

Transient Numerical Model

By Claudia C. Faunt, Joan B. Blainey, Mary C. Hill, Frank A. D’Agnese, and
Grady M. O’Brien

Chapter F of

Death Valley Regional Ground-Water Flow System, Nevada and California—Hydrogeologic Framework and Transient Ground-Water Flow Model

Edited by Wayne R. Belcher

Prepared in cooperation with the
U.S. Department of Energy
Office of Environmental Management, National Nuclear Security Administration, Nevada Site Office,
under Interagency Agreement DE-AI52-01NV13944, and
Office of Repository Development,
under Interagency Agreement DE-AI08-02RW12167

Scientific Investigations Report 2004-5205

U.S. Department of the Interior
U.S. Geological Survey

Contents

Introduction	265
Model Construction	265
Numerical Model Selection	266
Grid Definition	266
Temporal Discretization	266
Lateral Model Boundary Conditions	266
Hydraulic Properties	266
Hydrogeologic Units	268
Depth Decay of Hydraulic Conductivity	268
Vertical Anisotropy	268
Storage Properties	268
Hydrogeologic Structures	269
Ground-Water Recharge	269
Natural Ground-Water Discharge	271
Pumpage	278
Observations Used In Model Calibration	279
Heads, Head Changes, and Associated Errors	279
Ground-Water Discharge Observations and Errors.....	283
Boundary Flow Observations and Errors	283
Model Calibration	283
Approach.....	283
Sensitivity Analysis	283
Dimensionless Scaled Sensitivity	283
Composite Scaled Sensitivity	285
Parameter Correlation Coefficient	285
Nonlinear Regression	286
Uncertainty Evaluation	286
Unreasonable Parameter Estimates as Indicators of Model Error	287
Conceptual Model Variations	287
Horizontal Hydraulic Conductivity	288
Confining Units	288
Carbonate-Rock Aquifers	295
Volcanic-Rock Units	295
Basin-Fill Units.....	313
Depth Decay of Hydraulic Conductivity	313
Vertical Anisotropy	321
Storage Properties	321
Hydrogeologic Structures	322
Recharge	323
Ground-Water Discharge	326
Hydraulic-Head and Discharge Observations	326
Final Calibration of Model	327

Model Evaluation.....	327
Regional Water Budget	327
Evaluation of Model Fit to Observations	328
Ground-Water Discharge and Boundary Flow	331
Hydraulic Heads	332
Changes in Hydraulic Heads for the Transient Stress Periods	338
Normality of Weighted Residuals and Model Linearity	341
Evaluation of Estimated Parameter Values and Sensitivities	341
Evaluation of Boundary Flows	341
Evaluation of Hydrologically Significant Areas	341
Sheep Range	341
Pahrnagat Range	344
Northern Part of Death Valley and Sarcobatus Flat.....	344
Pahrump Valley	344
Penoyer Valley.....	345
Amargosa Desert.....	345
Nevada Test Site and Yucca Mountain	345
Model Evaluation Summary.....	346
Model Improvements	346
Data and Data Analysis	346
Model Construction and Calibration	346
Model Limitations	346
Observation Limitations	347
Quality of Observations	347
Interpretation of the Observations	347
Representation of Observations	347
Hydrogeologic Framework Limitations	347
Complex Geometry	347
Complex Spatial Variability	348
Flow Model Limitations	348
Representation of Physical Framework	348
Representation of Hydrologic Conditions	348
Representation of Time	348
Appropriate Uses of the Model	348
Summary	349
References Cited	350

Figures

F-1. Map showing location of model grid for the Death Valley regional ground-water flow system.....	267
F-2. Diagram showing example cross section across the model domain of subsurface configuration of model layers.....	269
F-3. Diagram showing oblique view of three-dimensional hydrogeologic framework model showing the distribution of the four major rock units using a series of north-south and east-west-oriented cross-sectional slices	271

F-4.	Schematic diagrams showing representation of hydrologic flow barrier (fault) in horizontal flow barrier (HFB) package of MODFLOW-2000.....	272
F-5—F-7.	Maps showing:	
F-5.	Hydrogeologic features interpreted as potential flow barriers and parameters used for horizontal flow barriers.....	273
F-6.	Recharge simulated in the Death Valley regional ground-water flow system model	274
F-7.	Model cell groups representing drains used to simulate natural ground-water discharge	275
F-8.	Graph showing pumping by model layers, 1913–98.....	278
F-9.	Map showing total withdrawal from pumpage by model cell, 1913–98.....	280
F-10.	(A) Map showing spatial distribution of hydraulic-head observations used in calibration of the Death Valley regional ground-water flow model; (B) graph showing the number of hydraulic-head observations representing both steady-state and transient conditions over time	284
F-11.	Graphs showing calculated uncertainty of head observations used to calibrate Death Valley regional ground-water flow system model: (A) Cumulative frequency; (B) percent contribution	287
F-12—F-34.	Maps showing hydraulic-conductivity zone parameters, unit thickness, and extent for:	
F-12.	Intrusive-rock confining unit.....	292
F-13.	Crystalline-rock confining unit.....	293
F-14.	Lower clastic-rock confining unit.....	294
F-15.	Upper clastic-rock confining unit and thrusted lower clastic-rock confining unit	296
F-16.	Sedimentary-rock confining unit.....	297
F-17.	Lower carbonate-rock aquifer (includes depth-decay parameters).....	300
F-18.	Upper carbonate-rock aquifer and thrusted lower carbonate-rock aquifer unit	301
F-19.	Older volcanic-rock unit.....	303
F-20.	Belted Range unit.....	304
F-21.	Crater Flat–Tram aquifer unit	305
F-22.	Crater Flat–Bullfrog confining unit.....	306
F-23.	Crater Flat–Prow Pass aquifer unit.....	307
F-24.	Wahmonie volcanic-rock and younger volcanic-rock unit.....	308
F-25.	Calico Hills volcanic-rock unit	309
F-26.	Paintbrush volcanic-rock aquifer.....	310
F-27.	Thirsty Canyon–Timber Mountain volcanic-rock aquifer.....	311
F-28.	Lava-flow unit	312
F-29.	Lower volcanic- and sedimentary-rock unit.....	315
F-30.	Upper volcanic- and sedimentary-rock unit.....	316
F-31.	Limestone aquifer and older alluvial confining units	317
F-32.	Older alluvial aquifer.....	318
F-33.	Younger alluvial confining unit.....	319
F-34.	Younger alluvial aquifer unit.....	320
F-35.	Graph showing hydraulic conductivity values decreasing with depth relative to the surface hydraulic conductivity.....	322

F-36.	Map showing recharge zone multiplication array representing infiltration rates and relative permeability in upper five model layers.....	325
F-37.	Graphs showing parameter values defining hydraulic conductivity for confining units and carbonate rocks, volcanic rocks, and basin-fill units.....	328
F-38.	Graphs showing parameter values defining flow barriers, drains, and depth decay, recharge, storage, specific yield, and ratio of horizontal to vertical anisotropy.....	329
F-39—F-45.	Graphs showing:	
F-39.	Total simulated and observed ground-water discharge from evapotranspiration and spring flow for steady state and transient stress periods of the transient model.....	332
F-40.	Simulated and observed annual discharge from regional springs in Pahrump Valley.....	333
F-41.	Weighted residuals and simulated equivalent for (A) hydraulic head, (B) head change, (C) constant-head flow and discharge.....	334
F-42.	Weighted observed value compared to weighted simulated values for (A) hydraulic head, (B) head change, and (C) constant-head flow and discharge.....	335
F-43.	Ground-water discharge weighted residuals (observed minus simulated).....	336
F-44.	Observed and simulated ground-water discharge by subregion: (A) Northern Death Valley, (B) Central Death Valley, and (C) Southern Death Valley with expected observed discharge variation.....	337
F-45.	Observed and simulated ground-water discharge observations by major discharge area with expected observation discharge variation.....	338
F-46.	Map showing steady-state stress period hydraulic-head residuals (observed minus simulated) and simulated potentiometric surface for uppermost active model layer.....	339
F-47.	Map showing steady-state stress period hydraulic-head weighted residuals (observed minus simulated) and simulated potentiometric surface for uppermost active model layer 16.....	340
F-48.	Graphs showing composite scaled sensitivities for all parameters.....	342
F-49.	Map showing model boundary and ground-water divide near Sheep Range with simulated potentiometric surface from model layers 1 and 16.....	343

Tables

F-1.	Thickness and depth to top of each layer of the flow model of the Death Valley regional flow system.....	268
F-2.	Flow through boundary segments of the Death Valley regional ground-water flow system model domain.....	270
F-3.	Major rock types of hydrogeologic units of the Death Valley regional ground-water flow system model.....	272
F-4.	Observed and simulated discharges for the cell groups representing drains for 1997 (stress period 86), Death Valley ground-water flow model.....	276
F-5.	Number of model cells representing wells and total pumpage by subregion from 1913 through 1998.....	281

F-6. Observations used in prepumped, steady-state stress period and pumped, transient stress periods of the model	282
F-7. Hierarchy of horizontal hydraulic-conductivity parameters and major characteristics guiding parameter definition	289
F-8. Calibrated horizontal hydraulic-conductivity parameters for confining units ..	291
F-9. Calibrated horizontal hydraulic-conductivity parameters for carbonate-rock aquifers	298
F-10. Calibrated horizontal hydraulic-conductivity parameters for the volcanic-rock units	302
F-11. Calibrated horizontal hydraulic-conductivity parameters for the basin-fill units ..	314
F-12. Calibrated depth-decay parameters	321
F-13. Calibrated vertical anisotropy parameters	323
F-14. Calibrated storage property values	323
F-15. Calibrated hydraulic characteristic parameters for hydrogeologic structures defined as horizontal-flow barriers	324
F-16. Calibrated recharge parameters used as multipliers for infiltration rates defined for the recharge zones	326
F-17. Calibrated drain conductance parameters.....	327
F-18. Simulated and observed water budget for the steady-state prepumping stress period and transient stress period 86 (year 1997).....	330
F-19. Summary statistics for measure of model fit.....	333

CHAPTER F. Transient Numerical Model

By Claudia C. Faunt, Joan B. Blainey, Mary C. Hill, Frank A. D’Agnese, and Grady M. O’Brien

Introduction

The construction, calibration, and evaluation of the transient numerical flow model of the Death Valley regional ground-water flow system (DVRFS) are described in this chapter. Parameter-estimation techniques were used to calibrate the model to prepumping steady-state conditions before 1913 and to transient-flow conditions from 1913 to 1998 after pumping of ground water began.

Previous studies by Prudic and others (1995) and Waddell (1982) showed that it is difficult to use computer models to effectively describe ground-water flow in an area as geographically large, and geologically and hydrologically complex, as the Death Valley region. Prudic and others (1995) reiterated that the validity of the assumptions and hydrologic values used in simulating ground-water flow in such an area can be argued.

Inevitably, simplifications and assumptions must be made to adapt the complex conceptual model for numerical simulation. The simplifications and assumptions made in the development of the DVRFS model include the following:

1. Regional ground-water flow is assumed to be through a porous medium. Although the water flows through fractures, faults, and solution openings in the rocks, these features are small enough and densely distributed enough, relative to the large scale of the model, that the rocks can be represented as a porous medium.
2. Horizontal hydraulic conductivity is assumed to be isotropic within a model cell. Heterogeneity is simulated by varying horizontal hydraulic conductivity of model cells or groups of cells. A vertical anisotropy factor is used to scale vertical hydraulic conductivity based on specified values of horizontal hydraulic conductivity. Major faults likely to be subvertical and barriers to horizontal flow are represented explicitly and contribute horizontal anisotropy to the model.
3. Prepumping conditions are assumed to have been at equilibrium and to have represented average annual conditions so that system recharge equaled system discharge. During 1913–98, ground-water pumpage is assumed to be the only transient stress on the system to cause the observed decline in water levels in wells and is the only transient change simulated. This assumption is made because:

(a) Any long-term decline in hydraulic heads caused by decreased recharge since the wet period during the late Wisconsin glacial period (20 thousand years ago [ka] to 10 ka) can be neglected. Declines in water levels since the Wisconsin glacial period have been suggested by Prudic and others (1995) and Grasso (1996) and likely would be limited to slowly declining heads and seepage from low-permeability rocks and areas isolated from the rest of the system by low-permeability rocks. Simulating heads still affected by elevated water levels in Wisconsin glacial period and neglecting the seepage could cause some model bias, but it is expected to be small. Also, the changes caused by this effect during the transient simulated period would be small (Prudic and others, 1995), so it is unlikely that drawdowns are affected.

(b) Decadal and seasonal fluctuations can be treated as noise in the observations. Thus, decadal and seasonal variations are accounted for through an analysis of observation errors, as discussed in the “Observations Used in Model Calibration” section of this chapter and in Chapter C (this volume).

Model Construction

The three-dimensional (3D) hydrogeologic data sets for the DVRFS described previously in this report (see Chapters B, C, and E) were discretized to develop the input arrays required for the model. Because the data sets were developed at grid cell resolutions ranging from 100 to 1,500 meters (m), their discretization to a common, larger grid cell resolution inevitably results in further simplification of the flow-system conceptual model and hydrogeologic framework model. This resampling and simplification of the 3D hydrogeologic data sets was apparent in (1) definition of the model grid, (2) assignment of boundary conditions, and (3) definition of model parameters.

A geographic information system (GIS) was used to ensure accurate spatial control of physical features and the finite-difference model grid. GIS also was used during calibration to manipulate and compare model input-data sets with model output.

Numerical Model Selection

The numerical modeling code used to simulate the DVRFS is the U.S. Geological Survey 3D ground-water flow model program MODFLOW-2000 with related packages (Harbaugh and others, 2000; Hill and others, 2000; Anderman and Hill, 2000, 2003; Hsieh and Freckleton, 1993). MODFLOW-2000 is a block-centered finite-difference code in which a 3D ground-water flow system is divided into a sequence of layers of porous material organized in a horizontal grid or array. MODFLOW-2000 (1) has the capabilities to represent the 3D complexities of the ground-water flow system; (2) contains methods for sensitivity analysis, calibration (including parameter estimation), and uncertainty evaluation; (3) includes a variety of hydrologic capabilities such as the simulation of wells and recharge; (4) can be applied to steady-state and transient flow conditions; and (5) is well documented, freely available, well tested, and widely accepted.

Grid Definition

The north-south-oriented grid for the flow model consists of 194 rows, 160 columns, and 16 layers, for a total of 496,640 cells with a constant grid-cell spacing of 1,500 m (fig. F-1). Because of the difference in grid definition between the mesh-centered hydrogeologic framework model (HFM) and the block-centered flow model, the HFM is one cell wider than the flow model. Finite-difference methods require that the model grid be constructed for the bounding rectangle of the DVRFS model domain, but only the cells within the model boundary are active and used to represent the flow system.

The model uses 16 layers to simulate the flow in the DVRFS. Most of these layers range in thickness from 50 to more than 300 m (table F-1 and fig. F-2). The thickness of model layer 16 varies and can extend as deep as 4,000 m below sea level; it is thickest in the Spring Mountains and isolated areas in the northeastern part of the model domain. With the exception of model layer 1, which has some thicker parts locally, model layer thickness generally increases with depth. This allows greater resolution at the top of the flow model where more hydrologic and geologic data are available.

The upper model layers are used to simulate relatively shallow flow primarily through basin-fill sediments and volcanic rocks and adjacent mountain ranges. The lower layers predominantly simulate deep flow through the regional carbonate-rock aquifer beneath the basin fill and mountain ranges. Model layer 1 is thick where low-permeability rocks, ground-water mounding, and/or steep hydraulic gradients are present. It is thickest in the Spring Mountains and parts of the Grapevine Mountains.

The top of model layer 1 is set to the simulated potentiometric surface of layer 1. The bottom of layer 1 was set to always be below this simulated potentiometric surface. In a few isolated areas, the heads in layer 1 are simulated above land surface. These areas are in mountain ranges with

low-permeability rocks and discharge areas. In the area around Mud Lake, heads also are simulated above land surface. This is not a realistic condition and most likely is a result of inaccurate portrayal of heads at the nearby constant-head boundaries.

In general, the model layers do not coincide with the hydrogeologic units (HGUs). The geometries of the HGUs in this system are complex because of considerable folding, faulting, and other processes, and it is not possible for model layers to conform to these irregular shapes (fig. F-2).

Temporal Discretization

For the DVRFS model, time is divided into steady-state or transient stress periods. The transient simulation begins with a prepumping steady-state period before 1913 in which no pumping is simulated. The subsequent 86-year period (1913–98) was divided into annual transient stress periods for which pumpage was defined. Within a single simulation, the same number of time steps, ranging from two to eight, was used in each stress period. The greater number of time steps did not improve model accuracy, and in the final calibrated model, two time steps per transient stress period are used.

Lateral Model Boundary Conditions

For previous simulations, the entire model boundary was represented as no flow and the only source of water in the model domain was recharge (D'Agnese and others, 1997, 2002). When using the recharge estimated from the net infiltration approximated by Hevesi and others (2003) (Chapter C, fig. C-8, this volume), ground-water levels and ground-water discharges could not be supported by the recharge, particularly in the north. Water-budget and Darcy-calculation estimates of flow from adjacent basins (Appendix 2, this volume) were used to help quantify flow into and out of the model domain. The type and location of the boundaries as well as the estimated flow are summarized in table F-2.

In order to simulate inflow or outflow across the model boundary, constant heads were specified in the cells along the boundary that are at or below the regional potentiometric surface. The hydraulic heads imposed at the constant-head cells were interpolated from the regional potentiometric surface (Appendix 1, this volume). As a result, the constant heads occur in different model layers along different parts of the boundary. The subsegment number and name are used as the observation name (table F-2). Observations are flows through subsegments defined as constant-head boundaries.

Hydraulic Properties

HGUs are the basis for assigning horizontal hydraulic conductivity, vertical anisotropy, depth decay of hydraulic conductivity, and storage characteristics to the cells of the model grid using the Hydrogeologic-Unit Flow (HUF) pack-

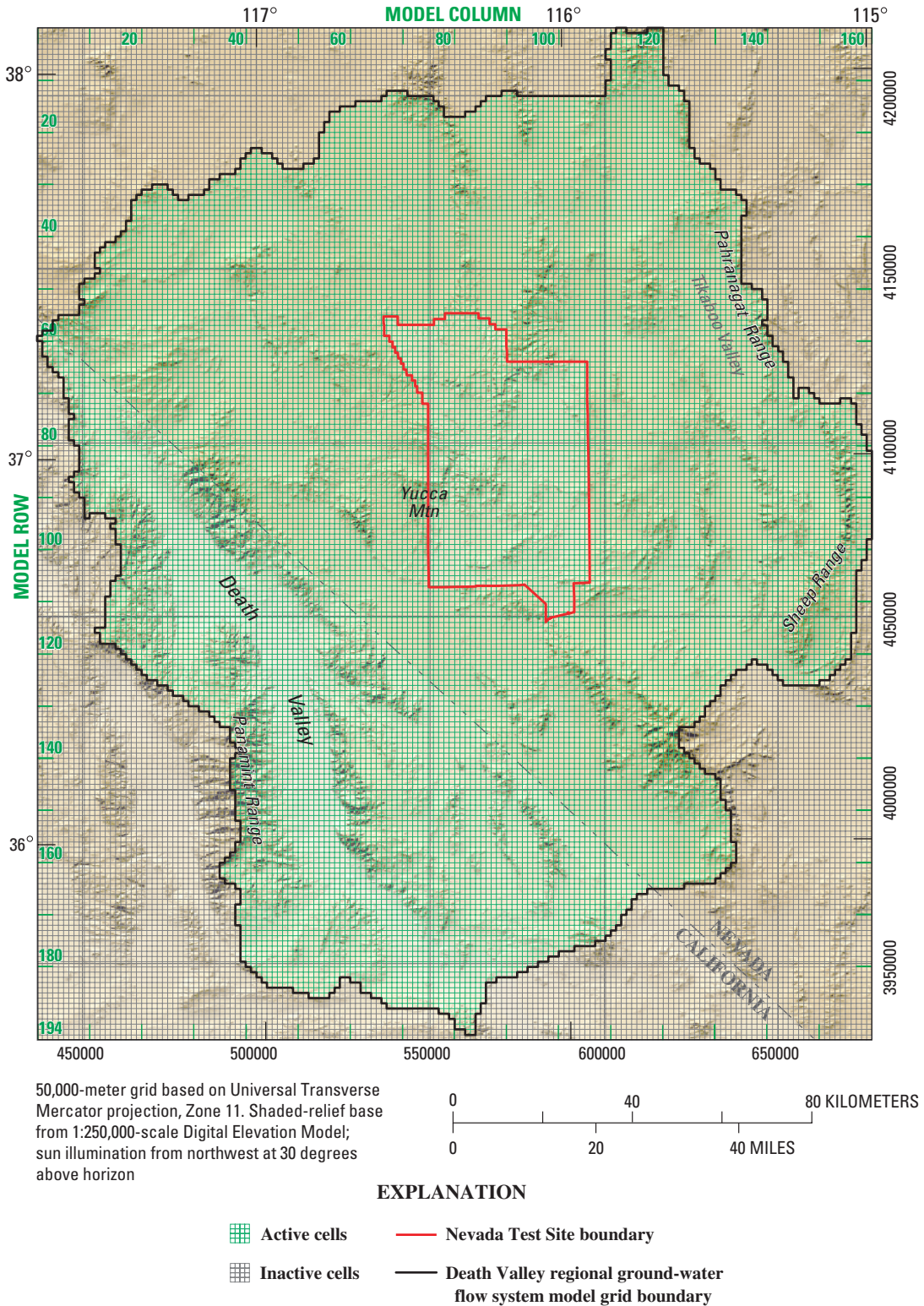


Figure F-1. Map showing location of model grid for the Death Valley regional ground-water flow system.

age (Anderman and Hill, 2000, 2003) for MODFLOW-2000. Model input arrays also were used to account for variations in the hydraulic properties within HGUs by zonation.

Hydrogeologic Units

The HUF package (Anderman and Hill, 2000, 2003) facilitates the discretization of the complicated geometry of the HGUs within the flow model. The HGUs are defined and assigned to model cells in the HUF package. Some model cells are filled by a single HGU; other model cells contain multiple HGUs. The HUF package vertically averages hydraulic properties for each cell based on the volume of the HGU occurring in the model cell.

Twenty-five HGUs (and two thrust units) were defined for the DVRFS (Chapter B, this volume). These HGUs were combined into four major rock types representing the initial HGU parameters for the flow model: confining units (K1), carbonate-rock aquifers (K2), volcanic-rock units (K3), and basin-fill units (K4) (fig. F-3 and table F-3). These major rock types are shown in a fence diagram of the model domain in figure F-3.

Only 5 of the 27 HGUs defined in the flow model are spatially significant: the lower carbonate-rock aquifer (LCA), lower volcanic- and sedimentary-rock unit (lower VSU), lower clastic-rock confining unit (LCCU), crystalline-rock confining unit (XCU), and intrusive-rock confining unit (ICU). The LCCU, XCU, and ICU are generally of low permeability and form confining units. The LCA forms the regional aquifer and transports most of the flow from the north and east toward Death Valley. Locally, the basin-fill units are important for ground-water development in Pahrump and Penoyer Valleys and Amargosa Desert. The volcanic-rock units of the south-western Nevada volcanic field (SWNVF) are important for ground-water flow and transport at the Nevada Test Site (NTS) and at Yucca Mountain (fig. F-3).

Table F-1. Thickness and depth to top of each layer of the flow model of the Death Valley regional flow system.

Model layer	Layer thickness (meters)	Minimum depth to top of layer (meters)
1	1 to 850	--
2	50	50
3	50	100
4	100	150
5	100	250
6	100	350
7	100	450
8	100	550
9	100	650
10	100	750
11	150	850
12	200	1,000
13	250	1,200
14	250	1,450
15	300	1,700
16	1,800 to 5,000	2,000

Depth Decay of Hydraulic Conductivity

To test the hypothesis that hydraulic conductivity decreases exponentially with depth (IT Corporation, 1996, p. 29), exponential decay was implemented in the HUF package of MODFLOW-2000 (Anderman and Hill, 2003), which allowed HGUs to be relatively impermeable at depth and relatively permeable near the land surface. The decay of hydraulic conductivity with depth is calculated as:

$$K_{Depth} = K_{Surface} 10^{-\lambda d} \quad (1)$$

where

K_{Depth} is the hydraulic conductivity at depth d [L/T],

$K_{Surface}$ is the hydraulic conductivity projected to the land surface [L/T],

λ is the depth-decay coefficient [L⁻¹],

and

d is the depth below land surface [L].

A value of $\lambda=1 \times 10^{-5}$ produces a hydraulic conductivity of 93 percent of the original value over 3,000 meters of depth; a value of $\lambda=1 \times 10^{-4}$ produces a hydraulic conductivity of 50 percent of the original value, and a value of $\lambda=1 \times 10^{-3}$ produces a hydraulic conductivity of 0.1 percent of the original value.

Vertical Anisotropy

Vertical anisotropy (the ratio of horizontal to vertical hydraulic conductivity) is defined for each HGU parameter by using the HUF package. Because of their layered nature, basin-fill sediments are likely to have significant vertical anisotropy. The assumed presence of solution features in carbonate rocks would indicate that these rocks have relatively small vertical anisotropy. The vertical anisotropy of other rocks and sediments would be expected to fall somewhere between these two extremes.

Storage Properties

In the HUF package, model layers can be defined as either confined or convertible between confined and unconfined (Anderman and Hill, 2003). Confined model layers are assigned a thickness that does not change during the simulation regardless of the simulated value of hydraulic head. In these layers, the storage coefficient generally equals the product of the specific storage and the model-layer thickness, where specific storage is defined for each HGU. If a cell contains more than one HGU, the specific-storage value for a cell equals a thickness-weighted average of the specific-storage values of the HGUs. All model layers were simulated as confined, and the storage consequences of water-table changes over time were simulated using a storage coefficient in the top model layer that was equivalent to a specific yield

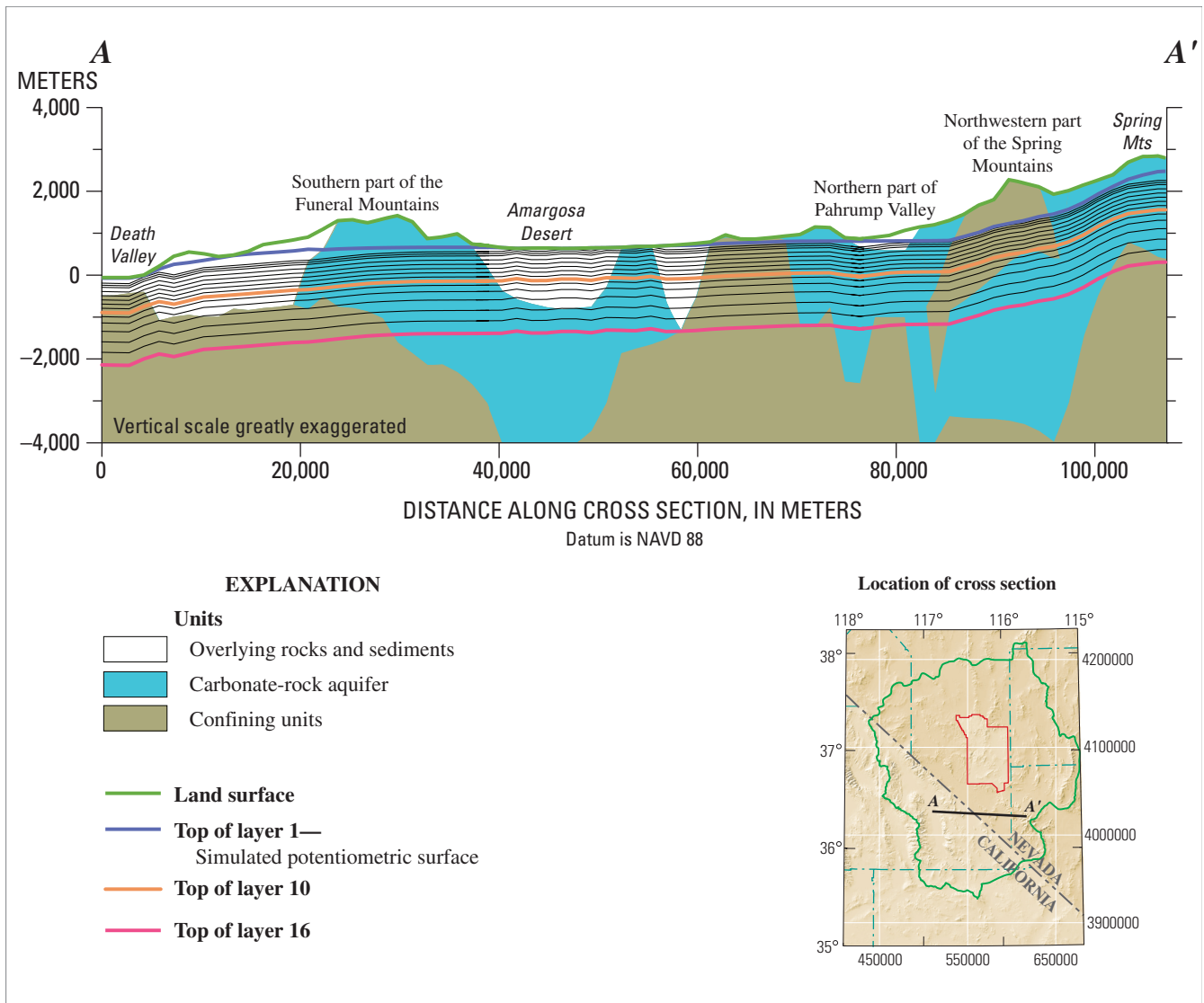


Figure F-2. Example cross section across the model domain of subsurface configuration of model layers.

(Anderman and Hill, 2003). The top model layer, layer 1, was defined as the simulated potentiometric surface in the unconfined part of the system.

Hydrogeologic Structures

A fault can be a barrier to flow for two reasons: (1) juxtaposition of low-permeability materials and relatively high-permeability materials, and (2) low-permeability material (fault gouge) in the fault zone itself, which forms a barrier to flow across the fault. Juxtaposition is represented in the flow model by the geometry of the HFM (described in Chapter E, this volume), and faults that contain fault gouge are simulated using the Horizontal-Flow Barrier (HFB) package (Hsieh and Freckleton, 1993). These flow barriers were located along cell boundaries to approximate the location of selected mapped faults (fig. F-4 and Chapter B, this volume). The model input

required for the HFB package is the hydraulic characteristic of the barrier; that is, the hydraulic conductivity of the barrier divided by the width of the barrier. It is assumed that the width is 1 m. The hydraulic conductivity is determined using estimated parameters. Faults in the model domain simulated as potential flow barriers are shown in figure F-5.

Ground-Water Recharge

The recharge rates were calculated using a net-infiltration model (Hevesi and others, 2003; Chapter C, this volume) with a 278.5-m grid (fig. C-8 in Chapter C) resampled to the 1,500-m DVRFS model grid using a nearest neighbor approach (fig. F-6). Recharge represented average annual conditions for the entire simulation. Initial recharge rates ranged from 0 to 0.000468 m/d (Chapter C, this volume).

Table F-2. Flow through boundary segments of the Death Valley regional ground-water flow system model domain.[--, standard deviation was considerably larger than the estimated flow and it was not quantified; m³/d, cubic meters per day]

Segment number and name (see fig. A2-3, this volume)	Conceptual boundary type	Comments	Observation name (subsegment number is last two digits) (see fig. A2-3, this volume)	Model boundary type ¹	Estimated boundary flow into (+) or out of (-) model domain (m ³ /d)	Standard deviation ² (m ³ /d)
1 Silurian	Flow in	Low-permeability rocks with hydraulic gradient nearly parallel to segment.	C_SILU0100	Constant head	500	500
2 Spring-Mesquite	No flow	Ground-water divide or hydraulic gradient parallel to segment; model boundary closely coincides with and is nearly parallel to the flow system boundary.	C_SPRM0200	No flow	0	--
3 Las Vegas	Flow out	Hydraulic gradient parallel to central part of segment, outflow from ends of segment is derived from recharge to the Spring Mountains and Sheep Range.	C_LASV0301 C_LASV0302 C_LASV0303	No flow No flow Constant head	-942 0 -3,633	-- -- 3,500
4 Sheep Range	Flow out	Outflow from most of the boundary is derived from inflow from Pahranaagat Valley and recharge to the Sheep Range; inflow on northern part of segment is derived from the Pahranaagat Valley.	C_SHPR0401 C_SHPR0402 C_SHPR0403 C_SHPR0404	Constant head Constant head Constant head Constant head	-4,410 -15,305 -4,959 5,927	4,000 15,000 4,500 5,500
5 Pahranaagat	Flow in and out	Southern part of segment has inflow adjacent to the Sheep Range. Most of the segment has outflow derived largely from Garden-Coal segment. Model boundary nearly parallel to flow-system boundary defined by a ground-water divide.	C_PAHR0501 C_PAHR0502 C_PAHR0503 C_PAHR0504 C_PAHR0505	Constant head Constant head No flow No flow Constant head	1,827 -2,346 -102 359 -2,521	1,500 2,000 -- -- 2,500
6 Garden-Coal	Flow in	Inflow mainly results in outflow to Pahranaagat segment.	C_GRDN0601 C_GRDN0602	No flow No flow	999 806	-- --
7 Stone Cabin-Railroad	Flow in	Hydraulic gradients poorly defined. Inflow likely on the basis of water budget and Darcy calculation.	C_GRDN0603 C_STNC0700	Constant head Constant head	2,334 12,476	2,000 12,000
8 Clayton	Flow in	Hydraulic gradient parallel to northern part of segment.	C_CLAY0800	Constant head	667	500
9 Eureka	Flow in	Hydraulic gradient parallel to segment.	C_EURS0900	Constant head	15,100	7,550
10 Saline	Flow in	Hydraulic gradient parallel to northern part of segment.	C_PANA1100	Constant head	15,000	7,500
11 Panamint	Flow in	Low-permeability rocks; steep hydraulic gradient.	C_OWLS1201 C_OWLS1202	No flow No flow	304 337	-- --
12 Owl'shead	Flow in	Low-permeability rocks, but hydraulic gradient across boundary.	C_OWLS1203 C_OWLS1204	Constant head No flow	1,682 59	1,500

¹A no-flow boundary segment is defined if the absolute value of the flow is less than 1,000 m³/d, except for the Silurian segment, where the local water budget strongly supports the small estimated value, and for the Clayton segment, where flow is likely.

²For flow estimates based on water-budget analyses (Appendix 2), the standard deviation was set to one-half of the estimated value. Otherwise, the standard deviation was set to the estimated flow value rounded down to the nearest 500.

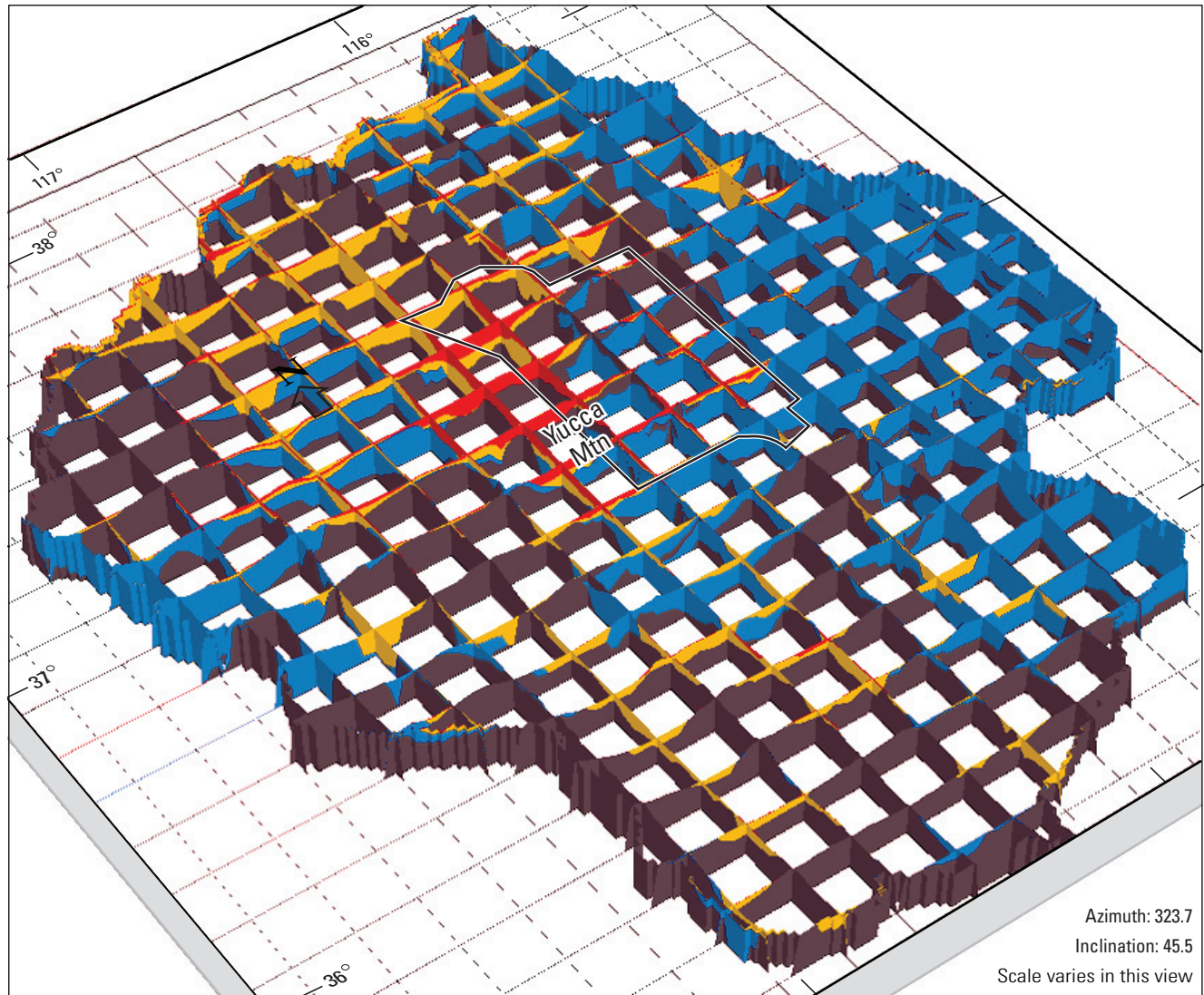


Figure F-3. Oblique view of three-dimensional hydrogeologic framework model showing the distribution of the four major rock units using a series of north-south and east-west-oriented cross-sectional slices.

Natural Ground-Water Discharge

Ground-water discharge by way of both evapotranspiration (ET) and spring flow is simulated using the Drain (DRN) package (Harbaugh and others, 2000) for MODFLOW-2000 (fig. F-7, table F-4). Discharge observations were developed from discharge data described in Chapter C (this volume), using average annual values for all data available for each observation. For cells covered only partly by an ET area, the

fractional area was specified in the Drain package. Unless there was a spring in the cell, only cells with ET areas greater than 4 percent of the cell area were included as drain cells in the model.

The Drain package simulates ground-water discharge through a head-dependent boundary. Ground water is simulated as discharging from a finite-difference cell in which a drain is defined when the simulated head in the cell rises above a specified drain altitude. The simulated discharge is

Table F-3. Major rock types of hydrogeologic units of the Death Valley regional ground-water flow system model.

Major rock type (parameter)	Hydrogeologic unit	
	Abbreviation	Name
Basin-fill units (K4)	YAA	Younger alluvial aquifer
	YACU	Younger alluvial confining unit
	OAA	Older alluvial aquifer
	OACU	Older alluvial confining unit
	LA	Limestone aquifer
	Upper VSU	Upper volcanic- and sedimentary-rock unit
	Lower VSU ¹	Lower volcanic- and sedimentary-rock unit
Volcanic-rock units (K3)	LFU	Lava-flow unit
	YVU	Younger volcanic-rock unit
	TMVA	Thirsty Canyon–Timber Mountain volcanic-rock aquifer
	PVA	Paintbrush volcanic-rock aquifer
	CHVU	Calico Hills volcanic-rock unit
	WVU	Wahmonie volcanic-rock unit
	CFPPA	Crater Flat–Prow Pass aquifer
	CFBCU	Crater Flat–Bullfrog confining unit
	CFTA	Crater Flat–Tram aquifer
	BRU	Belted Range unit
	OVU	Older volcanic-rock unit
	Lower VSU ¹	Lower volcanic- and sedimentary-rock unit
	UCA	Upper carbonate-rock aquifer
LCA, LCA_T1	Lower carbonate-rock aquifer and thrust	
Confining units (K1)	SCU	Sedimentary-rock confining unit
	UCCU	Upper clastic-rock confining unit
Carbonate-rock aquifer (K2)	LCCU, LCCU_T1	Lower clastic-rock confining unit and thrust
	XCU	Crystalline-rock confining unit
	ICU	Intrusive-rock confining unit

¹Lower VSU contains volcanic rocks and basin-fill deposits and is listed in both categories.

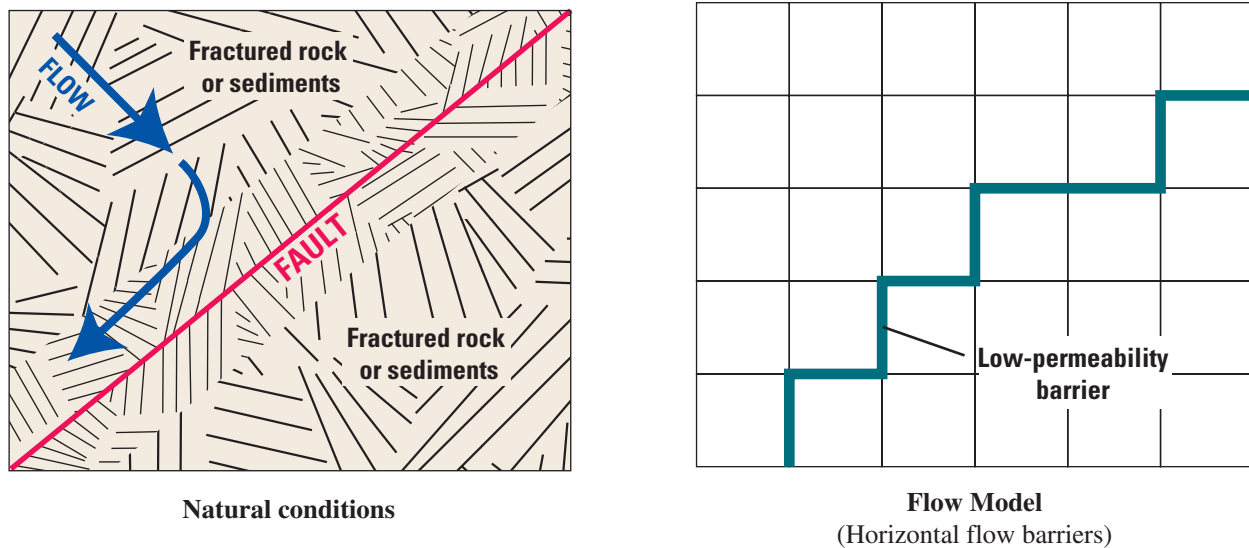


Figure F-4. Schematic diagrams showing representation of hydrologic flow barrier (fault) in horizontal flow barrier (HFB) package of MODFLOW-2000.

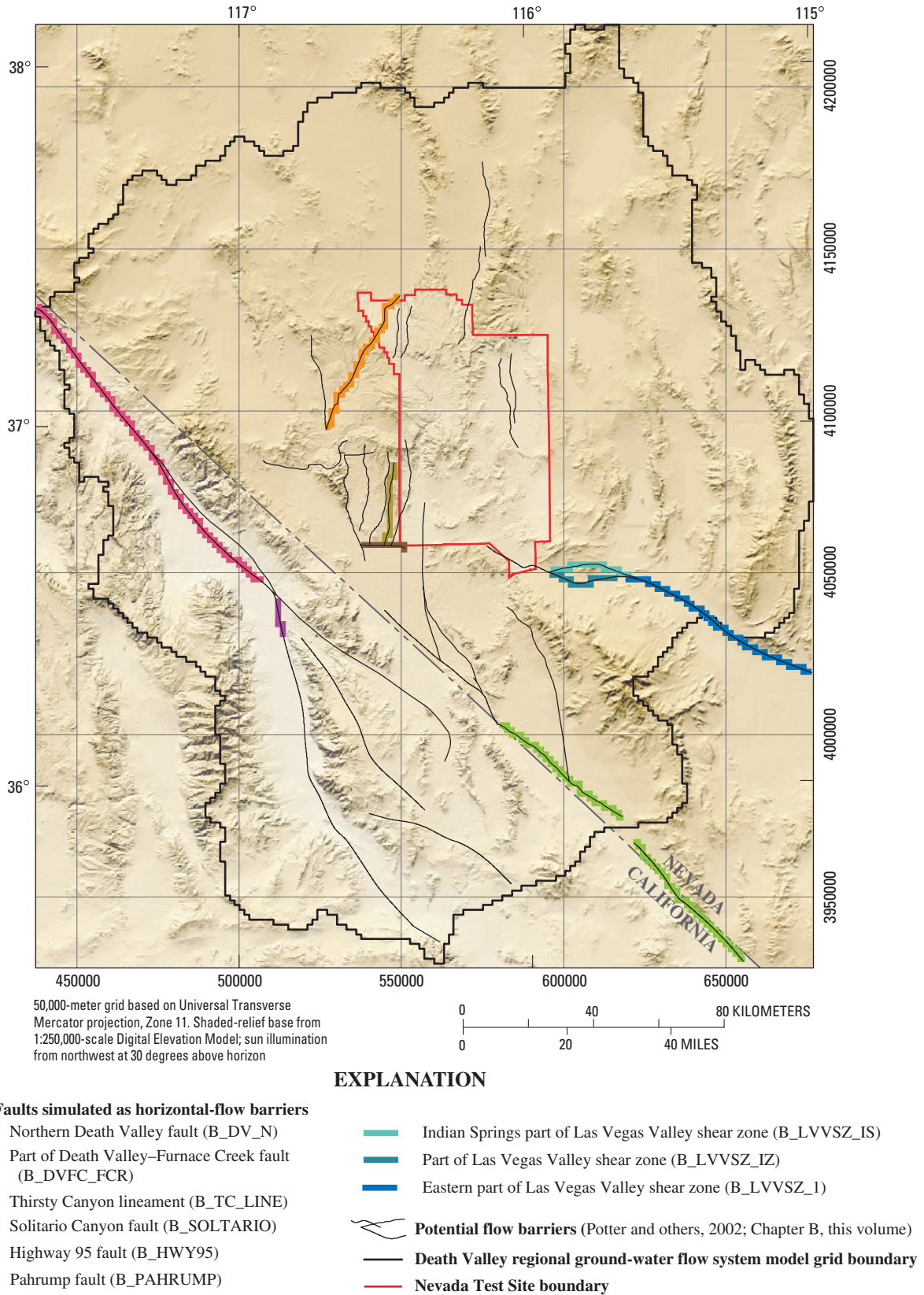


Figure F-5. Hydrogeologic features interpreted as potential flow barriers and parameters used for horizontal flow barriers.

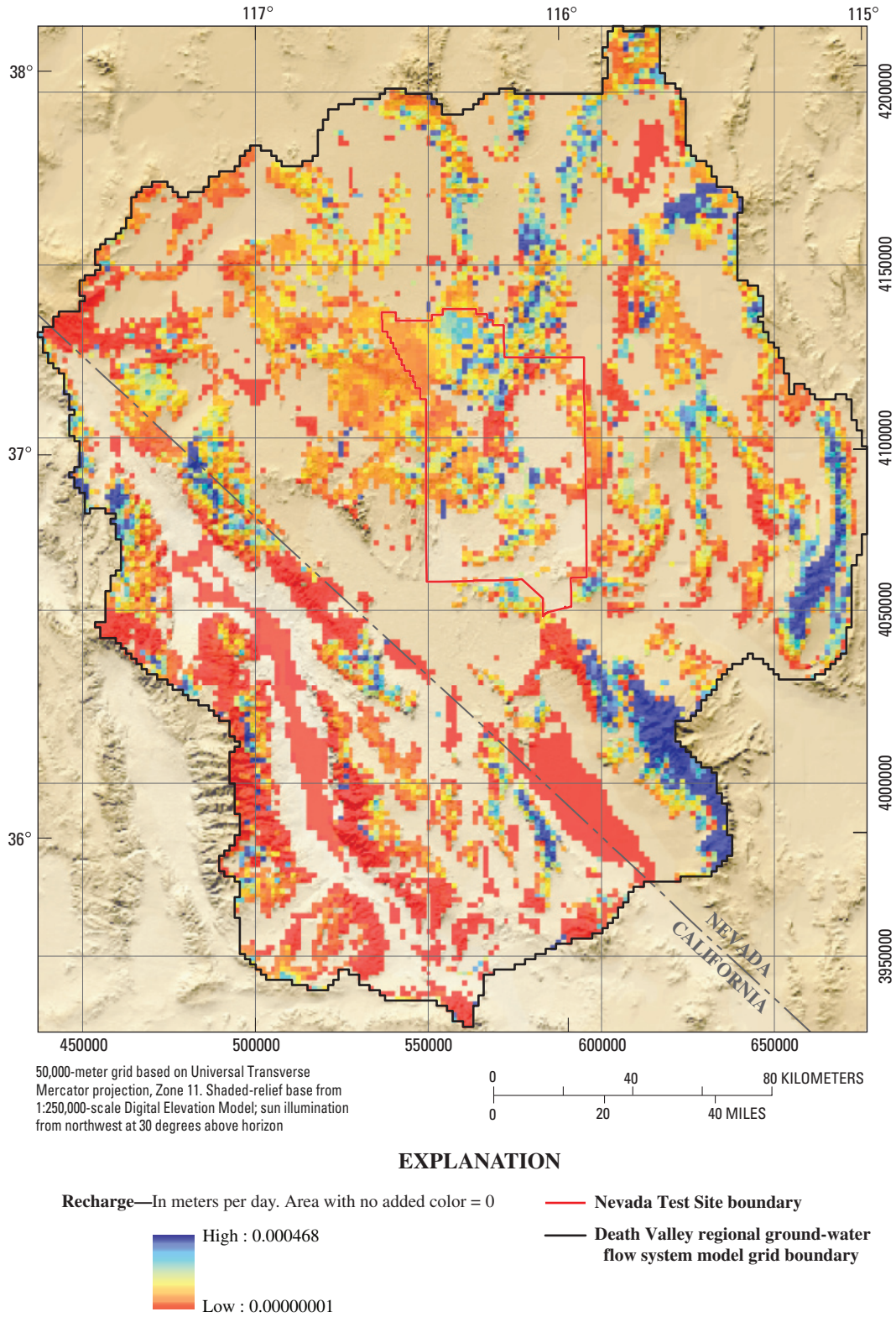
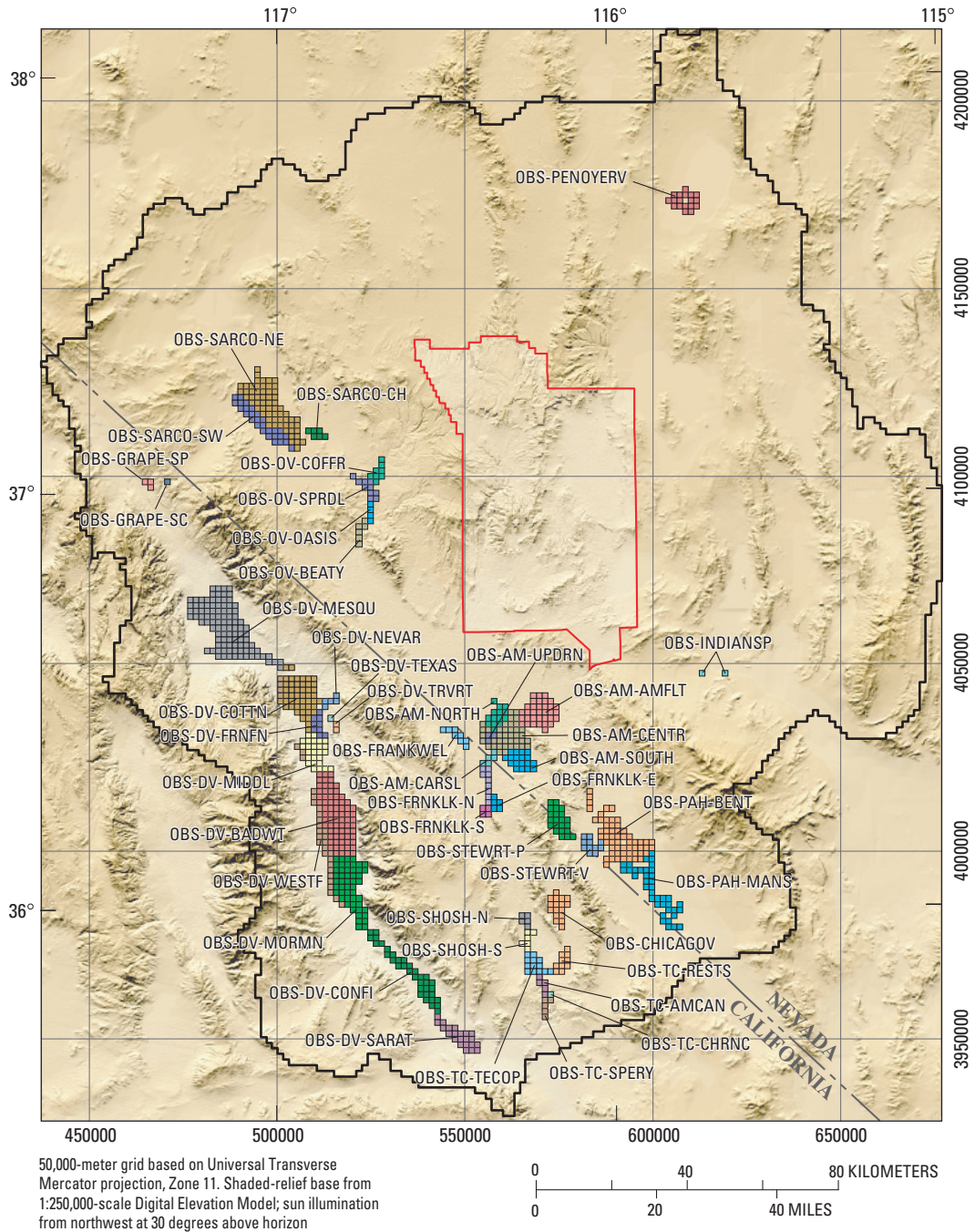


Figure F-6. Recharge simulated in the Death Valley regional ground-water flow system model.



EXPLANATION

- OBS-SARCO-NE **Model cell groups representing drains with observation name**—Observation descriptions provided in table F-4
- Death Valley regional ground-water flow system model grid boundary**
- Nevada Test Site boundary**

Figure F-7. Model cell groups representing drains used to simulate natural ground-water discharge.

Table F-4. Observed and simulated discharges for the cell groups representing drains for 1997 (stress period 86), Death Valley ground-water flow model.

[NA, not applicable]

Evapotranspiration (ET) zone	Observation name	Parameter name (conductance)	Observed discharge (cubic meters per day) (tables C-1 and C-2)	Simulated discharge (cubic meters per day)	Fractional difference	Coefficient of variation (D'Agnese and others, 2002)
Northern Death Valley Subregion						
Sarcobatus Flat ET			⁷ 44,662	39,340	0.12	NA
Northeastern	OBS-SARCO-NE	UP_PLY_DRN	⁷ 30,958	31,000	0.00	⁶ 0.46
Southwestern	OBS-SARCO-SW	UP_PLY_DRN	⁷ 12,174	7,290	0.40	⁶ 0.53
Twin Playas	OBS-SARCO-CH	UPPER_DRN	⁷ 1,530	1,050	0.31	⁶ 0.55
Grapevine Canyon Springs			³ 485	3,247	0.07	NA
Grapevine Springs area	OBS-GRAPE-SP	DEEP_DRN	³ 2,450	2,400	0.02	0.20
Staininger Springs area	OBS-GRAPE-SC	DEEP_DRN	³ 1,035	847	0.18	0.50
Part of Death Valley floor ET			29,002	44,900	-0.55	NA
Mesquite Flat	OBS-DV-MESQU	UP_DV_DRN	⁴ 29,002	44,900	-0.55	0.28
Central Death Valley Subregion—Pahute Mesa—Oasis Valley ground-water basin						
Penoyer Valley ET			12,833	4,890	0.62	NA
Penoyer Valley	OBS-PENOYERV	UPPER_DRN	⁵ 12,833	4,890	0.62	0.50
Oasis Valley ET			20,311	23,630	-0.16	NA
Upper	OBS-OV-COFFR	UPPER_DRN	² 4,390	2,700	0.38	⁶ 0.19
Upper middle	OBS-OV-SPRDL	UPPER_DRN	² 8,898	15,600	-0.75	⁶ 0.10
Lower middle	OBS-OV-OASIS	UPPER_DRN	² 3,629	3,910	-0.08	⁶ 0.10
Lower	OBS-OV-BEATY	UPPER_DRN	² 3,394	1,420	0.58	⁶ 0.13
Indian Springs	Not simulated	UPPER_DRN	² 74	NA	NA	0.19
Crystal Springs	Not simulated	UPPER_DRN	² 113	NA	NA	0.32
Upland Springs	Not simulated	UPPER_DRN	² 45	NA	NA	0.23
Central Death Valley Subregion—Ash Meadows ground-water basin						
Indian Springs area			2,240	0	1.00	NA
Indian and Cactus Springs	OBS-INDIANSP	UPPER_DRN	2,240	0	1.00	0.10
Ash Meadows ET			60,372	61,098	-0.01	NA
Northern	OBS-AM-NORTH ¹	UP_PLY_DRN/ DEEP_DRN	⁷ 18,337	11,800	0.36	⁶ 0.14
Central	OBS-AM-CENTR ¹	UP_PLY_DRN/ DEEP_DRN	⁷ 23,193	24,300	-0.05	⁶ 0.15
Southern	OBS-AM-SOUTH ¹	UP_PLY_DRN/ DEEP_DRN	⁷ 9,484	18,700	-0.97	⁶ 0.23
Amargosa Flat	OBS-AM-AMFLT	UPPER_DRN	⁷ 5,660	2,340	0.59	⁶ 0.32
Carson Slough drainage	OBS-AM-CARSL	UP_PLY_DRN	⁷ 468	318	0.32	0.50
Upper drainage	OBS-AM-UPDRN	UP_PLY_DRN	⁷ 3,230	3,640	-0.13	0.15
Franklin Well area ET			1,150	520	0.55	NA
Franklin Well	OBS-FRANKWEL	UP_PLY_DRN	⁷ 1,150	520	0.55	0.50
Franklin Lake ET			3,519	7,240	-1.06	NA
Northern-central	OBS-FRNKLK-N	UP_PLY_DRN	⁷ 2,350	4,460	-0.90	⁶ 0.26
Southwest	OBS-FRNKLK-S	UP_PLY_DRN	⁷ 741	1,410	-0.90	⁶ 0.49
Southeast	OBS-FRNKLK-E	UP_PLY_DRN	⁷ 428	1,370	-2.20	⁶ 0.71
Central Death Valley Subregion—Alkali Flat—Furnace Creek ground-water basin						
Part of Death Valley floor ET			80,048	125,700	-0.57	NA
Mormon Point	OBS-DV-MORMN	UP_DV_DRN	⁴ 13,356	18,800	-0.41	0.28
Badwater Basin	OBS-DV-BADWT	UP_DV_DRN	⁴ 20,098	24,400	-0.21	0.28
Middle Basin	OBS-DV-MIDDL	UP_DV_DRN	⁴ 6,625	23,700	-2.58	0.28
Furnace Creek Ranch	OBS-DV-FRNFN	UP_DV_DRN	⁴ 11,522	9,020	0.22	0.28
Cottonball Basin	OBS-DV-COTTN	UP_DV_DRN	⁴ 10,224	33,400	-2.27	0.28
West side vegetation	OBS-DV-WESTF	UP_PLY_DRN	⁴ 18,223	16,400	0.10	0.28
Death Valley area springs			7,737	7,230	0.07	NA
Nevaras Spring	OBS-DV-NEVAR ¹	DEEP_DRN	1,884	2,370	-0.26	0.15
Texas Spring	OBS-DV-TEXAS ¹	DEEP_DRN	1,220	1,450	-0.19	0.15
Travertine Spring	OBS-DV-TRVRT ¹	DEEP_DRN	4,633	3,410	0.26	0.10

Table F-4. Observed and simulated discharges for the cell groups representing drains for 1997 (stress period 86), Death Valley groundwater flow model.—Continued

[NA, not applicable]

Evapotranspiration (ET) zone	Observation name	Parameter name (conductance)	Observed discharge (cubic meters per day) (tables C-1 and C-2)	Simulated discharge (cubic meters per day)	Fractional difference	Coefficient of variation (D'Agnese and others, 2002)
Southern Death Valley Subregion						
Stewart Valley area ET			3,379	3,842	-0.61	NA
Upper Stewart Valley	OBS-STEWRT-V	UP_PLY_DRN	⁷ 2,383	672	0.33	⁶ 0.56
Lower Pahrump drainage	OBS-STEWRT-P	UP_PLY_DR	⁷ 996	3,170	-0.33	⁶ 0.16
Pahrump Valley area ET and springs						
Manse Spring (ET and spring flow) – steady state	OBS-PAH-MANS	UP_PAH_DRN	14,500	2,910	0.80	0.5
Manse fan (ET, spring dry) – 1960	OB-PAH-MANS	UP_PAH_DRN	5,375	2,480	0.54	0.5
Manse fan (ET, spring dry) – 1998	O-PAH-MANS	UP_PAH_DRN	821	1,370	-0.67	0.5
Bennetts Spring (ET and spring flow) – steady state	OBS-PAH-BENT	UP_PAH_DRN	17,900	19,600	-0.09	0.5
Pahrump fan (ET, spring dry) 1960	OB-PAH-BENT	UP_PAH_DRN	16,753	16,800	0.00	0.5
Pahrump fan (ET, spring dry) 1998	O-PAH-BENT	UP_PAH_DRN	2,557	7,650	-1.99	0.5
Tecopa Valley area ET						
Upper	OBS-TC-TECOP	UP_PLY_DRN	⁷ 12,097	1,470	0.88	⁶ 0.12
Middle	OBS-TC-AMCAN	UPPER_DRN	⁷ 3,360	853	0.75	⁶ 0.13
Lower	OBS-TC-SPERY	UPPER_DRN	⁷ 1,328	655	0.51	0.5
China Ranch	OBS-TC-CHNRC	UPPER_DRN	⁷ 1,766	263	0.85	0.5
Resting Springs	OBS-TC-RESTS	UPPER_DRN/ DEEP_DRN	⁷ 2,512	566	0.77	⁶ 0.16
Shoshone Valley area ET						
Upper	OBS-SHOSH-N	UPPER_DRN	⁷ 2,235	1,300	0.42	⁶ 0.16
Lower	OBS-SHOSH-S ²	UP_PLY_DRN/ DEEP_DRN	⁷ 4,780	2,350	0.51	⁶ 0.15
Chicago Valley area ET						
Chicago Valley	OBS-CHICAGOV	UP_PLY_DRN	⁷ 1,462	5,420	-2.71	⁶ 0.36
California Valley area ET						
California Ranch	Not simulated	NA	⁷ 326	NA	NA	0.22
Part of Death Valley floor ET						
Saratoga Springs	OBS-DV-SARAT	UPPER_DRN	⁴ 8,311	7,060	0.15	0.28
Confidence Mill site	OBS-DV-CONFI	UPPER_DRN	⁴ 3,236	5,800	-0.79	0.28

¹Observations for which 50 percent or more of the flow comes from springs.²Reiner and others, 2002.³Miller, 1977.⁴DeMeo and others, 2003.⁵Van Denburg and Rush, 1974.⁶R.K. Waddell, Geotrans, Inc., written commun., 2003.⁷Laczniaik and others, 2001.

calculated as the drain conductance multiplied by the difference in altitude between the simulated head and the drain. The drain conductances are defined using the hydraulic properties of materials through which water flows to the surface (“Parameter name” column in table F-4): (1) DEEP_DRN, warm-water discharge indicates rapid flow from depth and the drain cell is located at the shallowest occurrence of the LCA; (2) UPPER_DRN, flow is through surficial materials that are coarser than playa materials (YAA and OAA); (3) UP_PLY_DRN, flow is through surficial fine-grained playa materials (YACU and OACU); (4) UP_DV_DRN, flow is from springs in Death Valley with substantial salt concentrations; and (5) UP_PAH_DRN, all discharge areas in Pahrump Valley where estimates of discharge over time are available.

The drain conductances were estimated as part of model calibration. The drain altitudes were set equal to 10 m below the lowest land-surface altitudes for each group of cells (fig. F-7). This value is assumed to represent a reasonable altitude below which ET would not occur and to account for springs being located in land-surface depressions that are lower than would be evident in the top surface of the HFM. This altitude would approximate the extinction depth for ET as well. Drains representing springs are set to these altitudes but are connected to the topmost occurrence of the lower carbonate-rock aquifer at that cell location. This occurs in model layers 1 through 10.

Many discharge areas represent individual springs that are significantly smaller in area than the simulated 1,500-m grid cell. At this scale, it is not possible to represent variations in hydraulic gradient, fault and fracture geometry, and abrupt changes in lithology that influence ground-water discharge rates at a regional scale. In some cases, however, individual springs, such as Travertine, Texas, and Nevares Springs, were simulated. Discharge areas with flow rates less than 1,000 cubic meters per day (m³/d) were difficult to simulate, but the discharge contributions are relatively minor given the overall volumetric budget and model scale. Because of these simplifications in representing discharge areas in the model, errors in simulation can result.

Pumpage

Substantial volumes of ground-water discharge from the regional flow system through pumped wells are shown by model layer in figure F-8. Pumping from wells is simulated using the Multi-Node Well (MNW) package for MODFLOW-2000 (Halford and Hanson, 2002). In the DVRFS region wells typically are completed with screens that span multiple aquifers and thus multiple layers in the model. The MNW package uses the hydraulic conductivity and thickness to determine how much of the well pumpage is derived from each model layer. This allows pumpage to be redistributed as the estimates of the hydraulic-conductivity distribution change during model calibration.

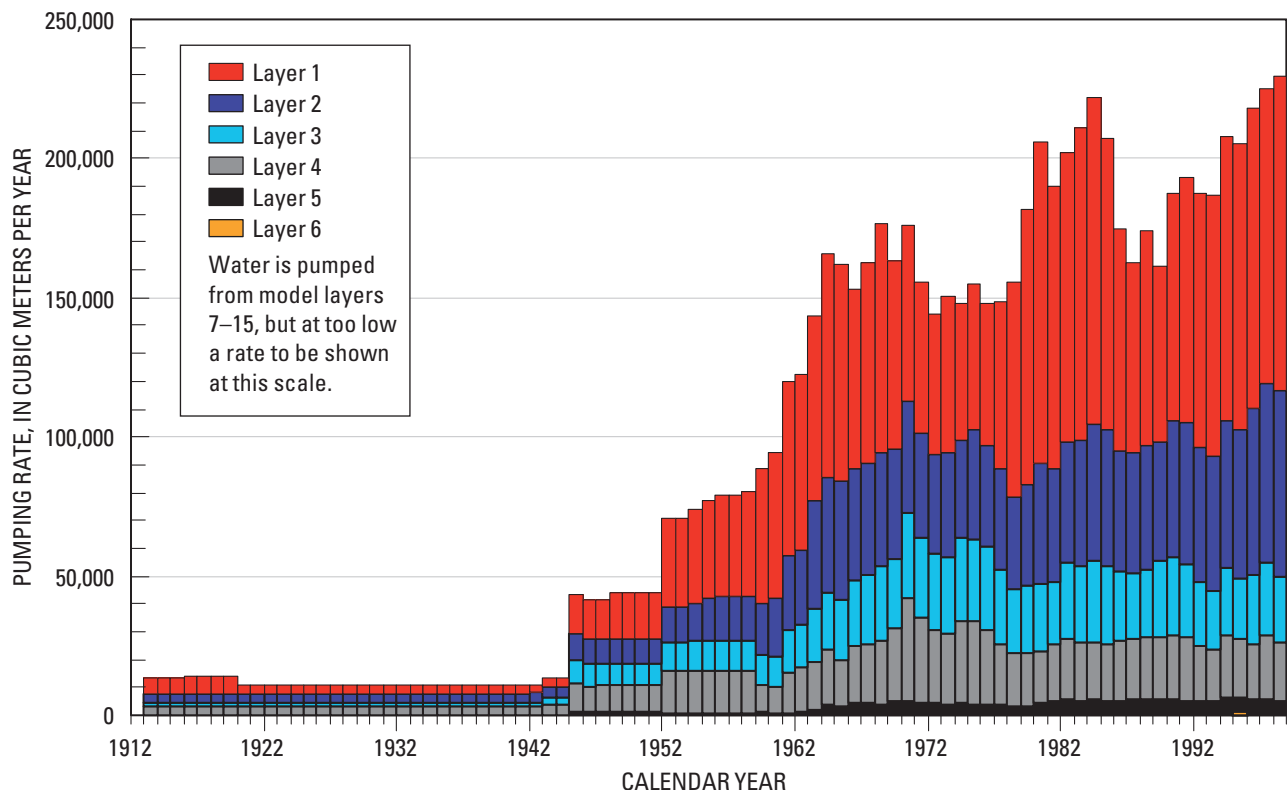


Figure F-8. Pumping by model layers, 1913-98.

Some return flow of pumpage through subsequent infiltration of excess irrigation, lawn water, or septic tank wastewater is likely to occur. The magnitude and timing of these returns have not been precisely quantified, but a method was developed to compute informal estimates of return flow (Chapter C, this volume). For each withdrawal point, return flow was estimated to be 20 percent of the estimated annual pumpage (Moreo and others, 2003), lagged by 7 years. The total pumpage for the wells in each cell is applied at the cell center (fig. F-9), resulting in 8,569 wells simulated by pumping in 432 cells (table F-5).

Observations Used In Model Calibration

Poorly quantified or unquantified characteristics of the system can be constrained on the basis of observations (composite field measurements used in calibrating the model). Observations used to calibrate the DVRFS model are those of hydraulic heads (water levels), changes in head over time due to pumpage, and discharge by ET and spring flow (table F-6). Estimated boundary flows (simulated as constant-head boundaries) are treated like observations but are less accurate than other observation types and are given less weight in the simulation.

Weighting values (or weights) are the inverse of the estimated variance of an observation. This weighting will result in parameter estimates with the smallest possible variance if (1) the estimated variances and the model are accurate, (2) the model is effectively linear, and (3) the number of observations is effectively large (Bard, 1974). In addition to variances, MODFLOW-2000 permits the designation of standard deviations or coefficients of variation (CVs), from which variances are calculated (Hill and others, 2000, p. 39–40, 53, 57, 65). These indicators of measurement precision are determined on the basis of an analysis of likely measurement error (Chapter C, this volume).

For the prepumped, steady-state stress period, all observations are considered representative of steady-state conditions. For the pumped, transient stress periods, some hydraulic-head and discharge observations are not influenced by pumping and thus are also considered representative of long-term steady-state conditions. Hydraulic-head observations influenced by pumping are treated as head-change observations. Natural discharge from ET and springs was considered to be constant and not influenced by pumping, with the exception of some springs in Pahrump Valley. It is assumed that constant-head observations used to simulate flow into and out of the model boundary are not influenced by pumping.

Heads, Head Changes, and Associated Errors

Water levels measured in boreholes and wells located within the model domain were used to develop hydraulic-head and head-change observations for calibration of the regional

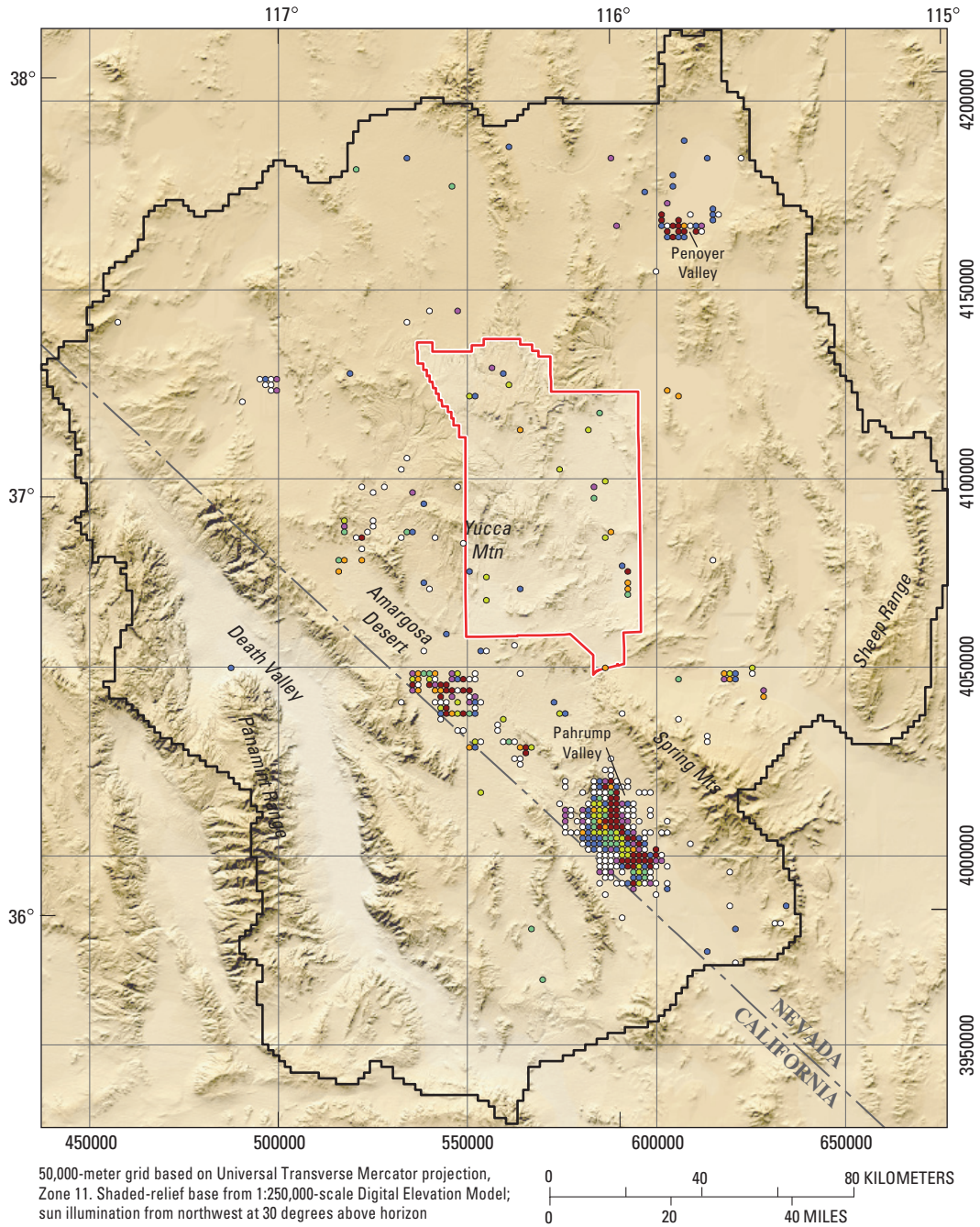
flow model. Only those water levels considered representative of regional ground-water conditions were used to calculate head observations (Chapter C, this volume). Prepumped, steady-state head observations were developed at 700 wells. Head observations at these wells were computed as the average of all water-level measurements throughout the entire record. For pumped, transient stress periods, hydraulic-head observations were computed as average annual water levels from nearly 15,000 water-level measurements considered representative of either steady-state or transient conditions (Chapter C, this volume). Head observations for wells having water-level measurements over multiple years were determined to be either affected or not affected by pumping. Head observations affected by pumping are treated in model calibration as a head change, which is calculated as the difference between the observation of interest and a reference observation (Hill and others, 2000, p. 33–34). The reference observation is the measurement prior to any pumping effect or the first measurement affected by pumping.

The areal distributions of the hydraulic-head and head-change observations are shown in figure F-10A. The number of observations representing steady-state and transient conditions over time is shown in figure F-10B, and the distribution of observations by the deepest open layer is shown in figure C-13 (this volume).

The open intervals of the wells were considered in determining the model layers associated with head and head-change observations (Chapter C, this volume). Most wells for which observations are available and that are open to multiple layers are on or near Pahute Mesa. Most head and head-change observations (82 percent) are from wells completed in the shallow part of the flow system (no deeper than model layer 5) and none are deeper than model layer 14. For wells open to more than one model layer, simulated heads are a weighted average calculated by MODFLOW-2000 using user-defined weights (Hill and others, 2000, p. 34–36).

The DVRFS model domain is dominated by observations in just a few areas: Pahrump Valley, Amargosa Desert, a few other small population centers, and the Nevada Test Site (fig. F-10A). Elsewhere, observations are sparse and the paucity of data is most pronounced in the distribution of hydraulic heads. Clustered data can be problematic if they dominate the regression analysis and result in a poor model fit in these areas.

In addition to the four sources of error discussed in Chapter C, two sources of error are associated with the modeling process: uncertainties in model discretization and pumpage estimates. Model-discretization errors result from inaccuracies in the geometric representation of HGUs and major structural features in the model (Hill and Tiedeman, 2003). The magnitude of these errors is assumed to be a function of nodal width, hydraulic gradient, and well-opening depth. The dependence on nodal width occurs because larger widths result in a less accurate representation of the geometry of HGUs and of major structural features relative to well location. The dependence on hydraulic gradient occurs because inaccurate geometric representations tend to shift the location of local hydraulic gradients. The depth dependence results from a decrease in



EXPLANATION

Simulated pumping well and total withdrawal by model cell—In cubic meters per day (1913–98)

- <50,000
- 50,000 to 100,000
- 100,000 to 500,000
- 500,000 to 1,000,000
- 1,000,000 to 5,000,000
- 5,000,000 to 10,000,000
- >10,000,000

- Death Valley regional ground-water flow system model grid boundary
- Nevada Test Site boundary

Figure F-9. Total withdrawal from pumpage by model cell, 1913–98.

Table F-5. Number of model cells representing wells and total pumpage by subregion from 1913 through 1998.

[Pumpage total in Chapter C (this volume) is slightly less because of rounding]

Division (see Chapter D, this volume)	Number of wells 1913–98	Number of cells in model	Pumpage 1913–98 (cubic meters)
Northern Death Valley subregion	16	11	1,110,751
Lida-Stonewall section	0	0	0
Sarcobatus Flats section	14	9	601,569
Grapevine Canyon–Mesquite Flat section	1	1	497,093
Oriental Wash section	1	1	12,088
Central Death Valley subregion	675	201	1,062,495,492
Pahute Mesa–Oasis Valley ground-water basin	109	63	299,170,575
Southern Railroad Valley/Penoyer Valley section	67	35	272,463,839
Kawich Valley section	6	5	4,208,641
Oasis Valley section	36	23	22,498,095
Ash Meadows ground-water basin	194	56	164,885,953
Tikaboo Valley section	0	0	0
Emigrant Valley section	4	2	15,196,498
Yucca–Frenchman Flat section	19	14	54,320,450
Pahrnagat section	0	0	0
Indian Springs section	87	15	32,383,220
Specter Range section	84	25	62,985,785
Alkali Flat–Furnace Creek ground-water basin	372	82	598,438,964
Fortymile Canyon section	7	5	14,041,836
Amargosa River section	357	69	583,275,400
Crater Flat section	7	7	1,107,050
Funeral Mountains section	1	1	14,678
Southern Death Valley subregion	7,878	220	2,212,287,835
Pahrump Valley	7,876	218	2,211,155,498
Shoshone-Tecopa	2	2	1,132,336
California Valley section	0	0	0
Ibex Hills section	0	0	0
Total	8,569	432	3,275,894,077

the knowledge of HGUs and structures with depth. Assuming these generalizations are correct, the potential for model discretization error increases with the size of the grid, the steepness of the hydraulic gradient, and the depth of the open intervals in observation wells and model layers.

Model-discretization error could be quantified in a number of ways. Here, this error is assumed to be normally distributed about the head observation with the 95-percent confidence interval being directly proportional to the nodal width and hydraulic gradient. Hydraulic gradients were calculated from the regional potentiometric surface map (D’Agnese and others, 1998), assuming that model-simulated hydraulic gradients will be similar to those represented by the map. The product of nodal width and hydraulic gradient approximates the head difference across a finite-difference cell and therefore is assumed to represent the error contributed by potential inaccuracies in the geometry of HGUs and the location of major structural features.

A scalar that is a function of the well-opening depth is used to incorporate the potential error attributed to a decrease in geologic certainty with depth. This depth scalar is calculated as 2 plus the quotient of the depth of the top of the open interval and the approximate thickness of the aquifer material

in the model (3,000 m). The depth scalar ranges from about 2 at the top of the flow system to 3 at the bottom of the flow system.

The 95-percent confidence interval is defined as four standard deviations, so the range defined by the model-discretization error is divided by four to obtain the standard deviation. The standard deviation for model-discretization error was computed as:

$$sd_5 = \{NW \times HG \times [(TOUPOPEN / MT) + 2]\} / 4 \quad (2)$$

where

sd_5 is the standard deviation of model-discretization error;

NW is nodal width, in meters, and is equal to 1,500 meters;

HG is hydraulic gradient;

$TOUPOPEN$ is top of upper well opening, in meters below land surface;

and

MT is the approximate thickness of aquifer material in the model and is equal to 3,000 meters for this calculation.

Table F-6. Observations used in prepumped, steady-state stress period and pumped, transient stress periods of the model.

[≤, less than or equal to; >, greater than]

Type of observation	Number of observations	
	Steady state	Transient (includes steady-state observations)
Head	700	2,227
Observations with few measurements	156	195
Observations with many measurements	544	2,032
Head change	0	2,672
Observed value ≤1.0 m	0	1,069
Observed value >1.0 m	0	1,603
Discharge from evapotranspiration or springs	45	49
Constant-head boundary flow	15	15

The resulting standard deviations seem reasonable for model-discretization error. Given that the maximum hydraulic gradient in this system is 0.15 and the maximum top well opening depth is 750 m, the maximum standard deviation that could be computed using equation 1 is 125 m. Standard deviations computed for head observations were much smaller, seldom exceeding 50 m.

Using the standard deviations of a head observation based on the five potential errors, the standard deviation, sd_h , of each observation was computed by the equation:

$$sd_h = (sd_1^2 + sd_2^2 + sd_3^2 + sd_4^2 + sd_5^2)^{1/2} \quad (3)$$

where

- sd_1 is standard deviation of well-altitude error;
- sd_2 is standard deviation of well-location error;
- sd_3 is standard deviation of nonsimulated transient error;
- sd_4 is standard deviation of measurement-accuracy error;

and

- sd_5 is standard deviation of model-discretization error.

Computed standard deviations of head observations used to calibrate prepumped, steady-state flow conditions ranged from less than 1 m to about 215 m, as shown on the vertical axis of the cumulative frequency diagram in figure F-11A. About 95 percent of the head observations had a standard deviation of less than 50 m and about 50 percent had a standard deviation of less than 10 m (fig. F-11A). The magnitudes of these standard deviations are larger

than those discussed in Chapter C because of the addition of model-discretization error (fig. F-11B). Figure F-11B shows the percentage contribution of the five types of errors (including model-discretization error) for the 700 head observations.

Differences between simulated and observed head changes are expected to be dominated by errors in the estimates of pumpage; thus, this is the only error considered in calculating the weighting of head-change observations. Withdrawal-estimate error does not affect head observations assumed to represent prepumped, steady-state flow conditions.

Pumpage-estimate error results from uncertainties in the pumping rate, the location of the pumped well, and the depth of pumped-well openings. Pumping rates were estimated by a variety of methods and data, including irrigated acreage, flow-meter measurements, water-use reports, and power-consumption graphs (Chapter C, this volume). Errors typical of these estimation techniques are discussed in Chapter C of this report.

The relation between pumping and head change is approximately linear, whereas that between pumped-well location and head change is less predictable. The linear relation between pumping and head change indicates that the error related to uncertainties in the pumping rate can be represented by a coefficient of variation (CV), which results in standard deviations that increase linearly with pumping rate. The result of a linear increase is that the weights are small for large pumping rates and large for small pumping rates. The strict use of a CV in this model was problematic because larger head-change observations were given unrealistically large standard deviations and small weights, and vice versa. To remedy this problem, a function was developed that maintained the basic premise of larger standard deviations for larger head changes but tempered the difference in the standard deviation between large and small head-change observations. The function used to calculate the standard deviation of a head-change observation is

$$sd_{hc} = 4 + [0.8 \times \log(hc_{obs}/40)] \quad \text{for } hc_{obs} > 1.0 \quad (4)$$

$$sd_{hc} = 1, \quad \text{for } hc_{obs} \leq 1.0$$

where

- sd_{hc} is the standard deviation used to weight observed head change;
- log denotes the natural log of the value in parentheses;
- and
- hc_{obs} is the head-change observation.

Standard deviations for head-change observations less than 1 were arbitrarily assigned a value of 1 to avoid very small errors that could cause numerical instability problems during calibration.

Ground-Water Discharge Observations and Errors

Discharge observations were developed primarily from discharge estimates that were derived from ET estimates and spring-flow measurements (Chapter C, this volume). Uncertainty in the discharge from each area was expressed as a CV. A higher CV implies less certainty in the estimate of ground-water discharge. Monte Carlo analyses were used to calculate CVs for the DVRFS (Lacznik and others, 2001, appendix). R.K. Waddell (GeoTrans, Inc., written commun., 2003) did a similar analysis for Pahrump Valley and updated the calculation by Lacznik and others. Both sets of CV calculations for discharge were compiled for the DVRFS model developed by D'Agnese and others (2002), and the compilation also was used in this study (table F-4). Where values were not available or new values were available, appropriate CVs were estimated or updated (table F-4).

Boundary Flow Observations and Errors

The boundary flow observations were obtained from the analysis in Appendix 2 (this volume) that estimates potential flow through 12 segments of the boundary of the DVRFS model domain. These values have a great deal of uncertainty associated with them but were used as observations during calibration. Standard deviations, and thus observation weights, were determined on the basis of the method used to determine the flow at the boundary (Appendix 2). For flow estimates based on water-budget analyses (Appendix 2), the standard deviation was set to one-half of the estimated value. Otherwise, the standard deviation was set to the estimated flow value rounded down to the nearest 500 m³/d.

Model Calibration

Model calibration is the process of changing model input values in an attempt to match simulated and actual conditions. Models typically are calibrated either by trial and error or by using formal parameter-estimation methods. Calibration of parameter values of the DVRFS model primarily relied on the parameter-estimation techniques available in MODFLOW-2000 and was achieved using a two-step process. First, the model was calibrated to prepumped (steady-state) flow conditions. Once calibrated, this model formed the initial conditions for the transient-flow model. The model was calibrated again to simulate transient-flow conditions for 1913–98.

Approach

Sensitivity analysis was used to evaluate the information provided by the observations for the estimation of all defined parameters, and nonlinear regression was used to estimate

parameter values that produced the best fit to observed hydraulic heads and discharges (Hill, 1998). For the DVRFS model, 100 parameters are used and more than 90 were estimated at some point during the modeling process. The maximum number of parameters estimated by nonlinear regression peaked at around 30.

Uncertain aspects of the hydrogeology were evaluated by constructing models with different hydraulic-property distributions and different methods to simulate ET, spring flow, recharge, and the boundary conditions. These models were evaluated through the sensitivity analysis and nonlinear regression methods. These evaluation tools are discussed briefly in the following sections, as well as how estimated parameter values considered unreasonable were used to detect model error. The linear confidence intervals used to evaluate the estimated parameter values also are discussed.

Sensitivity Analysis

Sensitivity analysis is used to assess the effects of different conceptual models (different model designs and parameter values) on the simulated heads and discharges, and to develop useful nonlinear regressions (Hill, 1998; Hill and Tiedeman, 2003). Changes in the conceptual model were assessed by evaluating the effect of the changes on model fit. These methods define parameter sensitivity as the partial derivative of the change in a simulated observation caused by a change in the parameter value. These sensitivities, when scaled properly, can be used to compare the importance of different observations to the estimation of a single parameter or the importance of different parameters to the simulation of an observed value (Hill, 1998, p. 15).

The sensitivity analysis focused on identifying parameter values that could be estimated by regression and identifying key observations that supported each parameter. As part of this analysis, three types of statistics were evaluated: (1) dimensionless scaled sensitivity, (2) composite scaled sensitivity, and (3) parameter correlation coefficient.

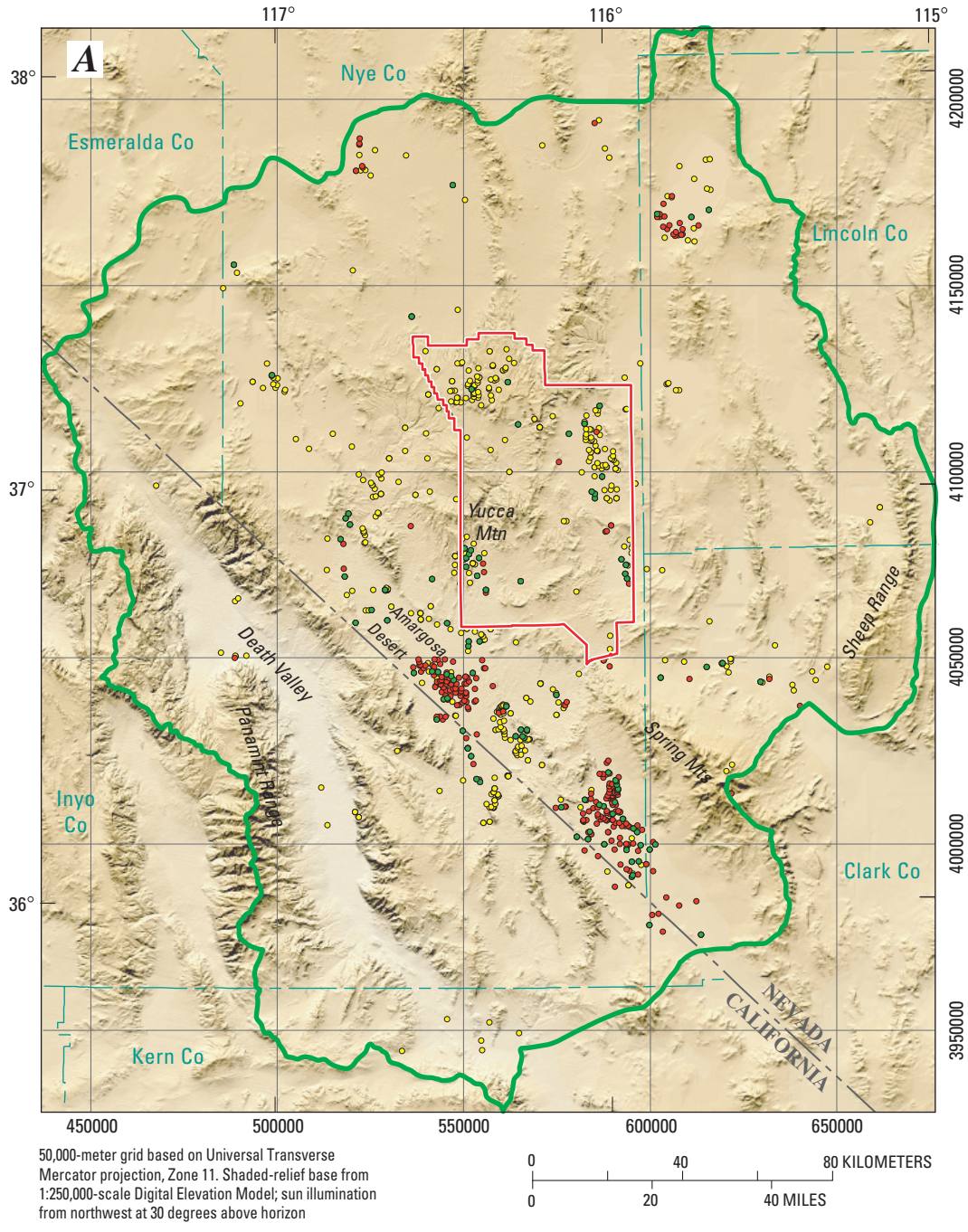
Dimensionless Scaled Sensitivity

Dimensionless scaled sensitivity (*DSS*) is used to evaluate the importance of an observation to the estimation of a single parameter. The *DSS* of each observation is calculated for each parameter as

$$DSS = w^{1/2}(\partial y' / \partial b)b \quad (5)$$

where

- w is the weight for observation y and is the inverse of the standard deviation of the observation;
- y' is the simulated value of the observation y ;
- and
- b is the parameter value.



EXPLANATION

- Death Valley regional ground-water flow system model boundary
- Nevada Test Site boundary
- Head and head-change observations**
- Steady state (prepumped) stress period
- Transient and steady-state stress periods
- Transient (pumped) stress period

Figure F-10. (A) Map showing spatial distribution of hydraulic-head observations used in calibration of the Death Valley regional ground-water flow model; (B) graph showing the number of hydraulic-head observations representing both steady-state and transient conditions over time.

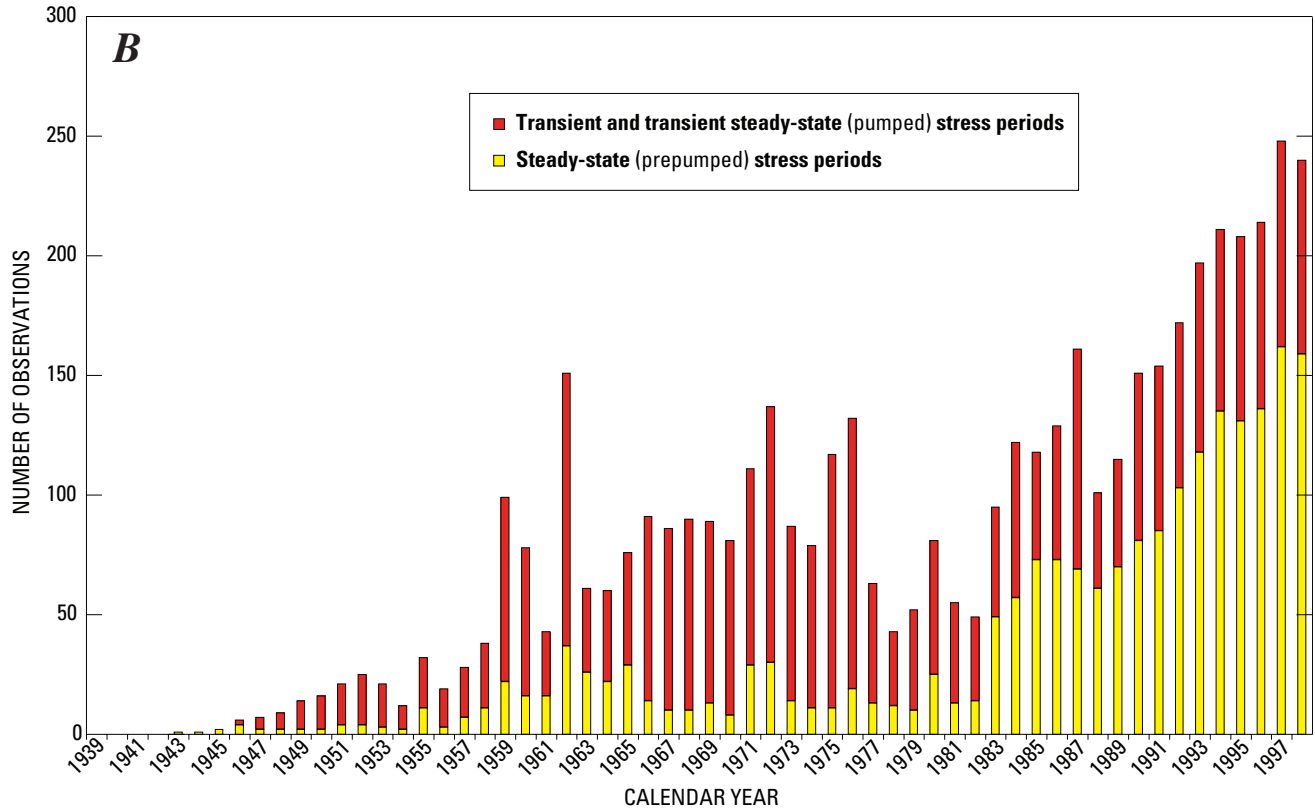


Figure F-10. (A) Map showing spatial distribution of hydraulic-head observations used in calibration of the Death Valley regional ground-water flow model; (B) graph showing the number of hydraulic-head observations representing both steady-state and transient conditions over time.—Continued

A parameter having a large *DSS* value for one observation and small values for all other observations is governed by that one observation. In this situation, any error in the one important observation will translate directly to the parameter and, therefore, the model. Parameters governed by only one observation are not estimated.

Composite Scaled Sensitivity

Composite scaled sensitivity (*CSS*) is used to evaluate the overall sensitivity of a parameter and is calculated as

$$CSS = \{[\sum_{i=1,n} (DSS)^2]/n\}^{1/2} \tag{6}$$

where *n* is the number of observations.

CSS typically is a good measure of the information observations contribute to the estimation of parameters. One exception is for parameters with values that change as the model is calibrated; for example, hydraulic heads at constant-head boundaries that were modified during calibration. *CSS* values are not presented for those types of parameters.

The relative size of *CSS* values can be used to assess whether additional parameters can be estimated. A relatively large *CSS* value indicates that observations contain enough information to represent that aspect of the system in more

detail, using additional parameters. A relatively small *CSS* value (about two orders of magnitude less than the largest *CSS* value) indicates that the observations provide insufficient information with which to estimate the parameter. Parameters with small *CSS* values generally were assigned a fixed value, and(or) lumped with a parameter with a similar value.

Parameter Correlation Coefficient

Parameter correlation coefficients (*PCC*) are used to evaluate whether parameter values can be estimated uniquely and are calculated for each parameter pair (*b*₁, *b*₂). *PCC* can be expressed as

$$PCC = Cov(b_1, b_2)/[\text{var}(b_1)^{1/2}\text{var}(b_2)^{1/2}] \tag{7}$$

where *Cov*(*b*₁, *b*₂) is the covariance for the parameter pair *b*₁ and *b*₂ and *var*(*b*₁) and *var*(*b*₂) are the variances for parameters *b*₁ and *b*₂.

A correlation coefficient having an absolute value close to 1.00 indicates that the two parameters involved likely cannot be estimated uniquely. Generally, absolute values greater than 0.95 are cause for concern, but values as small as 0.85 are reported in MODFLOW-2000 output because less correlated parameters can affect the uncertainty of parameter estimates. If parameter correlation was high, the value of the

correlated parameter with the smallest *CSS* was adjusted, unless the high correlation was between a depth-decay parameter and the associated hydraulic conductivity. In this case, the hydraulic-conductivity parameter was estimated.

Nonlinear Regression

Nonlinear regression is used to find parameter values that produce simulations that best fit the observations. The fit between model simulation and observations is quantified using an objective function, $S(\underline{b})$, that minimizes the sum of squared weighted residuals. The objective function is calculated as:

$$S(\underline{b}) = (\underline{y} - \underline{y}')^T \underline{W} (\underline{y} - \underline{y}') \quad (8a)$$

where

\underline{b} is an $np \times 1$ vector containing parameter values;

np is the number of parameters estimated by regression;

\underline{y} and \underline{y}' are $n \times 1$ vectors with elements equal to observed and simulated (using \underline{b}) values, respectively;

$\underline{y} - \underline{y}'$ is a vector of residuals, defined as the observed minus simulated values;

n is the number of measured and simulated hydraulic heads and flows;

\underline{W} is an $n \times n$ weight matrix;

and

T superscripted indicates the transpose of the vector.

The weight matrix diagonal elements are calculated as

$$w_{ii} = 1/(s_1^2 + s_2^2 + \dots + s_n^2) \quad (8b)$$

where

w_{ii} is a diagonal element of the weight matrix \underline{W} ,

s_1^2 is the estimated variance of error type 1,

s_2^2 is the estimated variance of error type 2,

and

s_n^2 is the estimated variance of error type n .

Although every potential error was not considered, it is expected that those that were considered were sufficient to obtain reasonable weighting of the observations. Parameter estimates obtained by nonlinear regression generally are not greatly affected by changes in weights within ranges supportable by an analysis of likely errors (Hill and Tiedeman, 2003). When errors are expected to produce a biased observation, the errors are accounted for through averaging or adjusting the observations. When errors are expected to be characterized as random, they are accounted for through observation weights.

MODFLOW-2000 calculates observation weights from user-defined variances, standard deviations, or CVs (Hill and others, 2000, p. 18–19). CVs equal the standard deviation divided by the observed value. For the DVRFS model, standard deviations are measures of hydraulic-head observation errors and CVs are specified as measures of ground-water discharge and head-change observation errors. Defining weights that reflect expected random observation error is necessary to accurately evaluate uncertainty (Hill and Tiedeman, 2003).

Model fit is evaluated using both unweighted and weighted residuals (the difference between observed and simulated values). Unweighted residuals have the same dimensions as the observations and can be misleading because observations are measured with different accuracy, and two unweighted residuals that are of equal value may not indicate an equally satisfactory model fit.

Weighted residuals reflect model fit relative to the expected observation error but are more difficult to interpret because they are dimensionless quantities that express model fit in terms of normalized values with respect to standard deviations of the observation errors. A weighted residual of 2.0, for example, indicates that the unweighted residual is twice the standard deviation of the observation error. For a hydraulic-head observation with a standard deviation of 10 m, a weighted residual of 2.0 corresponds to an unweighted residual of 20 m. Weighted residuals with larger absolute values indicate a less desirable model fit than do weighted residuals with smaller values.

Overall model fit can be measured using the standard error of the regression. The standard error of the regression is a dimensionless number, and smaller values generally are better. Generally, the better a model fits the observations, the more accurately the model represents the system. The standard error of regression is calculated as

$$\text{Standard error} = S(\underline{b})/(n - np) \quad (9)$$

Uncertainty Evaluation

Linear confidence intervals for the estimated parameter values are calculated using sensitivities calculated for the optimal parameter values. Linear confidence intervals are relevant only if weighted residuals are normally distributed and the model is effectively linear. A linear, 95-percent confidence interval on a parameter estimate that excludes reasonable values indicates model error or misinterpreted data on the parameter. Parameters with larger *CSS* values tend to have smaller confidence intervals.

Confidence intervals were used to assess whether all estimated parameters were warranted. For example, if the confidence intervals overlapped for two parameters representing the hydraulic conductivity of rock types of similar hydraulic properties, the rocks could be represented by a single hydraulic-conductivity parameter without adversely affecting model fit. Also, if the regression using fewer hydraulic-conductivity parameters yields a similar model fit to the

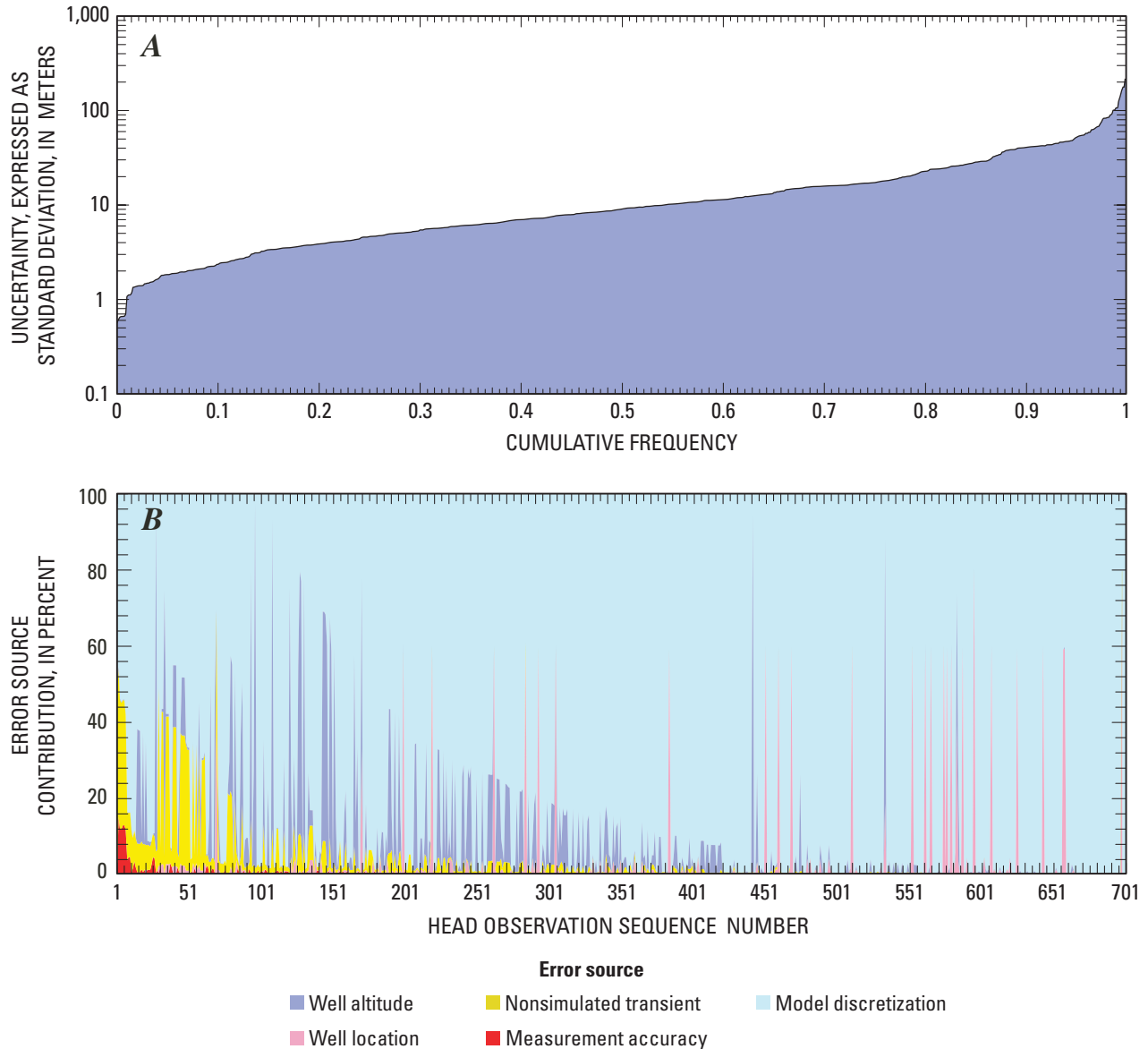


Figure F-11. Graphs showing calculated uncertainty of head observations used to calibrate Death Valley regional groundwater flow system model: (A) Cumulative frequency; (B) percent contribution.

observations, the available observations are insufficient to distinguish between the models. Thus, the model with more hydraulic-conductivity parameters represents a level of complexity that is not supported by the available data.

Unreasonable Parameter Estimates as Indicators of Model Error

An advantage to using regression to estimate parameter values is that the regression does not limit the estimates to reasonable values. Unreasonable estimated parameter values can indicate model error (Anderman and others, 1996; Poeter and Hill, 1997; Hill and others, 1998; and Hill, 1998, p. 13, 44). If a model represents a physical system adequately, and the observations used in the regression provide substantial

information about the parameters being estimated, it is reasonable to assume that parameter values would be realistic. Model error would be indicated by unreasonable estimates of parameters for which the data provide substantial information. These unreasonable parameter estimates would indicate that further calibration is necessary.

Conceptual Model Variations

During calibration, a number of conceptual models were evaluated using the regression methods of MODFLOW-2000. A best fit to hydraulic-head, ground-water discharge, and boundary-flow observations was calculated for each conceptual model. Evidence of model error or data problems was investigated after each model run. These analyses were

used in conjunction with hydrogeologic data to modify and improve the existing conceptual model, observation data sets, and weighting.

Horizontal Hydraulic Conductivity

Horizontal hydraulic-conductivity parameters were assigned using the zonation capability of the HUF package (Anderman and Hill, 2000). Zones are used to define areas with similar properties within individual HGUs. The only variations of horizontal hydraulic conductivity simulated within zones were those related to depth decay.

Hydrogeologic evidence was used to initially define areas of similar horizontal hydraulic conductivity within the HGUs (Chapter B, this volume). Most zones were defined to represent geologic materials that likely have fairly uniform hydraulic properties. In some situations, however, single zones represent materials with differing hydraulic properties, and the properties of the dominant material were specified. Parameters defining the horizontal hydraulic conductivity were associated with each zone. During calibration, however, it became apparent that in some areas sufficient detail was not available from the geologic-property zonations or that the zonations did not match the hydraulic conditions in an HGU or part of an HGU. In these cases, additional zones were added.

Zonation was used to subdivide the units following hierarchical approach, where the model showed sensitivity to a particular parameter. The first division was based on the four major rock types (K1–K4) (tables F–3 and F–7) and each was assigned a homogeneous and isotropic hydraulic-conductivity (K) parameter. The second division was based on major groupings of the hydrogeologic units listed (table F–7). The third division was based on the individual HGUs and identification of rocks that likely have similar hydraulic properties. The fourth and fifth divisions were based on identification of rocks that likely have similar hydraulic properties using hydrogeologic considerations and model fit to observations. The final set of 56 horizontal hydraulic-conductivity parameters was used to calibrate the model. During calibration, in order to reduce the number of parameters, relatively insensitive hydraulic-conductivity parameters were combined with parameters of similar hydraulic conductivity. As a result, in some cases the hierarchy is not maintained, and rocks from different HGUs and different orders of parameters were grouped and the naming convention modified. Calibrated horizontal hydraulic-conductivity parameters are listed in tables by the four major rock types in following sections; accompanying maps show the extent of each HGU and its associated parameters and the value of the hydraulic-conductivity parameter projected to the land surface.

Confining Units

The geometry and location of the low-permeability units likely is more important than the specific value of horizontal hydraulic conductivity. Because the flow through these units

is generally small, small changes in flow rate do not appreciably affect the discharge rates or water levels. In some cases, however, the hydraulic conductivity of these rocks is important to the magnitude and direction of ground-water flow and water levels. This is particularly true on the constant-head boundaries.

Zone arrays and parameters were used to refine the distribution of hydraulic-conductivity parameters for the confining units (clastic and crystalline rocks) (table F–8). The hydraulic-conductivity parameters for the crystalline-rock and clastic-rock confining units are defined by spatial zones and have varying degrees of effect on the flow model. CSS values for the ICU and XCU hydraulic-conductivity parameters were generally low. Where the hydraulic-conductivity parameters for the crystalline-rock and clastic-rock confining units were estimated to have similar properties, the zones were combined into one parameter.

The ICU was split into those areas inside and outside the major caldera centers (table F–8 and fig. F–12). This was done because the source for the intrusive rocks in the calderas likely is similar to, or the same as, the source of the volcanic rocks associated with the caldera.

It was necessary to simulate several zones in the XCU to accurately represent hydraulic gradients through the constant-head boundaries, heads, and discharges. The zonation for the XCU was initially based on the zonation described for the clastic units (Chapter B, this volume). Because these crystalline rocks are highly susceptible to deformation, zones based on structure (Chapter B, this volume) also were added. In the final calibration, and on the basis of the hydrologic information supplied to the simulation, only three zones were resolvable in the XCU (table F–8 and fig. F–13).

The LCCU (and LCCU_T1) was subdivided into several hydraulic-conductivity parameter zones on the basis of lithology and structure (Chapter B, this volume) (table F–8 and fig. F–14). The main facies transition within the LCCU is from an eastern region dominated by thick intervals of coarse clastics interbedded with shale (zones K1LCCU_XCU, K11C_XILCU, and K122fgLCCU; fig. F–14) to a more shale-dominated region with significant amounts of carbonate rocks (zone K122esLCCU; fig. F–14). The far northwestern part of the model domain contains a significant thickness of carbonate rocks (Sweetkind and White, 2001) with high permeability due to fractures. This area and the area along the Panamint Range in the western part of the model domain were combined into their own zone (zone K122esLCCU; fig. F–14). Because these zones alone were not enough to simulate some of the steep hydraulic gradients in the region, additional zones based on regional differences in deformational style (Chapter B, this volume) were added. Although the LCCU parameters generally have low hydraulic conductivity, higher hydraulic-conductivity values in zone K1223LCCU were required to simulate flow from Pahrump Valley to the Shoshone-Tecopa basin and then into the southern part of Death Valley (zone K1223LCCU, fig. F–14) because of a significant thickness of carbonate rocks in the LCCU in this area (Chapter B, this volume). The LCCU_T1 was simulated as a separate zone.

Table F-7. Hierarchy of horizontal hydraulic-conductivity parameters and major characteristics guiding parameter definition.

First-order parameters (major rock types)	Second-order parameters (major groupings of hydrogeologic units)	Third-order parameters (hydrogeologic units and(or) zones with similar characteristics)	Fourth- and fifth-order parameters (hydrogeologic units and(or) zones with similar characteristics)	Parameters used in final calibration		
K1 Confining units – crystalline and clastic rocks	K11 Crystalline rocks	K111 Intrusive-rock confining unit (ICU)	Zoned inside or outside calderas	K11C_XILCU K11_ICU		
		K112 Crystalline-rock confining unit (XCU)	Zoned inside or outside calderas	K11DV_XCU K1LCCU_XCU K11C_XILCU		
	K12 Clastic rocks	K121 Sedimentary-rock confining unit (SCU)				
		K122 Clastic-rock confining units	K1221 Upper clastic-rock confining unit (UCCU)		K1221UCCU	
			K1222 Lower clastic-rock confining units (LCCU, LCCU_T1) zoned based on facies and deformation			K12223LCCU K122fgLCCU K122esLCCU
						K11C_XILCU K232_LCA
	K2 Carbonate rocks	K21 Western facies of lower carbonate-rock aquifer (LCA)	K211 Low deformation			
			K212 Deformed (oroflexes)		K232_LCA	
		K22 Eastern facies of lower carbonate-rock aquifer (LCA) – low permeability	K221 Regional anticline			K221_LCA K242G_LCA
				K222 Disrupted by extension or calderas		K221_LCA
K23 Poorly known areas of the lower carbonate-rock aquifer (LCA)			K231 Near extension			K232_LCA
		K232 Near moderate extension K233 Near oroflex			K232_LCA K232_LCA	
K24 Eastern facies of lower carbonate-rock aquifer (LCA), thrust lower carbonate-rock aquifer (LCA_T1), and upper carbonate-rock aquifer (UCA) – permeable		K241 Low deformation	K2411 Stable blocks		K241SM_LCA K2SHPLCA	
				K2412 Semi-stable blocks	K2412_LCA K2412fLCA K2_DV_LCA K242G_LCA K241LCA_T1	
				K2413 Thrusted lower carbonate-rock aquifer (LCA_T1)		
			K242 Moderate deformation	K2421 Rotated range blocks	K241SMWLCA K2421_LCA K242G_LCA K242YN_LCA K2YMLCA K242A_LCA K2422b_LCA K244_LCA	
	K2422 Basin-Range blocks					
K2423 Regional fold		K243_UCA				

Table F-7. Hierarchy of horizontal hydraulic-conductivity parameters and major characteristics guiding parameter definition.

—Continued

First-order parameters (major rock types)	Second-order parameters (major groupings of hydrogeologic units)	Third-order parameters (hydrogeologic units and(or) zones with similar characteristics)	Fourth- and fifth-order parameters (hydrogeologic units and(or) zones with similar characteristics)	Parameters used in final calibration
			K2424 Oroflexed stable block	K2SHPLCA
		K243 High deformation	K2431 Shear zone	K2SHPLCA K243_LCA
			K2432 Detachment	K243PP_LCA K243GV_LCA
			K2433 Multiply-deformed areas	K2421_LCA K243_LCA
			K2434 Upper carbonate-rock aquifer (UCA)	K243_UC
K3 Volcanic rocks	K31 Younger volcanic rocks, tuffs and lava flows (LFU, YVU)	K311 Younger volcanic-rock unit (YVU)		K32BR4CH13
		K312 Lava-flow unit (LFU)	Zoned based on facies change	K42UP_VSU K3LFU_am
	K32 Southwestern Nevada volcanic field rocks	K321 Thirsty Canyon–Timber Mountain volcanic-rock aquifer (TMVA)	Zoned based on brittleness and alteration	K3C_TM K3211TMVA
		K32 Paintbrush volcanic-rock aquifer (PVA)	Zoned based on inside or outside caldera	K3C_PVA K3PVA
		K323 Calico Hills volcanic-rock confining unit (CHVU)	Zoned based on brittleness and alteration	K32CH24LF K32BR4CH13
		K324 Wahmonie volcanic-rock unit (WVU)		K32BR4CH13
		K325 Crater Flat Group volcanic rocks	K3251 Crater Flat–Prow Pass aquifer (CFPPA)	K321521_PP
			K3252 Crater Flat–Bullfrog confining unit (zoned based on brittleness and alteration) (CFBCU)	K3215BCU1 K3215BCU34
			K3253 Crater Flat–Tram aquifer (CFTA)	K3215TR
		K326 Belted Range unit (BRU)	Zoned based on brittleness and alteration	K3BRU123
	K33 Older volcanic unit (OVU)	Zoned based on inside/outside SWNVF		K33_OVU K33_OVUsw
K4 Basin fill	K41 Alluvial aquifers (YAA, OAA, LA)			K4_VF_AQ K4_VF_OAA
	K42 Alluvial confining units (YACU, OACU, upper VSU, lower VSU)	K421 Younger and older alluvial confining units (YACU, OACU)		K4_VF_CU
		K422 Volcanic- and sedimentary-rock unit (upper and lower VSU)	Zones based on facies changes	K4UP_VSUC K4UP_VSUP K42UP_VSU K42222_VSU K422LNEVSU K422LNWVSU K4222S_VSU K422DV_VSU K422GW_VSU K4222P_VSU K422GV_VSU

Table F-8. Calibrated horizontal hydraulic-conductivity parameters for confining units.

[Abbreviations: ICU, intrusive-rock confining unit; XCU, crystalline-rock confining unit; LCCU, lower clastic-rock confining unit; LCCU_T1, thrustled lower clastic-rock confining unit; UCCU, upper clastic-rock confining unit; NA, not available]

Parameter name	Description	Minimum – maximum hydraulic conductivity (meters per day) from Belcher and others (2001)	Composite scaled sensitivity	Hydraulic conductivity at land surface (meters per day)	Coefficient of variation ¹	Average depth (meters)	Hydraulic conductivity at average depth (meters per day)
K11_ICU	Extra-caldera ICU.	6×10^{-4} – 1.4	0.616	2.463×10^{-3}	0.0014	3,372	0.002461
K11DV_XCU	XCU rocks in the Death Valley area. Complex geologic structures and lack of subsurface data result in highly interpretive geometry, extent, and property distribution for rocks in this zone.	NA	0.831	1.086×10^{-1}	0.0017	2,625	0.002564
K11C_XILCU	Intracaldera ICU.	3×10^{-8} – 5	0.389	1.940×10^{-3}	0.0047	24,092	0.001938
K1LCCU_XCU	Intracaldera parts of XCU rocks. In general, these rocks form a barrier to flow. Deformed LCCU including Stirling Quartzite around calderas. (1) LCCU in southern part of DVRFS model domain, including the Saratoga Springs area. (2) XCU that generally form a barrier to flow. Where exposed, the rocks are often core complexes of detachment faults.	3×10^{-8} – 5 3×10^{-8} – 5	0.384	4.082×10^{-3}	0.0047	4,643	0.000005
K1222LCCU	(1) Thick section of LCCU (Stirling Quartzite) interpreted as extending beneath Pahrump Valley and to the west toward Shoshone and Tecopa basins. The rocks in this area are affected by extensional faulting that may increase the permeability of the more competent parts of this unit. (2) Deformed part of LCCU (Stirling Quartzite); north central swath of model domain northern part of Death Valley. (3) LCCU_T1.	3×10^{-8} – 5	0.648	1.568×10^{-3}	0.0007	2,528	0.001567
K1222fgLCCU	(1) Spring Mountains and Sheep Range with deformed LCCU and LCCU_T1 (Stirling Quartzite). (2) Yucca Mountain and the Amargosa Desert characterized by undeformed LCCU (Stirling Quartzite). (3) Northeastern part of DVRFS model domain (no Stirling Quartzite).	3×10^{-8} – 5	0.100	6.000×10^{-5}	0.0002	3,561	0.000060
K1222sLCCU	(1) Deformed LCCU in the Panamint Range-Death Valley area. (2) Deformed part of LCCU (Stirling Quartzite) in extreme northwestern part of DVRFS model domain (finer grained). Thick localized section of clastic rocks (UCCU) in Eleana Range separating the regional carbonate-rock aquifer into upper and lower parts.	3×10^{-8} – 5	0.284	1.846×10^{-1}	0.12	3,561	0.1844
K1221UCCU		0.0002 – 0.4	0.346	3.878×10^{-2}	0.0358	1,019	0.001147

¹Values were log transformed.²Average depth from most spatially expansive unit, XCU.

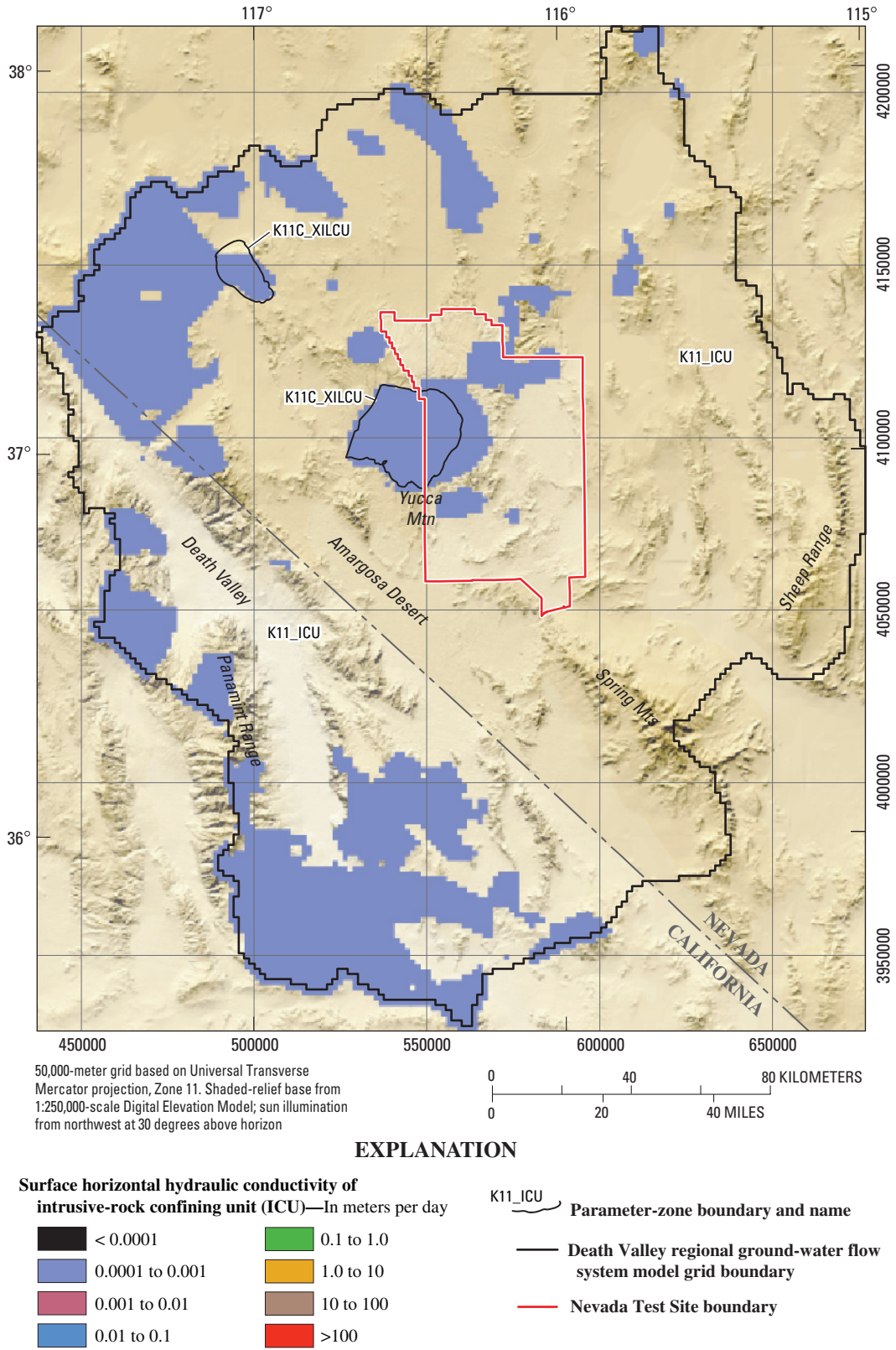
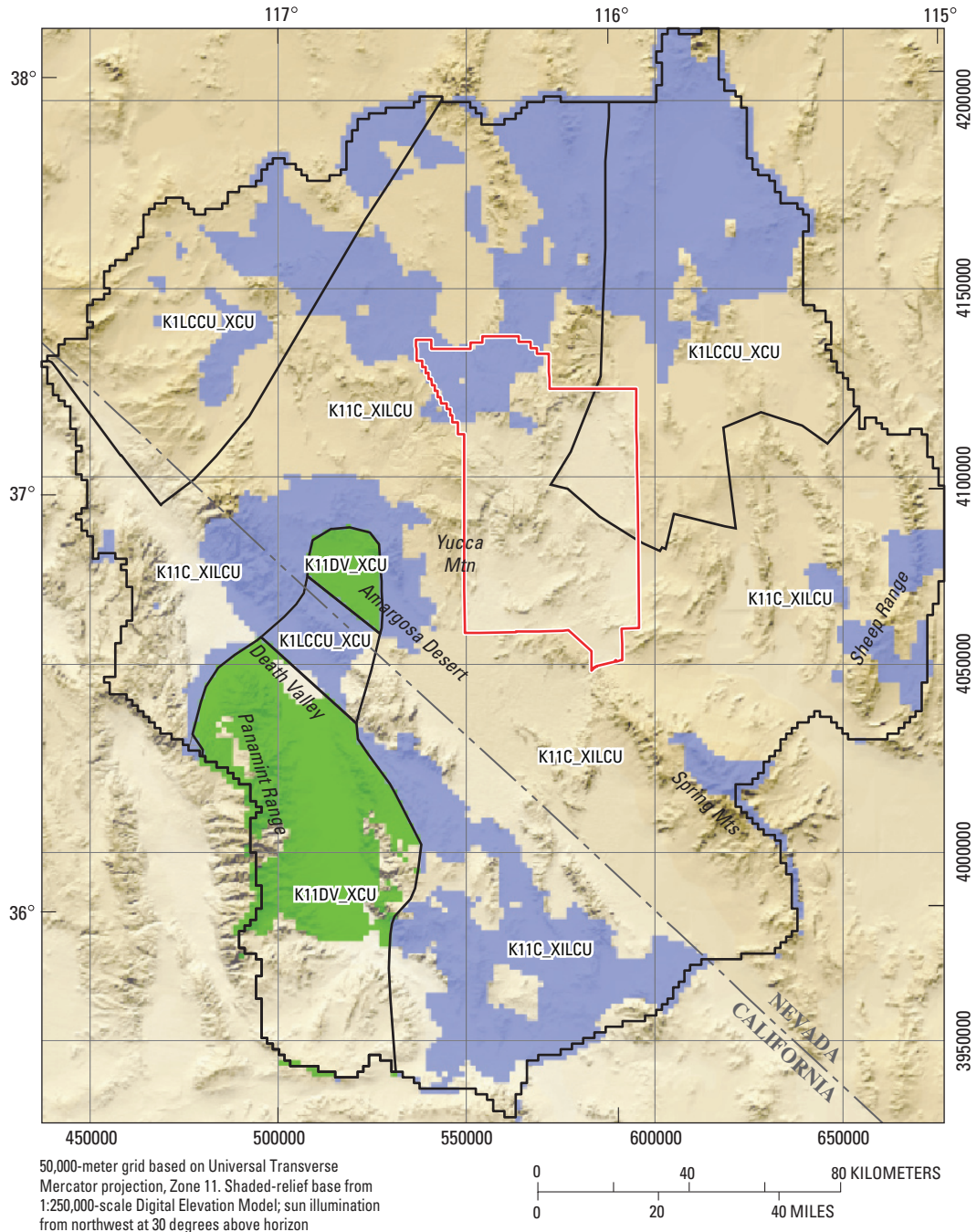


Figure F-12. Hydraulic-conductivity zone parameters, unit thickness, and extent for intrusive-rock confining unit.



EXPLANATION

Surface horizontal hydraulic conductivity of crystalline-rock confining unit (XCU)—

In meters per day

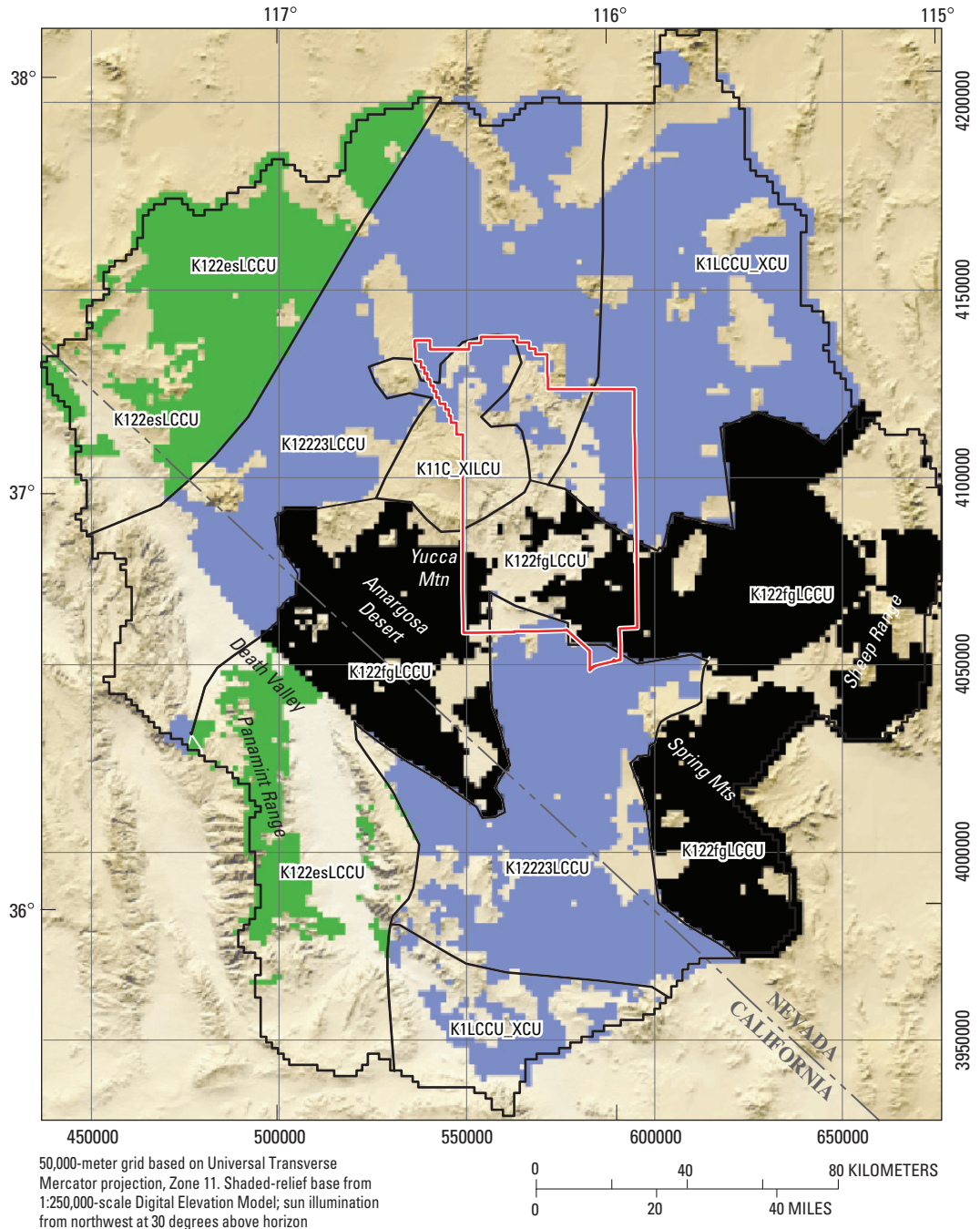
	< 0.0001		0.1 to 1.0
	0.0001 to 0.001		1.0 to 10
	0.001 to 0.01		10 to 100
	0.01 to 0.1		>100

K11C_XILCU Parameter-zone boundary and name

Death Valley regional ground-water flow system model grid boundary

Nevada Test Site boundary

Figure F-13. Hydraulic-conductivity zone parameters, unit thickness, and extent for crystalline-rock confining unit.



EXPLANATION

Surface horizontal hydraulic conductivity of lower clastic-rock confining unit (LCCU)—In meters per day		K122esLCCU	Parameter-zone boundary and name
< 0.0001	0.1 to 1.0	—	Death Valley regional ground-water flow system model grid boundary
0.0001 to 0.001	1.0 to 10	—	Nevada Test Site boundary
0.001 to 0.01	10 to 100		
0.01 to 0.1	>100		

Figure F-14. Hydraulic-conductivity zone parameters, unit thickness, and extent for lower clastic-rock confining unit.

During calibration, the properties of the LCCU_T1 were found to be similar to the K122fgLCCU parameter, and the unit was combined with this parameter. Parts of the LCCU_T1 that may also have relatively higher hydraulic-conductivity values were combined into the K12223LCCU zone (fig. F-15).

An important feature in the flow model is the steep hydraulic gradient west of Yucca Flat that wraps around to Yucca Mountain and that is formed by the low permeability of the UCCU (fig. F-15). Because of this, the UCCU was separated as an individual parameter (K1221UCCU). Because of its geologic origin, the SCU commonly is of higher permeability and was also separated as a different parameter (K4UP_VSUP) (fig. F-16).

For some of the confining units, the hydraulic conductivity at the land surface is the same as or of higher magnitude than that of the aquifers. Depth-decay parameters, however, cause hydraulic conductivities to decrease rapidly with depth. Thus, where most of the flow occurs, these units have a much lower relative hydraulic-conductivity value. Calibrated hydraulic-conductivity values at the land surface and at an average depth are presented in table F-8. The assignment of relatively high hydraulic conductivities for the confining units at land surface also is reasonable because of the effects of weathering on the rocks (Bedinger and others, 1989).

Carbonate-Rock Aquifers

The HGUs constituting the carbonate rocks were initially grouped into one hydraulic-conductivity parameter (K2), and the resulting CSS value was more than four times greater than the parameters defining the other major rock types. Because of this sensitivity, this hydraulic-conductivity parameter was then subdivided into a series of hierarchical hydraulic-conductivity parameters (table F-9) based on geologic zonations (Chapter B, this volume). Initially, the LCA was split into eastern and western facies and poorly defined areas. The eastern facies was then split into permeable and low-permeability zones on the basis of the degree of rock deformation (Chapter B). The permeable eastern zones also include the LCA_T1 and the UCA. Recharge zone multipliers and flow out of the constant-head boundary at the Sheep Range were sensitive to the LCA_T1 parameter. The LCA was further subdivided into spatial zones defined on the basis of structural-physiographic subsections described in more detail in Chapter B.

Delineating the zones in the LCA described in Chapter B (this volume) helped improve model fit and the simulation of regional potentiometric features, but more zones were required to simulate discharge or heads in some areas (fig. F-17). Additional zones were added to the LCA in areas immediately north and east of the Las Vegas Valley shear zone (LVVSZ), where oroflexural bending occurs and may cause preferential flow directions along this structural fabric. Because of the

sensitivity of the LCA_T1 parameter (K241LCA_T1), the LCA_T1 and UCA were broken out as separate parameters (fig. F-18).

Because of depth decay, either the hydraulic-conductivity values at depth are greater in the confining units than the LCA, or both values are so small that flow through the units is insignificant. In some areas, however, such as north of Yucca Mountain and along the Eleana Range, this reversal in relative permeability may indicate an unrealistic interpretation in the HFM and(or) perched water levels.

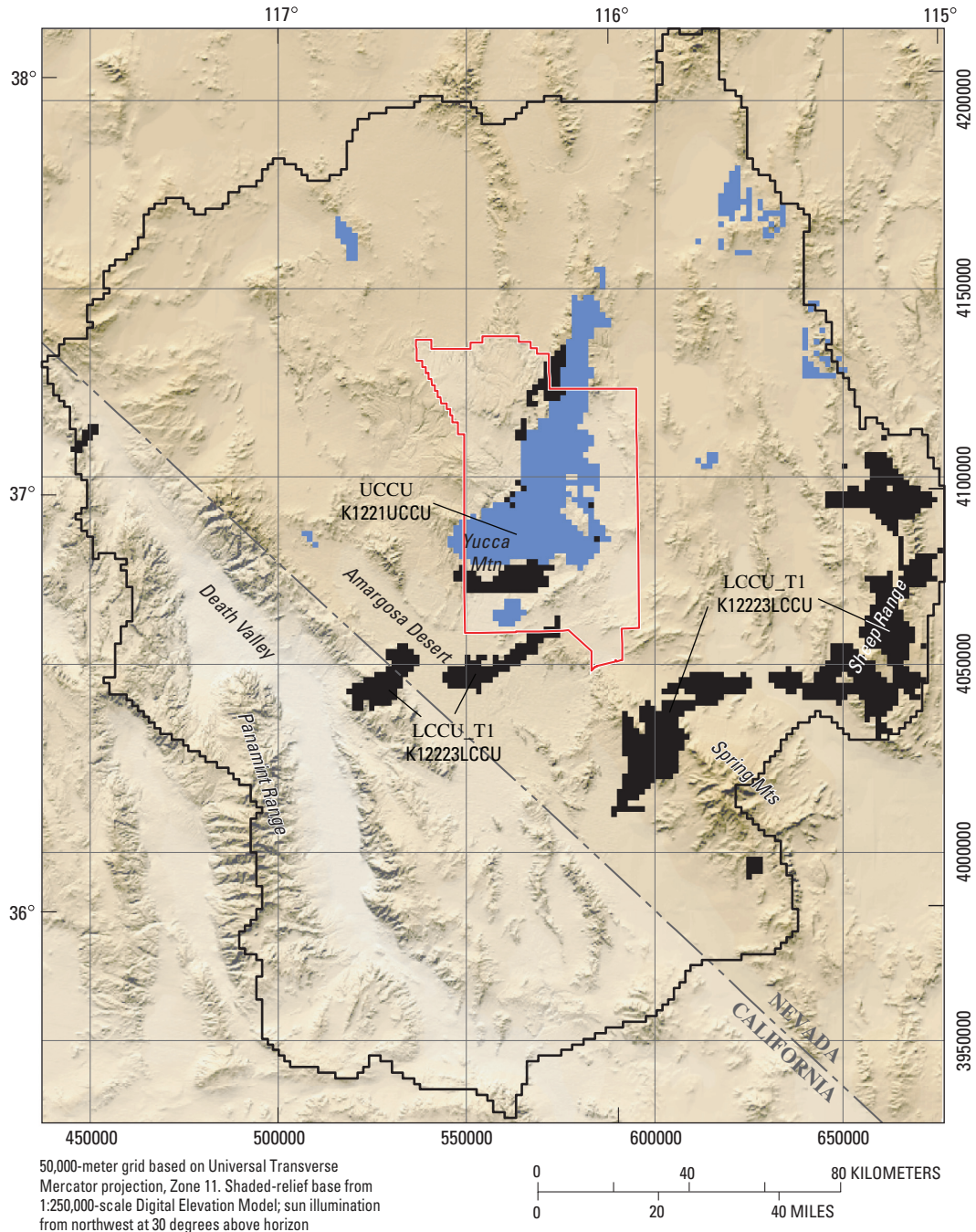
Volcanic-Rock Units

The hydrologic characteristics of the volcanic rocks are more difficult to define than those of the other units because of their great variability in aquifer test results and complex stratigraphy. In a general way, however, some hydrologic properties do correlate with stratigraphy. Because the HFM is based on stratigraphy, the HGU classifications were used first to subdivide the volcanic-rock units (K3) into three second-order parameters (table F-7), which then were subdivided further on the basis of caldera locations, welding, and(or) alteration (table F-10):

1. Older volcanic-rock unit (OVU) (fig. F-19)
2. SWNVF rocks (BRU, CFTA, CFBCU, CFPPA, WVU, CHVU, PVA, TMVA) (figs. F-20—F-27)
3. Younger volcanic rocks, tuffs, and lava flows (YVU, LFU) (figs. F-24 and F-28).


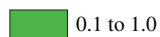
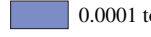


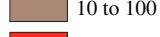
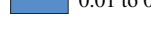
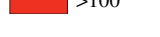
The OVU (fig. F-19) was subdivided into two general groups: (1) volcanic rocks associated with, and perhaps originating from, the SWNVF (K33_OVUsw) and (2) volcanic rocks that originated outside the SWNVF (K33_OVU) (Chapter B, this volume). The OVU within the SWNVF (K33_OVUsw) acts as a confining unit because of its generally nonwelded to partially welded nature, and widespread zeolitic alteration (Chapter B, this volume) (fig. F-19 and table F-10). The OVU outside the SWNVF (K33_OVU) can form local aquifers (Chapter B, this volume). The K33_OVU zone does not appear to have regionally connected fractures and serves as a regional confining unit (fig. F-19, table F-10).

Within the SWNVF units, the PVA and TMVA were assumed to have similar properties and were initially combined. Likewise, the CHVU and the WVU were combined on the basis of their similar geologic characteristics. During calibration, estimates of the hydraulic-conductivity parameters for the volcanic-rock units did not follow the zonation of brittle and altered rock described in Chapter B (this volume) and likely indicates the uncertainty of this zonation. Although the zones based on these properties were used to subdivide the HGUs, the calibrated hydraulic-conductivity value commonly did not agree with the expected value based on the hydraulic properties used for the zonation.



EXPLANATION

Surface horizontal hydraulic conductivity of upper clastic-rock confining unit (UCCU) and lower clastic-rock confining unit-thrust (LCCU_T1)—In meters per day

	< 0.0001		0.1 to 1.0
	0.0001 to 0.001		1.0 to 10
	0.001 to 0.01		10 to 100
	0.01 to 0.1		>100

K1221UCCU Parameter-zone name



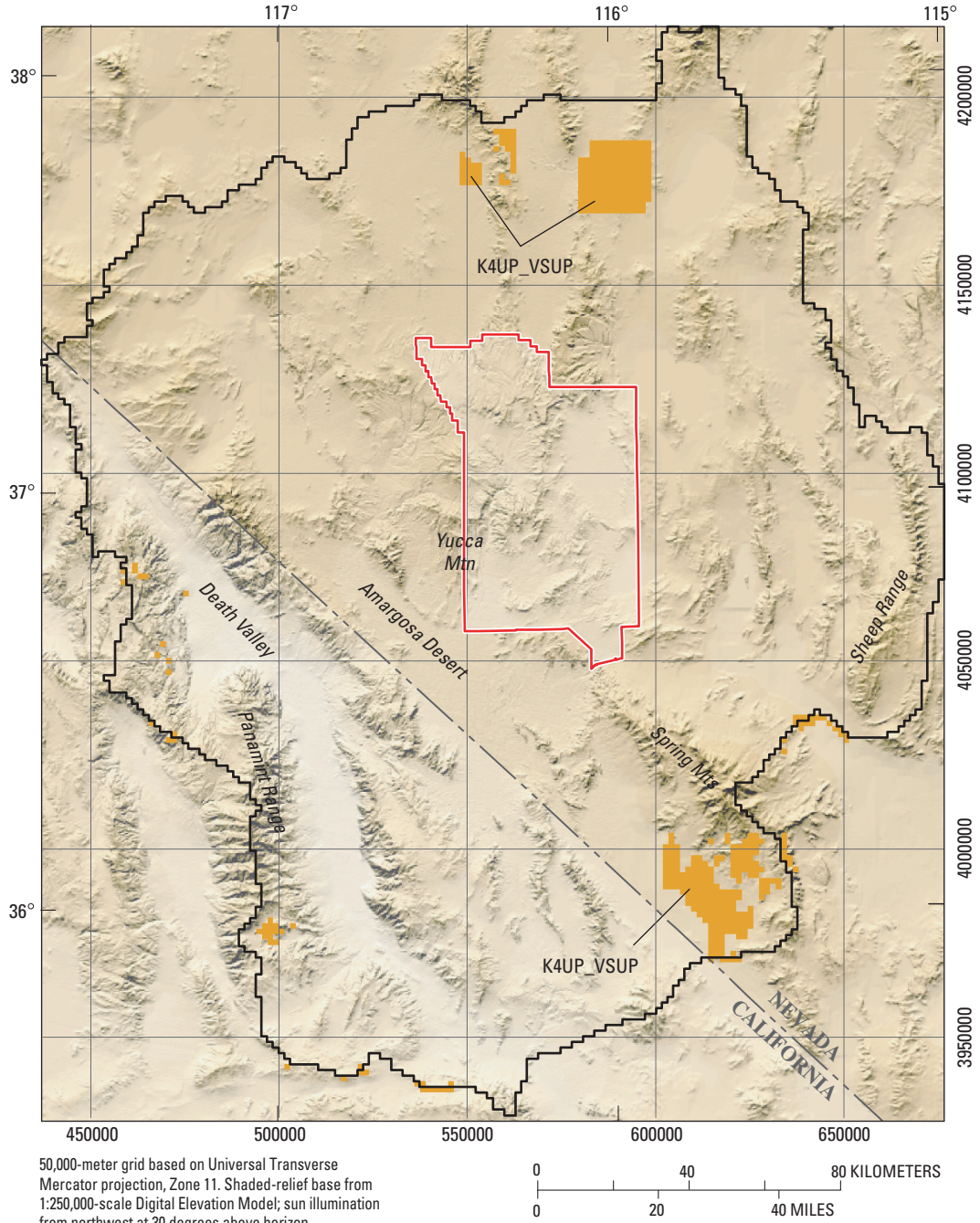
-  Death Valley regional ground-water flow system model grid boundary
-  Nevada Test Site boundary

Figure F-15. Hydraulic-conductivity zone parameters, unit thickness, and extent for upper clastic-rock confining unit and thrust lower clastic-rock confining unit.



EXPLANATION

Surface horizontal hydraulic conductivity of sedimentary-rock confining unit (SCU)—In meters per day		K4UP_VSUP	Parameter-zone name
< 0.0001	0.1 to 1.0		Death Valley regional ground-water flow system model grid boundary
0.0001 to 0.001	1.0 to 10		Nevada Test Site boundary
0.001 to 0.01	10 to 100		
0.01 to 0.1	>100		

Figure F-16. Hydraulic-conductivity zone parameters, unit thickness, and extent for sedimentary-rock confining unit.

Table F-9. Calibrated horizontal hydraulic-conductivity parameters for carbonate-rock aquifers.

[LCA, lower carbonate-rock aquifer; LCA_TI, thrustbed lower carbonate-rock aquifer; NA, not applicable; UCA, upper carbonate-rock aquifer]

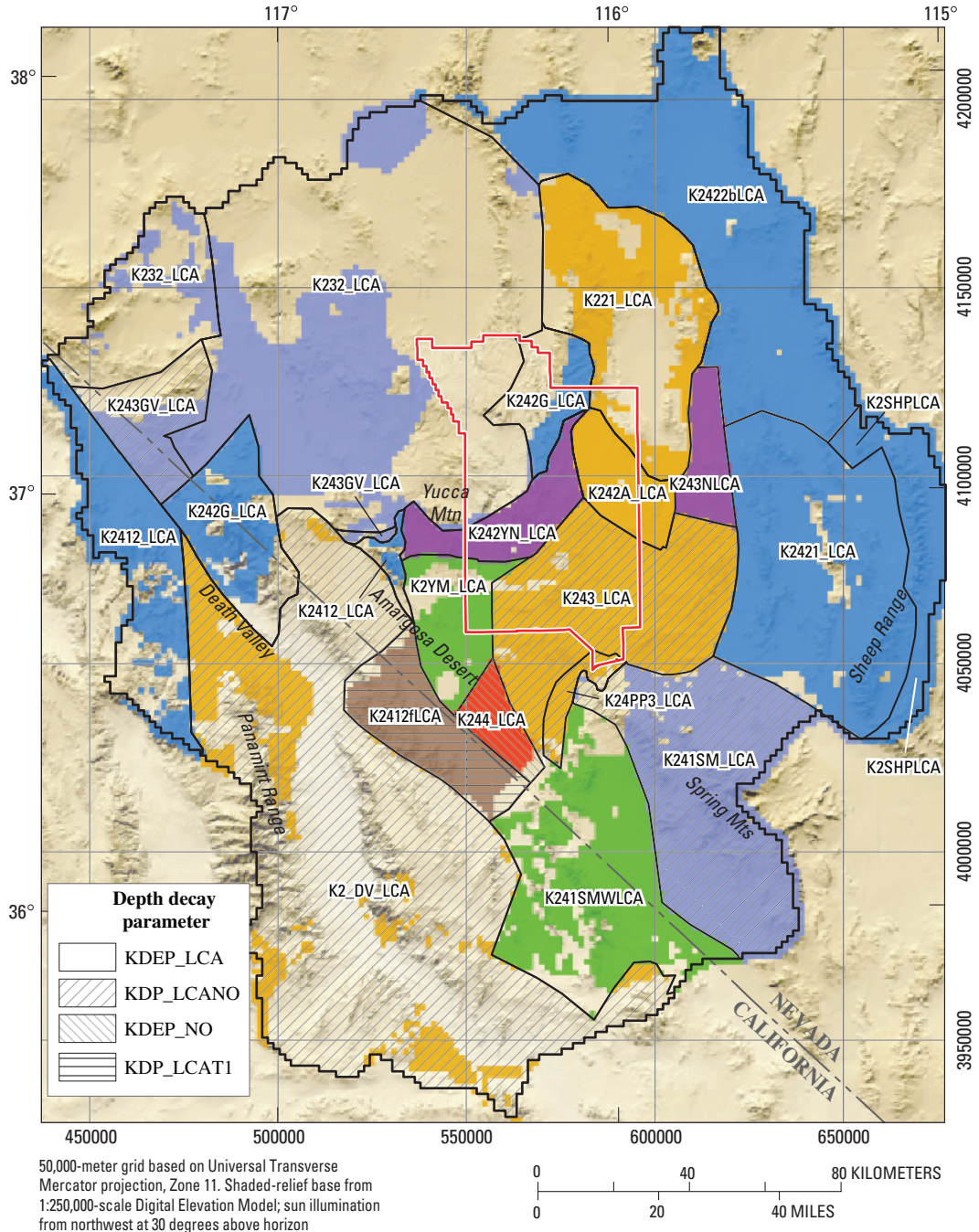
Parameter name	Description	Composite scaled sensitivity	Hydraulic conductivity at land surface ¹ (meters per day)	Coefficient of variation ²	Average depth, in meters	Hydraulic conductivity at average depth (meters per day)
K232_LCA	(1) Poorly defined areas with moderate extension (K23); character of LCA is highly uncertain. (2) Western facies (K21), low deformation; carbonate rocks are interbedded with shales.	0.096	1.000×10^{-3}	0.0041	1,956	6.37×10^{-4}
K221_LCA	Eastern (K22) low-permeability facies along regional anticline; the LCA may not exist in this area and is poorly defined.	0.171	6.089×10^0	0.5	1,396	4.41
K241SM_LCA	Eastern permeable facies with low deformation along stable block of the Spring Mountains.	0.735	1.510×10^{-3}	0.00029	2,670	1.26×10^{-3}
K241LCA_TI	Upper plate of thrustbed LCA.	0.252	9.865×10^{-1}	0.5	1,056	0.0257
K241SMWLCA	Eastern permeable facies with moderate deformation along highly extended rotated range blocks.	0.361	3.7749×10^{-1}	0.31	1,353	0.275
K2_DV_LCA	Eastern low-permeability facies disrupted by extension along Death Valley.	0.049	3.000×10^0	0.5	981	2.81
K2412_LCA	Eastern permeable facies with low deformation along semi-stable blocks.	0.472	8.059×10^{-2}	0.038	2,041	5.04×10^{-1}
K2412FLCA	Eastern permeable facies with low deformation along semi-stable blocks of the Funeral Range.	0.825	1.206×10^1	0.5	2,042	1.04×10^{-2}
K242G_LCA	(1) Eastern permeable facies with low deformation along semi-stable blocks (K241) of the Grapevine Mountains. (2) Eastern permeable facies with moderate deformation (K242) of basin-range blocks. (3) Eastern low permeability facies along regional anticline (K221) on eastern part of Pahute Mesa; LCA may not exist in this area and is poorly defined.	2.883	6.463×10^{-2}	0.014	2,741	0.0344
K242YN_LCA	LCA along northern part of Yucca Mountain.	0.134	1.170×10^{-4}	0.00089	2,741	6.225×10^{-5}
K242A_LCA	Eastern permeable facies with moderate deformation (K242) around Yucca Flat.	0.195	3.393×10^0	0.5	2,180	2.05
K2SHPLCA	(1) Eastern permeable facies with low deformation along stable block of the Sheep Range. (2) Eastern permeable facies with moderate deformation of oroflexed stable block (strike-slip faults). (3) Eastern permeable facies with high deformation in regional shear zones (Pahrnagat shear zone).	0.097	6.511×10^{-2}	0.19	3,152	0.0315
K2YMLCA	Eastern permeable facies with moderate deformation around Yucca Mountain.	0.442	4.2262×10^{-1}	0.41	2,766	0.225

Table F-9. Calibrated horizontal hydraulic-conductivity parameters for carbonate-rock aquifers.—Continued

[LCA, lower carbonate-rock aquifer; LCA_T1, thrustled lower carbonate-rock aquifer; NA, not applicable; UCA, upper carbonate-rock aquifer]

Parameter name	Description	Composite scaled sensitivity	Hydraulic conductivity at land surface ¹ (meters per day)	Coefficient of variation ²	Average depth, in meters	Hydraulic conductivity at average depth (meters per day)
K2421_LCA	(1) Eastern permeable facies with moderate deformation along highly extended rotated range blocks. (2) Eastern permeable facies with high deformation in multiply-deformed areas (oroflexes, extension, shear and regional folding).	0.930	1.573×10^{-2}	0.005	2,681	8.48×10^{-3}
K2422b_LCA	Eastern permeable facies with moderate deformation of basin-range blocks.	0.272	6.454×10^{-2}	0.033	2,314	0.0291
K243_LCA	(1) Eastern permeable facies with high deformation in regional shear zones (Mine Mountain shear zone). (2) Eastern permeable facies with high deformation in multiply deformed areas (oroflexes, extension, shear and regional folding).	2.438	2.189×10^0	0.5	2,398	1.78
K243_UCA	(1) UCA. (2) Eastern permeable facies with moderate deformation of regional fold along Spotted Range syncline.	0.0159	1.000×10^{-4}	NA	341	3.08×10^{-5}
K243PP_LCA	Eastern permeable facies with high deformation in upper plate of brittle detachments.	0.162	1.000×10^0	0.5	836	0.946
K243GV_LCA	(1) Eastern permeable facies with high deformation in upper plate of brittle detachments along Grapevine Mountains and Bare Mountain. (2) Poorly known areas near oroflex; character of LCA is highly uncertain.	0.086	2.398×10^{-3}	0.0036	1,367	2.19×10^{-3}
K244_LCA	Eastern permeable facies with moderate deformation centered around Ash Meadows.	0.014	2.000×10^2	NA	2,201	200.0

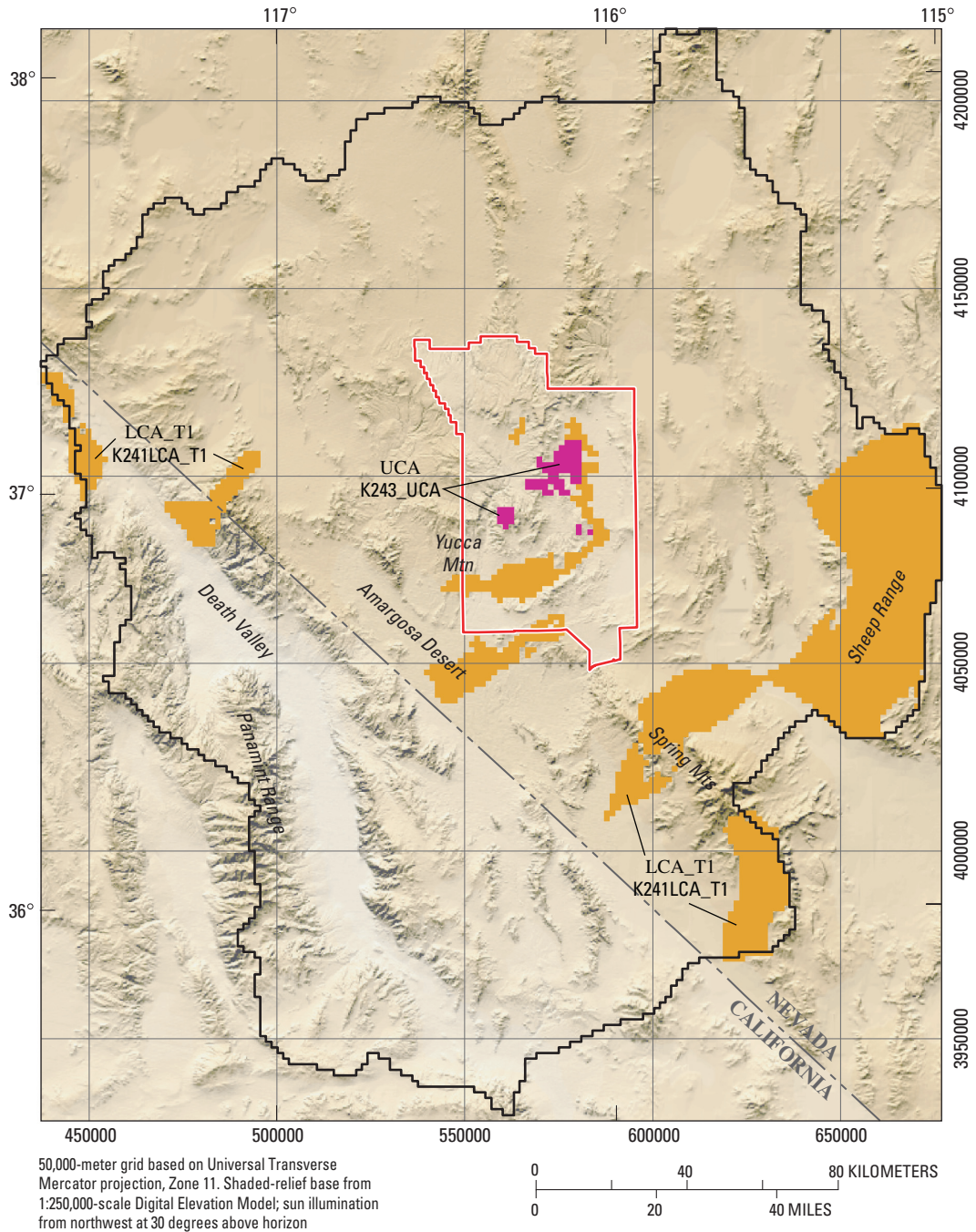
¹Minimum and maximum hydraulic conductivity in meters per day for the UCA and LCA are 0.0001 to 820 (Belcher and others, 2001).²Values were log transformed.



EXPLANATION









Surface horizontal hydraulic conductivity of lower carbonate-rock aquifer (LCA)—In meters per day		Parameter-zone boundary and name
< 0.0001	0.1 to 1.0	Death Valley regional ground-water flow system model grid boundary
0.0001 to 0.001	1.0 to 10	Nevada Test Site boundary
0.001 to 0.01	10 to 100	
0.01 to 0.1	>100	

Figure F-17. Hydraulic-conductivity zone parameters, depth-decay parameters, unit thickness, and extent for lower carbonate-rock aquifer. Depth-decay parameter values presented in table F-12 and figure F-35.



EXPLANATION

Surface horizontal hydraulic conductivity of upper carbonate-rock aquifer (UCA) and lower carbonate-rock aquifer-thrust (LCA_T1)—In meters per day

	< 0.0001		0.1 to 1.0
	0.0001 to 0.001		1.0 to 10
	0.001 to 0.01		10 to 100
	0.01 to 0.1		>100

K243_UCA Parameter-zone name



-  Death Valley regional ground-water flow system model grid boundary
-  Nevada Test Site boundary

Figure F-18. Hydraulic-conductivity zone parameters, unit thickness, and extent for upper carbonate-rock aquifer and thrusted lower carbonate-rock aquifer unit.

Table F-10. Calibrated horizontal hydraulic-conductivity parameters for the volcanic-rock units.

Parameter name	Description	Minimum – maximum hydraulic conductivity, in meters per day, from Belcher and others, 2001	Composite scaled sensitivity	Hydraulic conductivity at land surface (meters per day)	Coefficient of variation ¹	Average depth (meters)	Hydraulic conductivity at average depth (meters per day)
K311 YVU	(lumped with part of CHVU; K32BR4CH13)	0.002–4	0.0904	5.094×10 ⁻²	0.23	38	0.0410
K312 LFU	(part lumped with VSU (upper); K42UP_VSU)	³ 2×10 ⁻⁴ –20	1.029	8.440	0.5	144	3.71
K3LFU_am	LFU in Amargosa Desert area	³ 2×10 ⁻⁴ –20	0.280	5.662×10 ⁻¹	0.44	588	0.197
K3C_TM	TMVA – brittle (either altered or not)	²⁷ 7×10 ⁻⁷ –17	0.08808	0.3162	NA	248	0.0767
K321ITMVA	TMVA – not brittle (either altered or not)	²⁷ 7×10 ⁻⁷ –17	0.2820	2.885×10 ²	¹¹ 0.29	248	70.00
K3C_PVA	Intracaldera PVA	⁴ 0.002–4	0.1776	1.328×10 ⁻¹	0.42	¹² 38	0.107
K3PVA	Extra-caldera PVA						
K32CH24LF	(1) CHVU – altered, brittle (2) CHVU – not altered, not brittle (3) LFU – all areas except Amargosa Desert						
K32BR4CH13	(1) BRU – not brittle, not altered (2) WVU (3) CHVU – not altered, brittle (4) CHVU – altered, not brittle	⁵ 0.008–4	0.2840	1.604×10 ⁻¹	0.11	¹³ 175	0.05917
K321521_PP	CFPPA	⁶ 0.001–180	0.5710	1.661×10 ²	0.5	693	3.183
K3215BCU1	CFBCU – not altered, brittle	⁶ 0.001–180	0.04711	1.000×10 ⁻²	0.26	561	0.000406
K3215BCU34	CFBCU – not brittle (either altered or not)	⁷ 0.0003–55	0.3780	1.241	0.49	562	0.05012
K3215TR	CFTA	⁸ 0.003–2	0.1347	5.597×10 ⁻²	0.49	721	0.000914
K3BRU123	(1) BRU – not altered, brittle (2) BRU – altered, brittle (3) BRU – altered, not brittle	⁹ 0.01–4	0.1597	1.894	0.5	561	0.07693
K33_OVU	OVU outside SWNVF	¹⁰ 1×10 ⁻⁶ –1	0.01341	9.900×10 ⁻³	0.021	142	0.004388
K33_OVUsw	OVU inside SWNVF	¹⁰ 1×10 ⁻⁶ –1	0.1867	4.8638×10 ⁻²	0.061	509	0.002658

¹Values were log transformed.²Range listed is for the PVA.³Range listed is for the TMVA.⁴Range listed is for the LFU, which includes the range of the CHVU.⁵Minimum value listed is for CHVU and the maximum value listed is for the BRU.⁶Range listed is for the CFPPA.⁷Range listed is for the CFBCU.⁸Range listed is for the CFTA.⁹Range listed is for the BRU.¹⁰Range listed is for the OVU.¹¹Parameter was not log transformed.¹²Average depth is for the LFU, the most spatially extensive unit.¹³Average depth is for the BRU, the most spatially extensive unit.

[BRU, Belted Range unit; CFBCU, Crater Flat–Bullfrog confining unit; CFPPA, Crater Flat–Prow Pass aquifer; CFTA, Crater Flat–Tram aquifer; CHVU, Calico Hills volcanic-rock unit; LFU, lava-flow unit; OVU, older volcanic-rock unit; PVA, Paintbrush volcanic-rock aquifer; SWNVF, southwestern Nevada volcanic field; TMVA, Thirsty Canyon–Timber Mountain volcanic-rock aquifer]

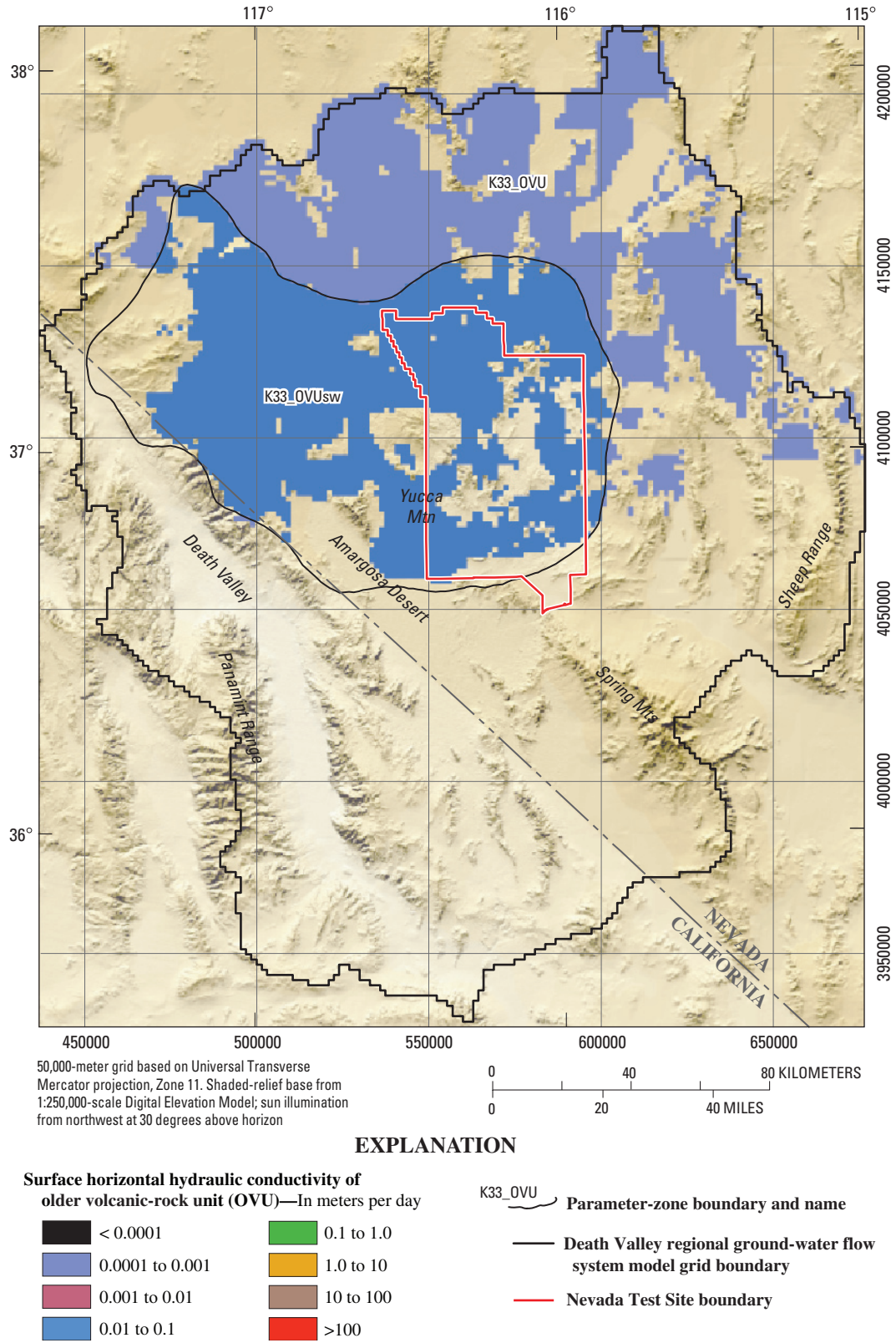


Figure F-19. Hydraulic-conductivity zone parameters, unit thickness, and extent for older volcanic-rock unit.

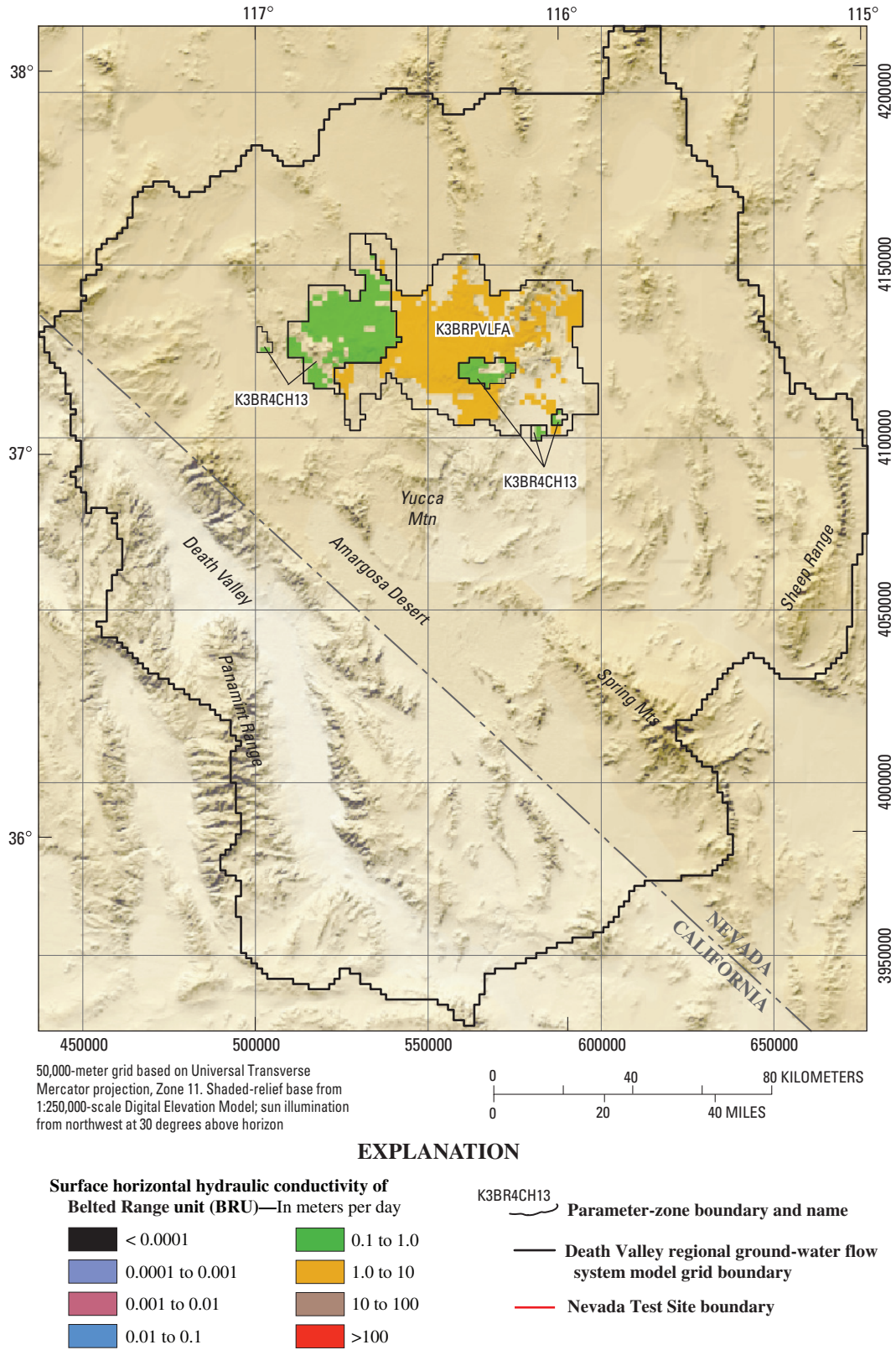
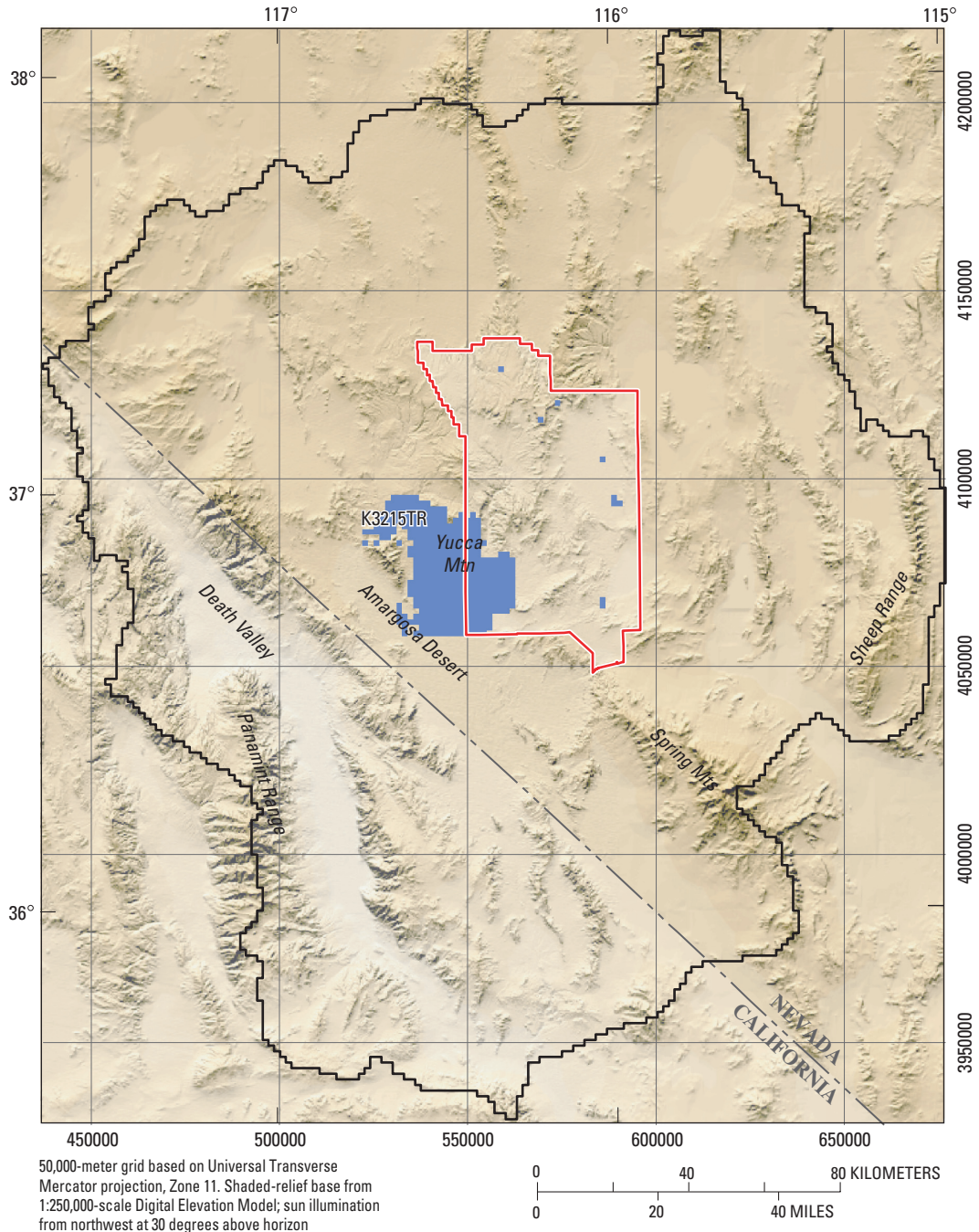


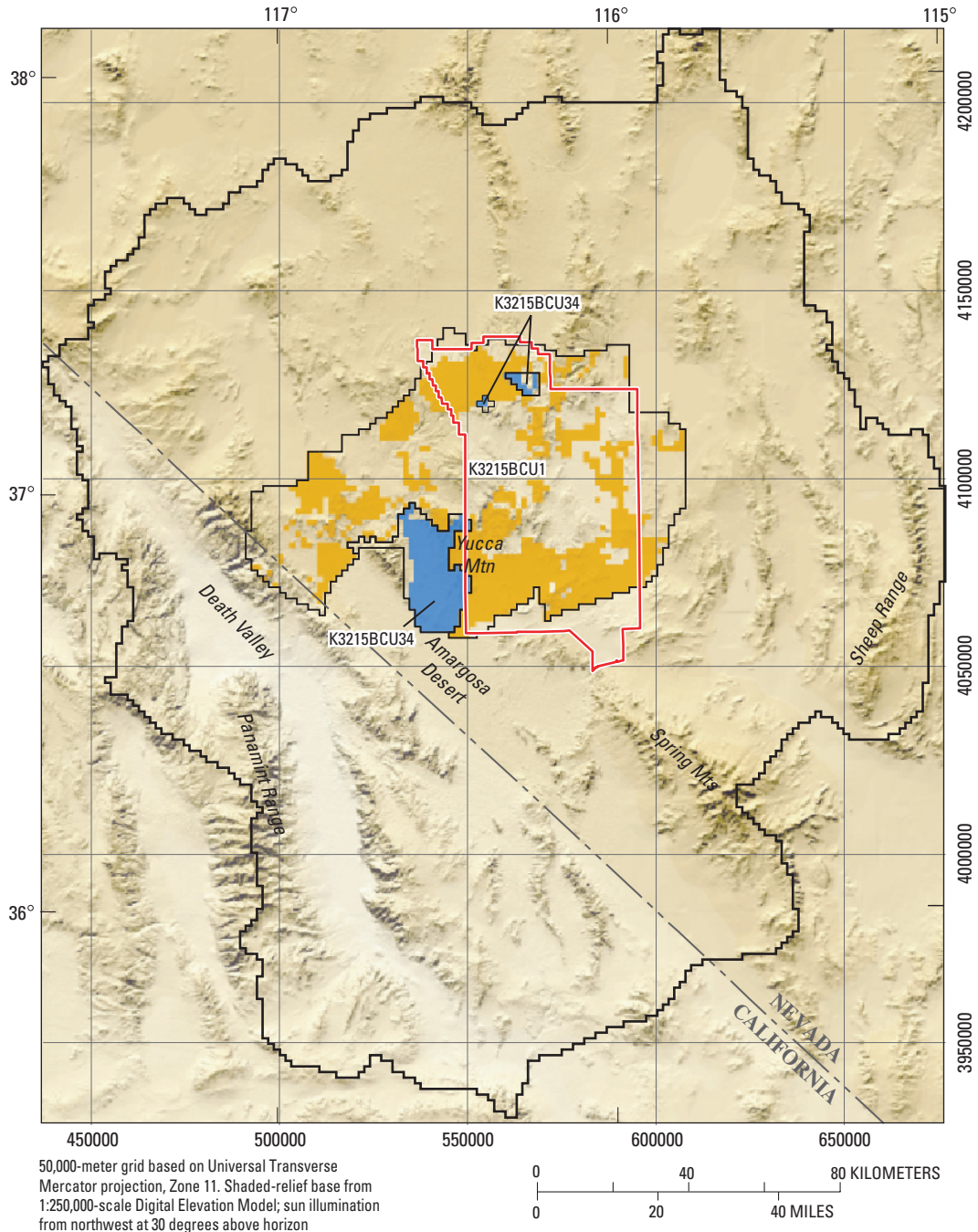
Figure F-20. Hydraulic-conductivity zone parameters, unit thickness, and extent for belted Range unit.



EXPLANATION

Surface horizontal hydraulic conductivity of Crater Flat-Tram aquifer (CFTA)—In meters per day		K3215TR Parameter-zone name
< 0.0001	0.01 to 1.0	Death Valley regional ground-water flow system model grid boundary
0.0001 to 0.001	1.0 to 10	Nevada Test Site boundary
0.001 to 0.01	10 to 100	
0.01 to 0.1	>100	

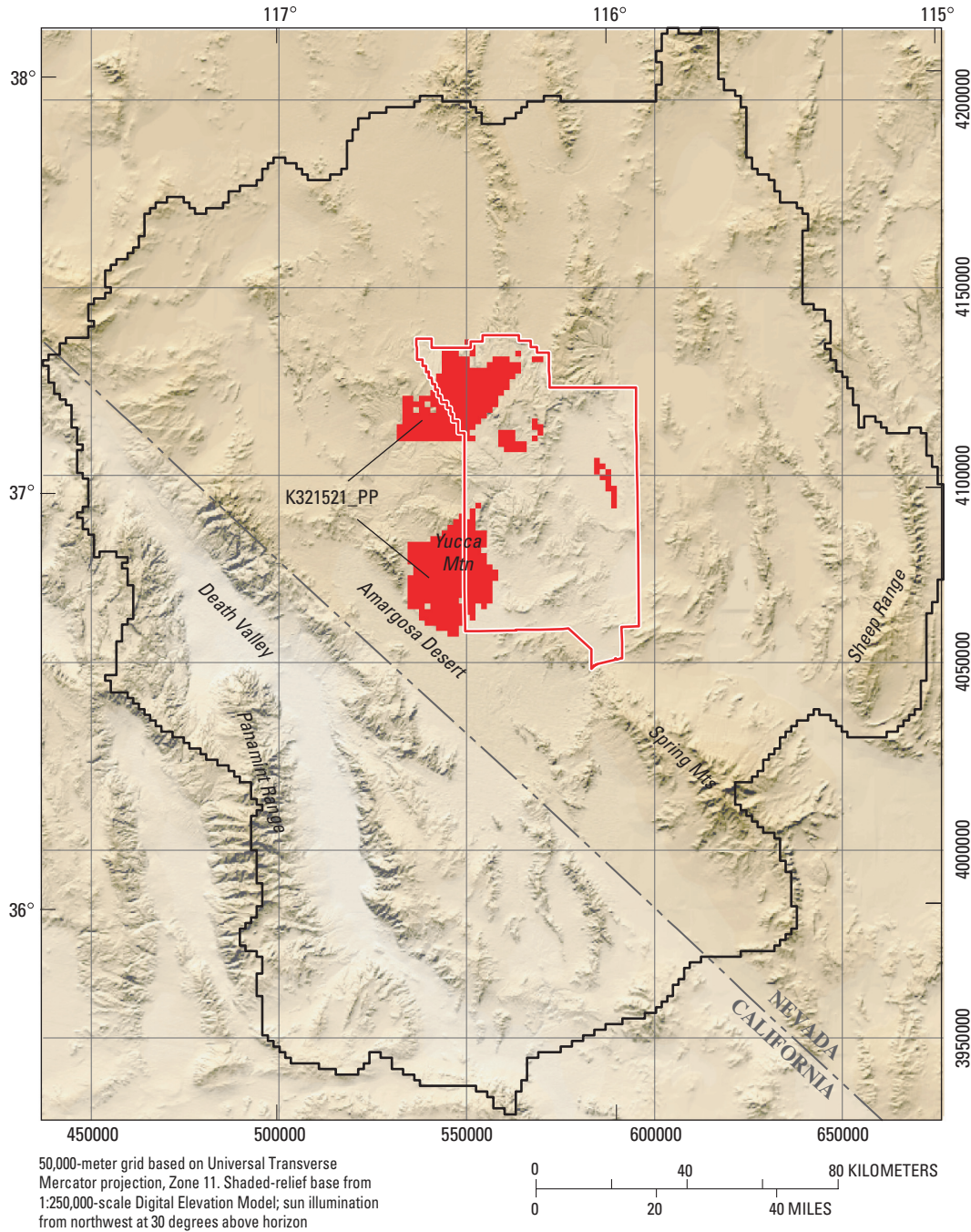
Figure F-21. Hydraulic-conductivity zone parameters, unit thickness, and extent for Crater Flat-Tram aquifer unit.



EXPLANATION

Surface horizontal hydraulic conductivity of Crater Flat-Bullfrog confining unit (CFBCU)— In meters per day		K3215BCU34 Parameter-zone boundary and name
< 0.0001	0.1 to 1.0	Death Valley regional ground-water flow system model grid boundary
0.0001 to 0.001	1.0 to 10	Nevada Test Site boundary
0.001 to 0.01	10 to 100	
0.01 to 0.1	>100	

Figure F-22. Hydraulic-conductivity zone parameters, unit thickness, and extent for Crater Flat-Bullfrog confining unit.



EXPLANATION

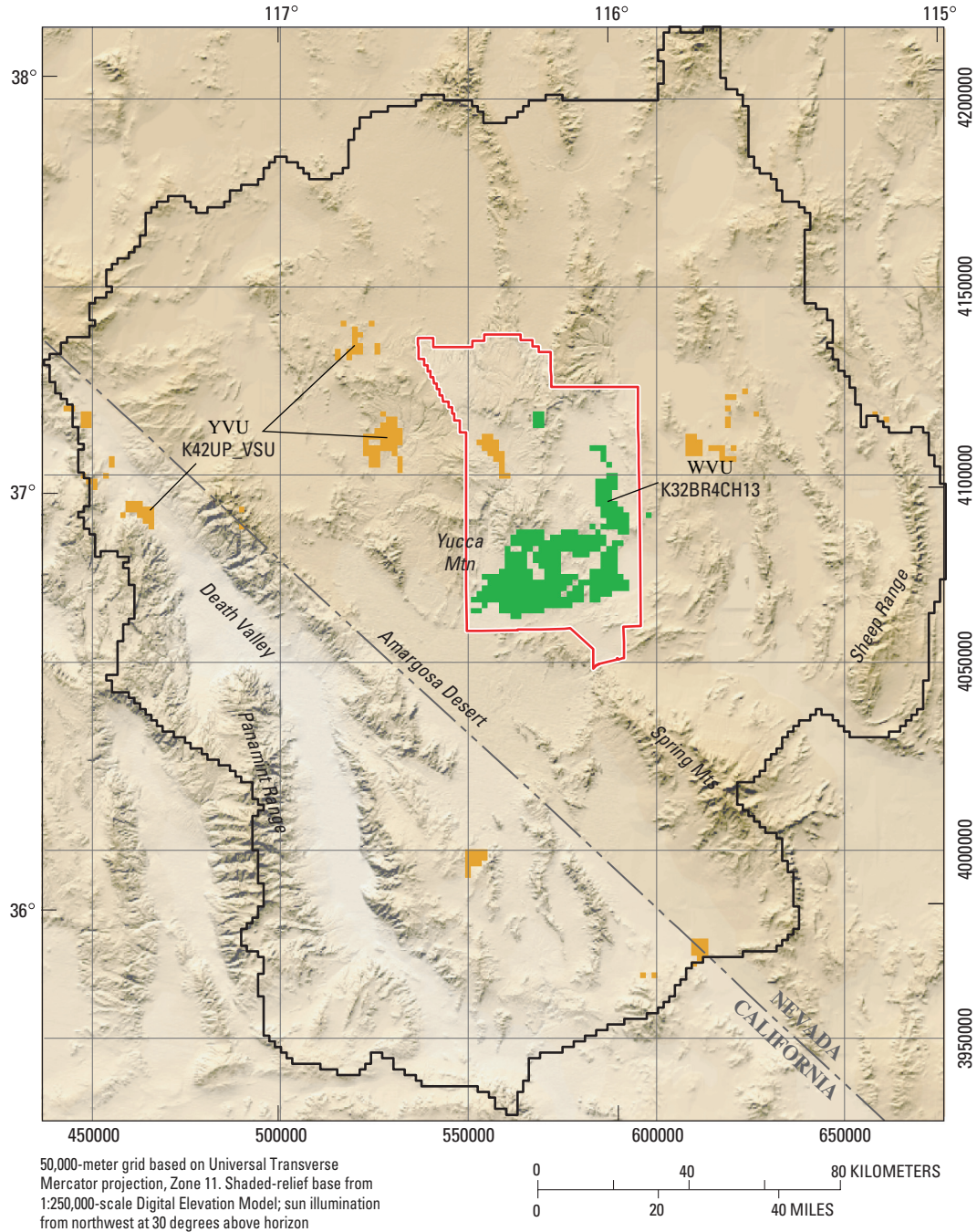
Surface horizontal hydraulic conductivity of Crater Flat-Prow Pass aquifer (CFPPA)—
In meters per day

- | | |
|-----------------|------------|
| < 0.0001 | 0.1 to 1.0 |
| 0.0001 to 0.001 | 1.0 to 10 |
| 0.001 to 0.01 | 10 to 100 |
| 0.01 to 0.1 | >100 |

K321521_PP Parameter-zone name

- Death Valley regional ground-water flow system model grid boundary
- Nevada Test Site boundary

Figure F-23. Hydraulic-conductivity zone parameters, unit thickness, and extent for Crater Flat-Prow Pass aquifer unit.



EXPLANATION

Surface horizontal hydraulic conductivity of Wahmonie volcanic-rock unit (WVU) and young volcanic-rock unit (YVU)—In meters per day

< 0.0001	0.1 to 1.0
0.0001 to 0.001	1.0 to 10
0.001 to 0.01	10 to 100
0.01 to 0.1	>100

K42UP_VSU Parameter-zone name

- Death Valley regional ground-water flow system model grid boundary
- Nevada Test Site boundary

Figure F-24. Hydraulic-conductivity zone parameters, unit thickness, and extent for Wahmonie volcanic-rock and younger volcanic-rock unit.

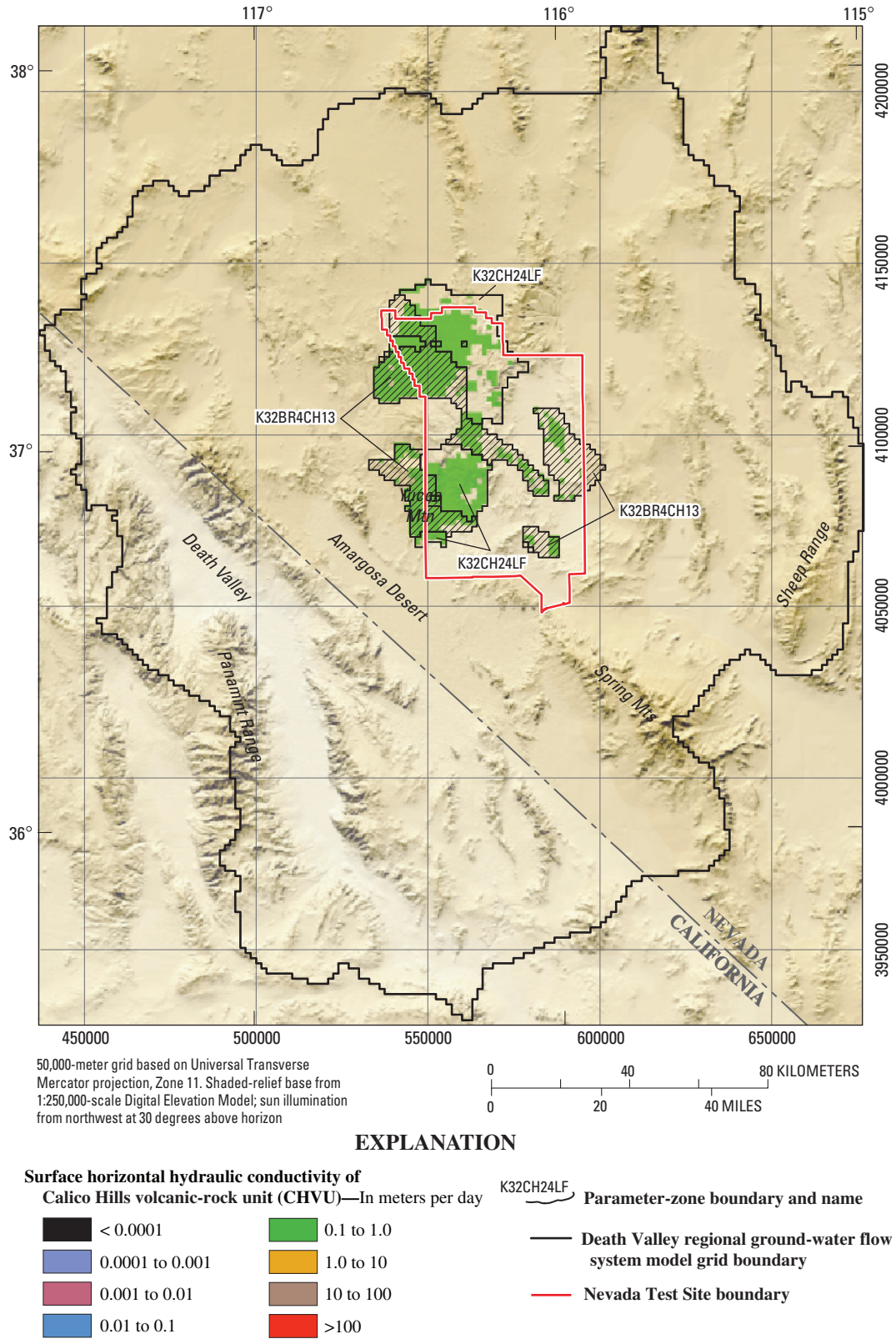
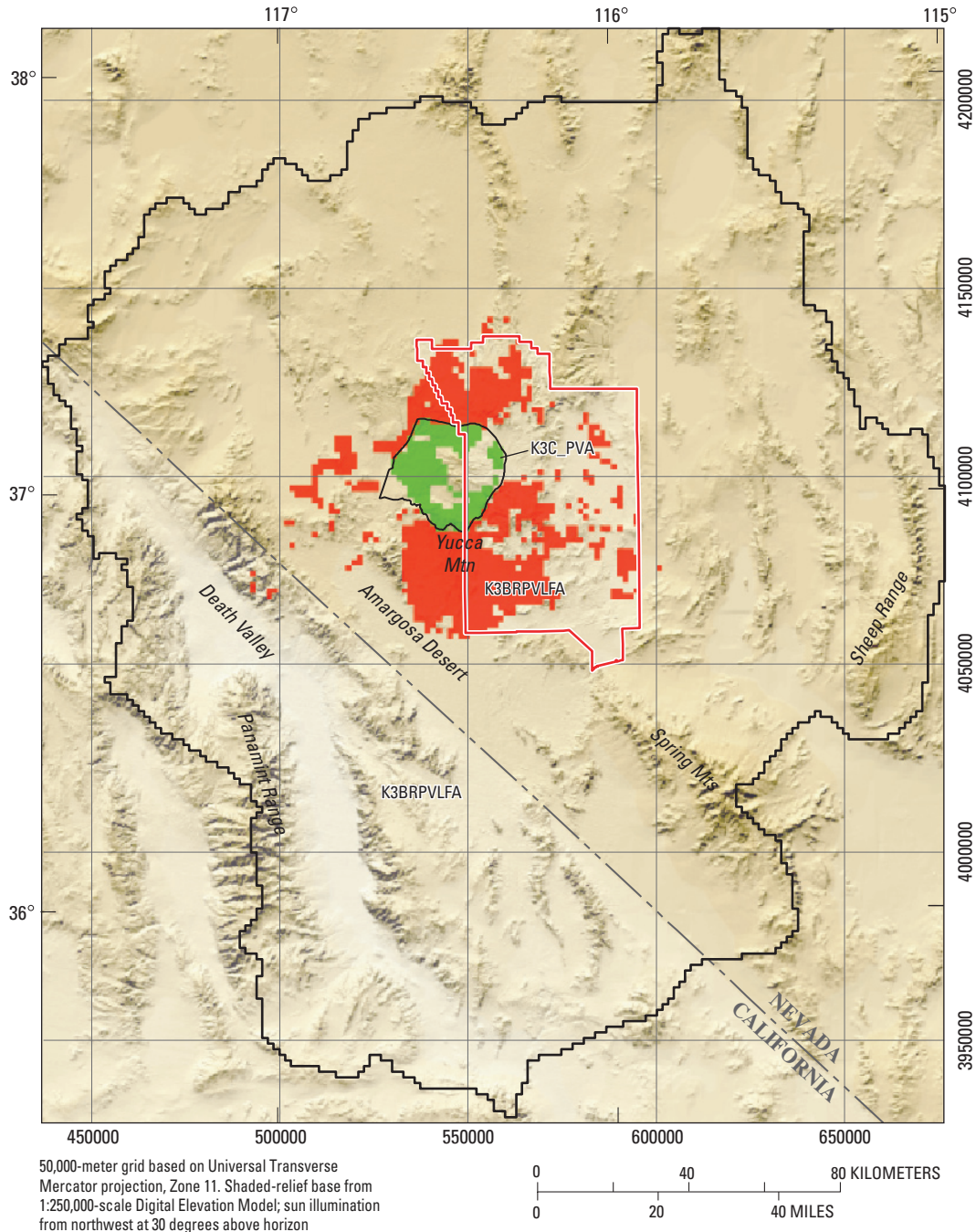










Figure F-25. Hydraulic-conductivity zone parameters, unit thickness, and extent for Calico Hills volcanic-rock unit.



EXPLANATION

Surface horizontal hydraulic conductivity of Paintbrush volcanic-rock aquifer (PVA)—
In meters per day

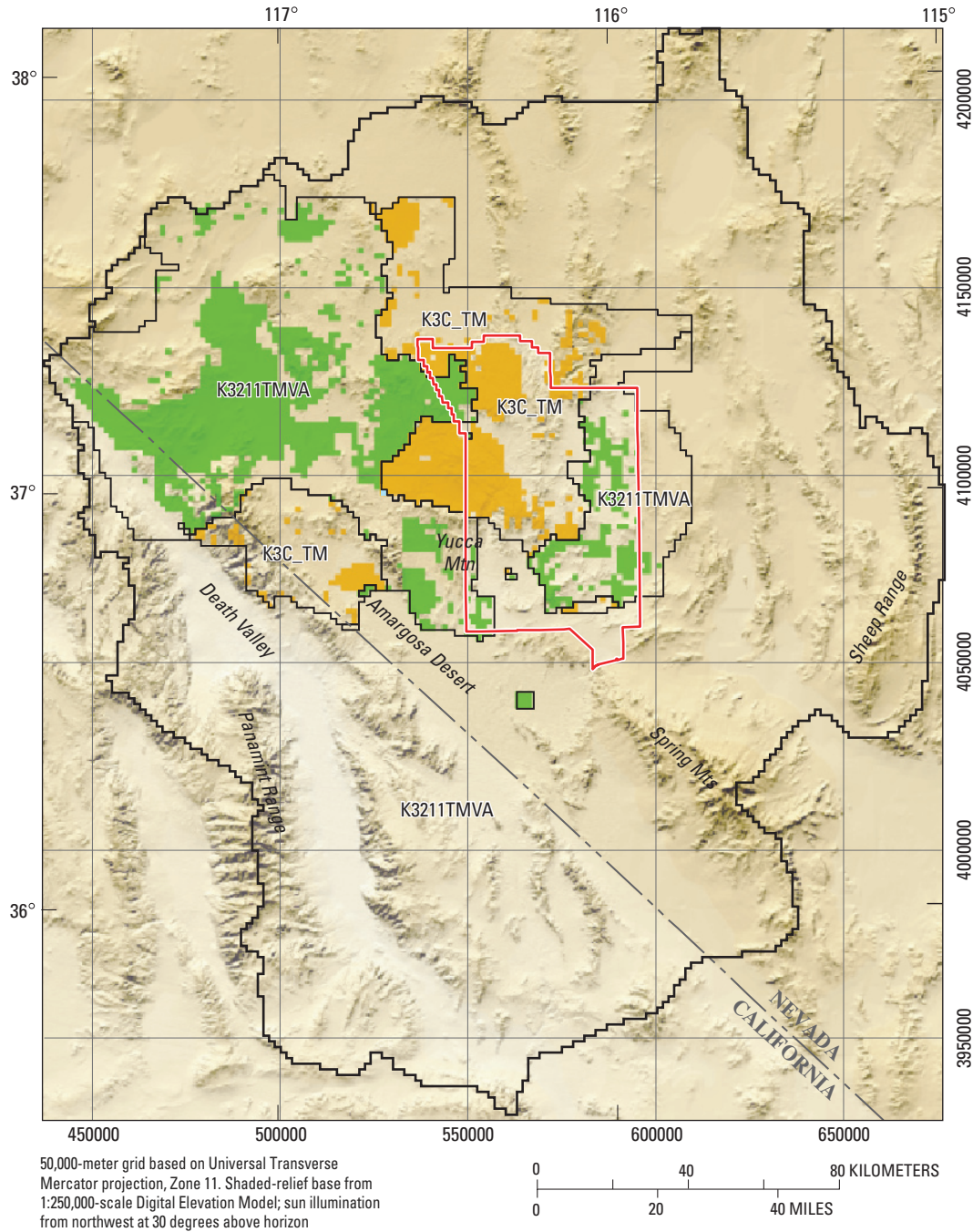
- | | |
|---|--|
|  < 0.0001 |  0.1 to 1.0 |
|  0.0001 to 0.001 |  1.0 to 10 |
|  0.001 to 0.01 |  10 to 100 |
|  0.01 to 0.1 |  >100 |

 **K3C_PVA** Parameter-zone boundary and name

 **Death Valley regional ground-water flow system model grid boundary**









 **Nevada Test Site boundary**

Figure F-26. Hydraulic-conductivity zone parameters, unit thickness, and extent for Paintbrush volcanic-rock aquifer.



EXPLANATION

Surface horizontal hydraulic conductivity of Timber Mountain-Thirsty Canyon volcanic-rock aquifer (TMVA)—In meters per day

- | | |
|---|--|
|  < 0.0001 |  0.1 to 1.0 |
|  0.0001 to 0.001 |  1.0 to 10 |
|  0.001 to 0.01 |  10 to 100 |
|  0.01 to 0.1 |  >100 |




-  **K3C_TM** Parameter-zone boundary and name
-  Death Valley regional ground-water flow system model grid boundary
-  Nevada Test Site boundary

Figure F-27. Hydraulic-conductivity zone parameters, unit thickness, and extent for Thirsty Canyon-Timber Mountain volcanic-rock aquifer.

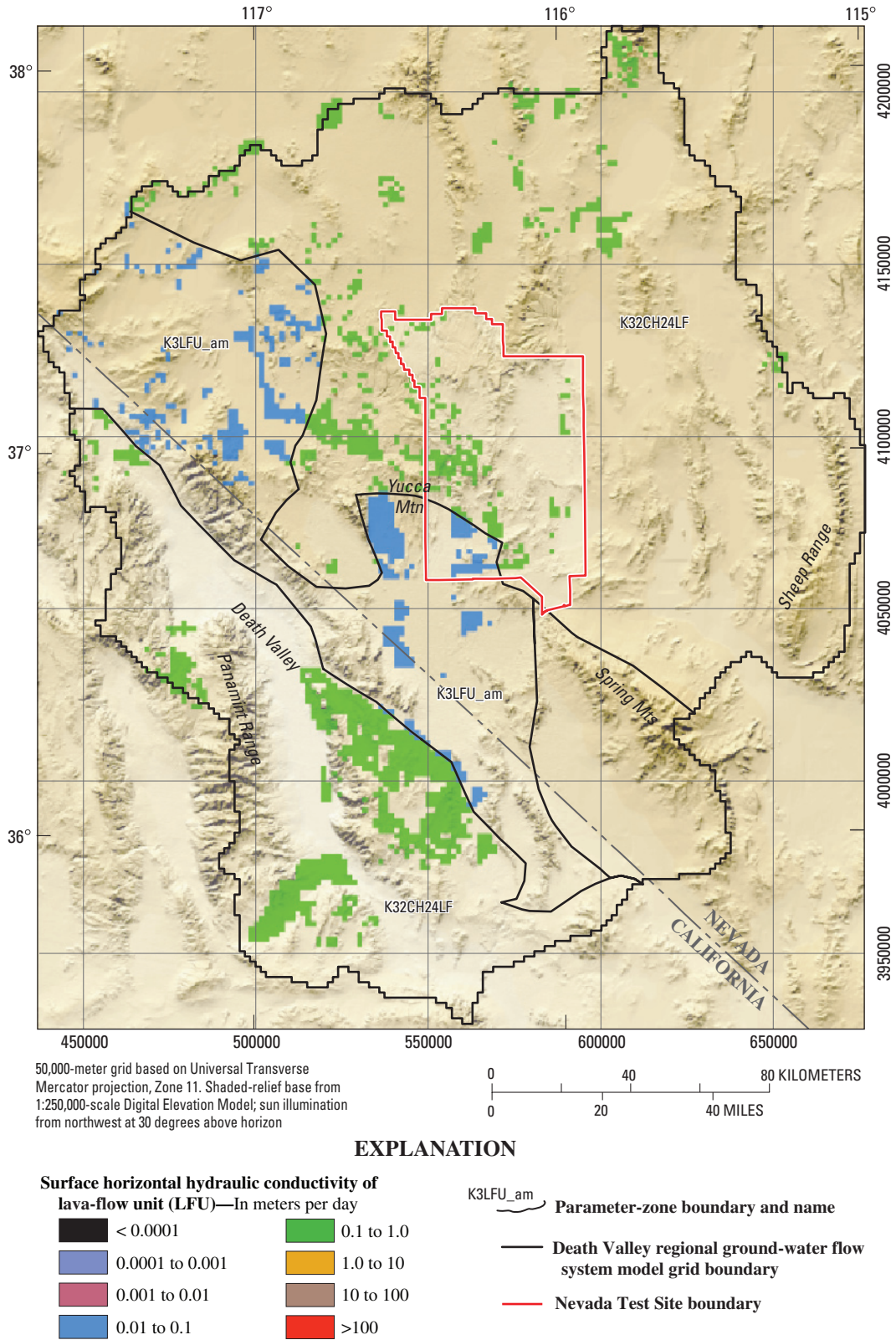


Figure F-28. Hydraulic-conductivity zone parameters, unit thickness, and extent for lava-flow unit.

Some volcanic HGUs, such as the WVU, did not have enough hydraulic information to subdivide into zones and thus were left intact and commonly combined with other HGUs. In one case, that of the PVA, the property zonations did not appear to support the hydraulic data at all. The PVA was divided on the basis of its relative location inside or outside caldera centers (fig. F-26), which likely coincides with fracture density.

Basin-Fill Units

The HGUs constituting the basin-fill units were initially grouped into one hydraulic-conductivity parameter (K4). These units were initially split into two hydraulic-conductivity parameters representing aquifers (YAA, LA, and OAA) and confining units (YACU, OACU, and upper and lower VSU (table F-11)). The upper and lower VSUs were assigned into a parameter defining units that tend to be confining units even though they can be both confining units and aquifers.

Because the upper and lower VSUs can represent both aquifers and confining units, they were split on the basis of depositional characteristics of the basins. Hydraulic-conductivity zone parameters for these basin-fill units were defined on the basis of facies (figs. F-29 and F-30). The lower VSU was initially subdivided by facies (Chapter B, this volume). During calibration, this unit was further subdivided, especially in Pahrump Valley (fig. F-29). The basin-fill deposits in Pahrump Valley likely are more carbonate-rich and possibly of different character. The playa deposits in Pahrump Valley contain large amounts of fine-grained clays typical of a dry playa. The lower VSU also was important for matching heads and discharges near Sarcobatus Flat (fig. F-29) and flow in from the constant-head boundary (Clayton and the western part of Stone Cabin–Railroad boundary segments) (fig. A2-3 in Appendix 2). As a result, the lower VSU section representing the SWNVF sediments was split into an SWNVF area and a northeast and northwest component (fig. F-29 and table F-11).

The upper VSU was zoned on the basis of the location of the YACU and OACU because these relatively low permeability, fine-grained deposits were assumed to persist through time. This resulted in parameter zones (K4UP_VSUC, K4UP_VSUP, and K42UP_VSU) with similar depositional environments (fig. F-30 and table F-11).

The upper part of the basin-fill deposits is composed of a sequence of older and younger deposits defined by grain size. The older basin-fill are composed of the OACU (fig. F-31) and the OAA (fig. F-32), whereas the younger basin-fill units are composed of the YACU (fig. F-33) and the YAA (fig. F-34). The coarse-grained deposits are represented by the YAA and OAA (and fine-grained deposits represented by the YACU and OACU. Localized limestone aquifers in the basin-fill deposits were represented by the LA, which was

combined into the hydraulic-conductivity parameter representing basin-fill aquifers (K4_VF_AQ). During calibration, these units were lumped and split as necessary.

Parameter zones also were used to assess the importance of the lower and upper VSU units in controlling ground-water discharge (figs. F-29—F-30 and table F-11). The YACU and finer grained parts of the VSUs limit the flow of ground water to discharge areas and pumping centers, especially near Ash Meadows and in Pahrump Valley.

CSS values of many of the basin-fill units are much larger in the transient calibration than in the steady-state calibration. Additional parameters were created in the basin-fill units and the lower and upper VSU to discern confining units and aquifers (figs. F-29—F-34 and table F-11). Specific storage parameters and hydraulic conductivities were adjusted by examining the simulated and observed changes in both discharge and hydraulic-head observations over time.

Depth Decay of Hydraulic Conductivity

Depth decay of hydraulic conductivity was simulated using the HUF package (Anderman and Hill, 2003) (table F-12 and fig. F-35). Because of the uncertainty in depth decay of hydraulic conductivity and the great effect this can have on model calibration, the initial parameter values were inserted on the basis of previous estimates of hydraulic-conductivity decay with depth (IT Corporation, 1996, figs. 6-1—6-3). In general, depth decay was important in all of the volcanic-rock units, all of the basin-fill units, and of somewhat lesser importance in the carbonate-rock aquifer, as indicated by IT Corporation (1996). Depth decay applied to zones within the LCCU, SCU, XCU, and ICU confining units was helpful for improving the model. Initially, depth decay of hydraulic conductivity was assigned to all areas of the carbonate-rock aquifer. In some areas, depth decay reduced model fit and made calibrations less than optimal. In these areas, the rate of decrease in hydraulic conductivity with depth was reduced. Although this change is subjective, it improved model fit.

Depth decay produces some values of hydraulic-conductivity that are outside expected values. This may indicate that values of the depth-decay parameters are in error or that the decay of hydraulic conductivity with depth is not an exponential function (eq. 1). In addition, hydraulic-conductivity values become extremely small at depth for many of the units (table F-12). In reality, the hydraulic conductivity may not decrease below a certain threshold value. The flow system can be simulated adequately without this parameter. Because depth-decay of hydraulic conductivity is more important in simulating the contaminant migration than ground-water flow, transport simulations could be helpful to quantify this value.

Table F-11. Calibrated horizontal hydraulic-conductivity parameters for the basin-fill units.

[Abbreviations: LA, limestone aquifer; OAA, older alluvial aquifer; OACU, older alluvial confining unit; SCU, sedimentary-rock confining unit; VSU, volcanic- and sedimentary-rock units; YAA, younger alluvial aquifer; YACU, younger alluvial confining unit; YVU, younger volcanic-rock unit]

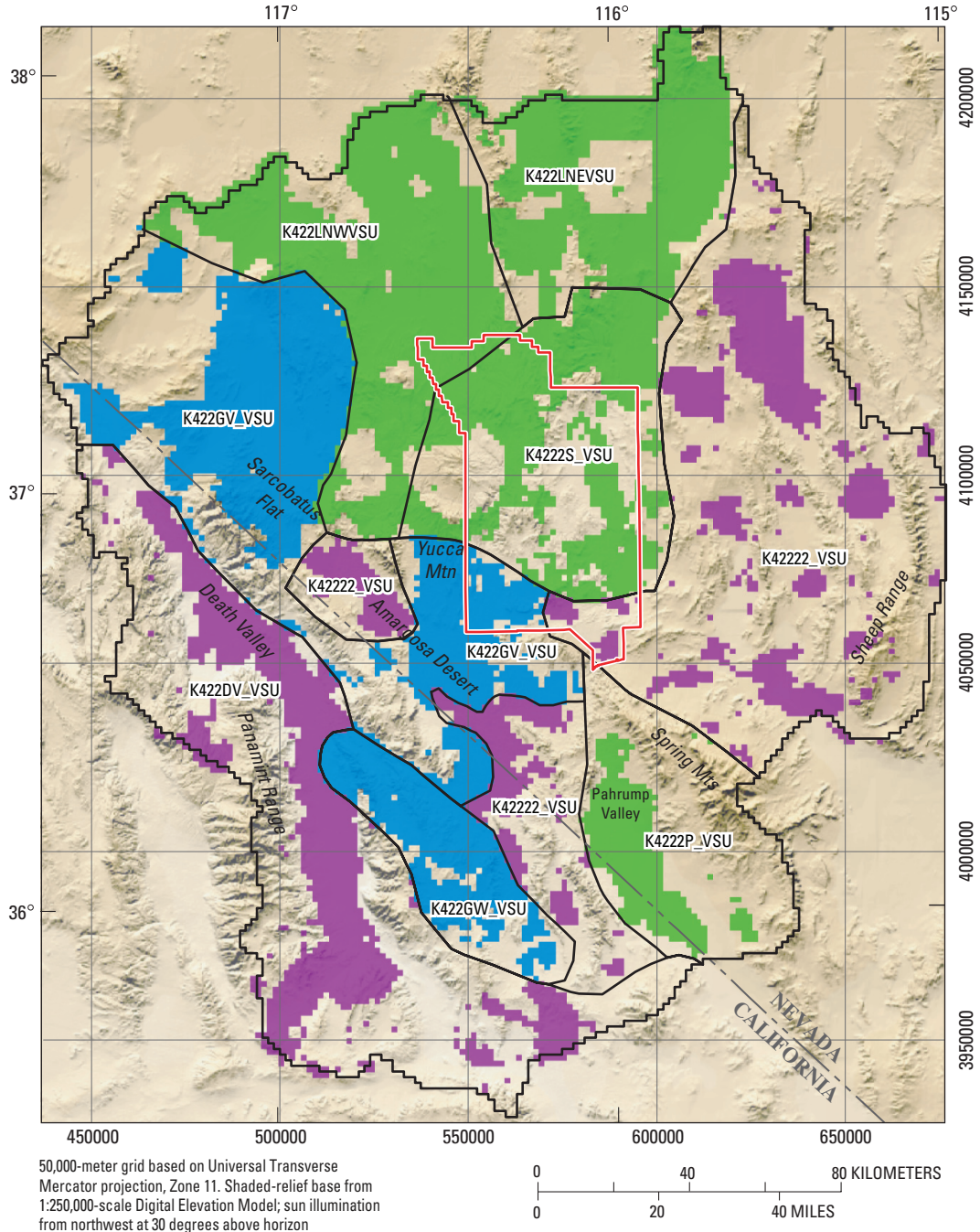
Parameter name	Description	Minimum – maximum hydraulic conductivity (meters per day) from Belcher and others (2001)	Composite scaled sensitivity	Hydraulic conductivity at land surface (meters per day)	Coefficient of variation ¹	Average depth (meters)	Hydraulic conductivity at average depth (meters per day)
K4_VF_AQ	(1) Basin-fill aquifers (coarser grained) (LA, YAA) (2) SCU	¹ 6×10 ⁻⁵ –130	0.342	5.972×10 ⁻¹	0.5	10	0.4467
K4_VF_OAA	OAA	¹ 6×10 ⁻⁵ –130	0.0349	5.920×10 ⁻²	0.5	39	0.000197
K4_VF_CU	Basin-fill confining units (finer grained) (YACU, OACU)	² 0.003–34	0.547	1.580	0.5	43	0.4655
K4UP_VSUC	Upper VSU (below YACU or OACU); finer grained	⁴ 0.00004–6	0.578	9.397×10 ⁻¹	0.13	164	0.18256
K4UP_VSUP	Upper VSU (below YACU) in Pahrump Valley; finer grained	⁴ 0.00004–6	0.253	2.077×10 ¹	0.5	160	4.169
K42UP_VSU	(1) Upper VSU ; coarser grained (anywhere not below YACU or OACU) (2) YVU	⁴ 0.00004–6	0.572	7.057	0.5	159	1.438
K42222_VSU	Lower VSU; mixture of fluvial and lacustrine sediments (LCCU-derived, nonvolcanic, and finer grained sediments); small area of Amargosa Desert added during calibration	⁴ 0.00004–6	0.130	5.000×10 ⁻³	0.01	401	0.004476
K422LNEVSU	Lower VSU; SWNVF sediments – northeast	⁴ 0.00004–6	0.311	1.847×10 ⁻¹	0.0001	721	0.15135
K422LNWVSU	Lower VSU; SWNVF sediments – northwest	⁴ 0.00004–6	0.770	1.917×10 ⁻¹	0.04	1,144	0.1397
K4222S_VSU	Lower VSU; SWNVF sediments	⁴ 0.00004–6	0.927	1.264×10 ⁻¹	0.06	1,296	0.088357
K422DV_VSU	Lower VSU; coarse syntectonic sediments (nonvolcanic) in Death Valley	⁴ 0.00004–6	0.399	8.804×10 ⁻³	0.02	608	0.007442
K422GW_VSU	Lower VSU; Greenwater volcanic sediments	⁴ 0.00004–6	1.078	1.524×10 ⁻²	0.003	572	0.013008
K4222P_VSU	Lower VSU; fluvial and lacustrine sediments with few volcanic units in Pahrump Valley	⁴ 0.00004–6	0.0866	5.812×10 ⁻¹	0.5	601	0.49227
K422GV_VSU	Lower VSU; mixture of sediments with diverse lithologies in the Amargosa Desert area	⁴ 0.00004–6	0.325	4.630×10 ⁻²	0.02	689	0.038276

¹Values were log transformed.

²Range listed is for the alluvial aquifer (AA), which is the combined YAA and OAA and includes the range of the SCU.









³Range listed is for the alluvial confining unit (ACU), which is the combined YACU and OACU.

⁴Range listed is for the combined YVU/VSU.



EXPLANATION

Surface horizontal hydraulic conductivity of lower volcanic- and sedimentary-rock unit (lower VSU)—In meters per day

- | | |
|---|--|
|  < 0.0001 |  0.1 to 1.0 |
|  0.0001 to 0.001 |  1.0 to 10 |
|  0.001 to 0.01 |  10 to 100 |
|  0.01 to 0.1 |  >100 |

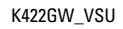


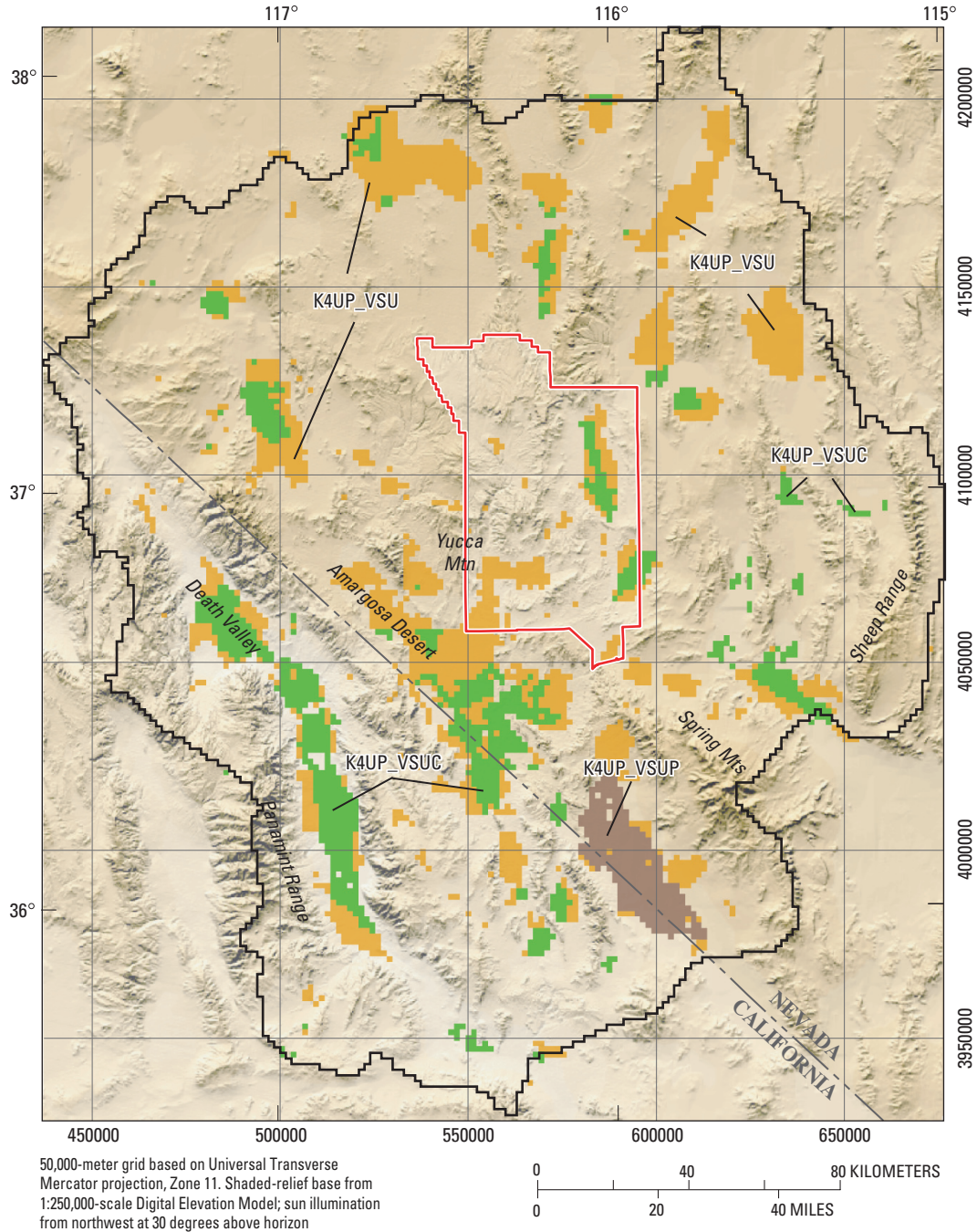

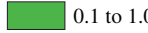
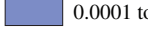



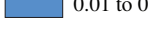

-  **Parameter-zone boundary and name**
-  **Death Valley regional ground-water flow system model grid boundary**
-  **Nevada Test Site boundary**

Figure F-29. Hydraulic-conductivity zone parameters, unit thickness, and extent for lower volcanic- and sedimentary-rock unit.



EXPLANATION

Surface horizontal hydraulic conductivity of upper volcanic- and sedimentary-rock unit (upper VSU)—In meters per day

- | | |
|---|--|
|  < 0.0001 |  0.1 to 1.0 |
|  0.0001 to 0.001 |  1.0 to 10 |
|  0.001 to 0.01 |  10 to 100 |
|  0.01 to 0.1 |  >100 |

K4UP_VSUP Parameter-zone name


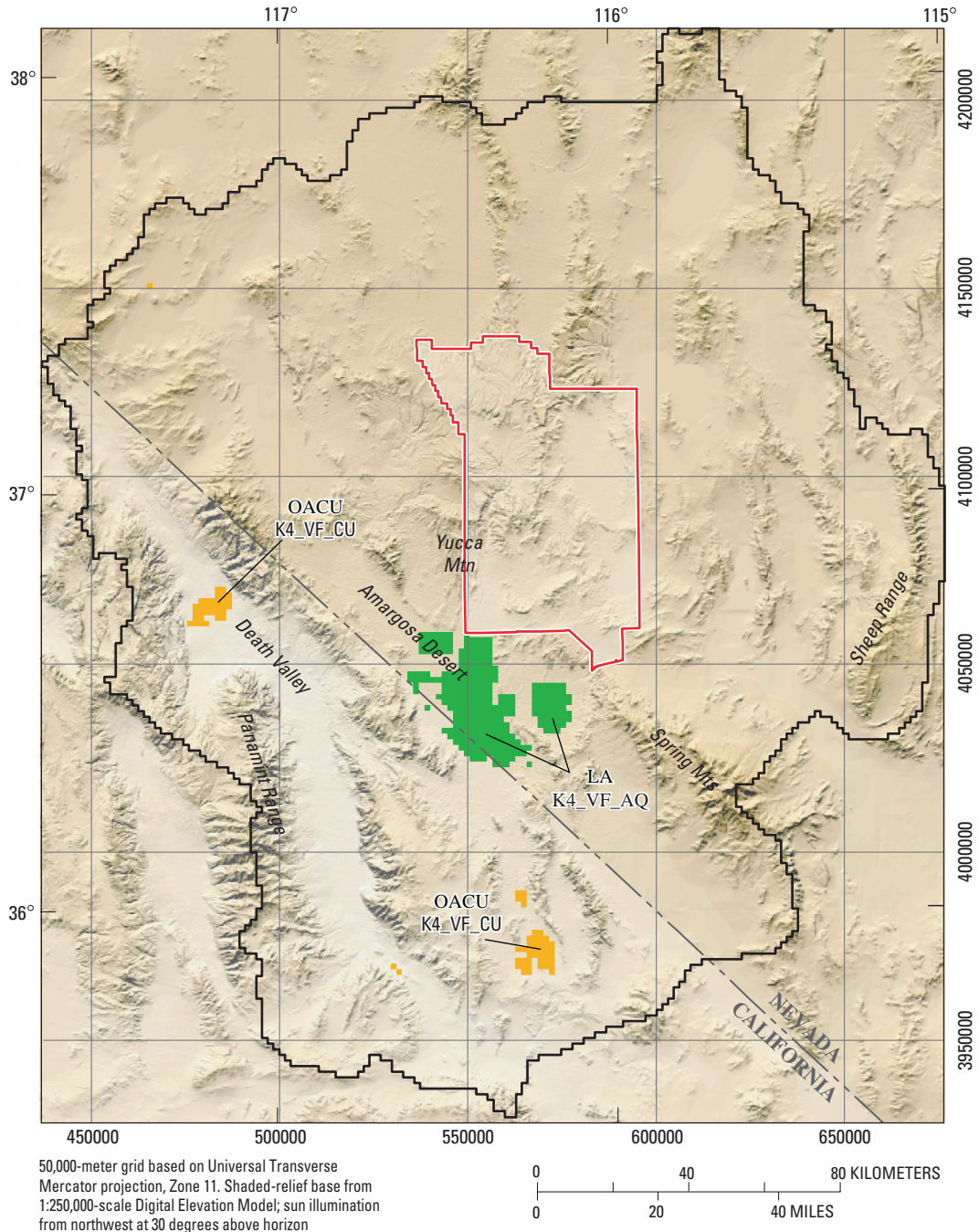








-  Death Valley regional ground-water flow system model grid boundary
-  Nevada Test Site boundary

Figure F-30. Hydraulic-conductivity zone parameters, unit thickness, and extent for upper volcanic- and sedimentary-rock unit.



EXPLANATION

Surface horizontal hydraulic conductivity of limestone aquifer (LA) and older alluvial confining unit (OACU)—In meters per day

 < 0.0001	 0.1 to 1.0
 0.0001 to 0.001	 1.0 to 10
 0.001 to 0.01	 10 to 100
 0.01 to 0.1	 >100

K4_VF_CU Parameter-zone name



-  **Death Valley regional ground-water flow system model grid boundary**
-  **Nevada Test Site boundary**

Figure F-31. Hydraulic-conductivity zone parameters, unit thickness, and extent for limestone aquifer and older alluvial confining units.

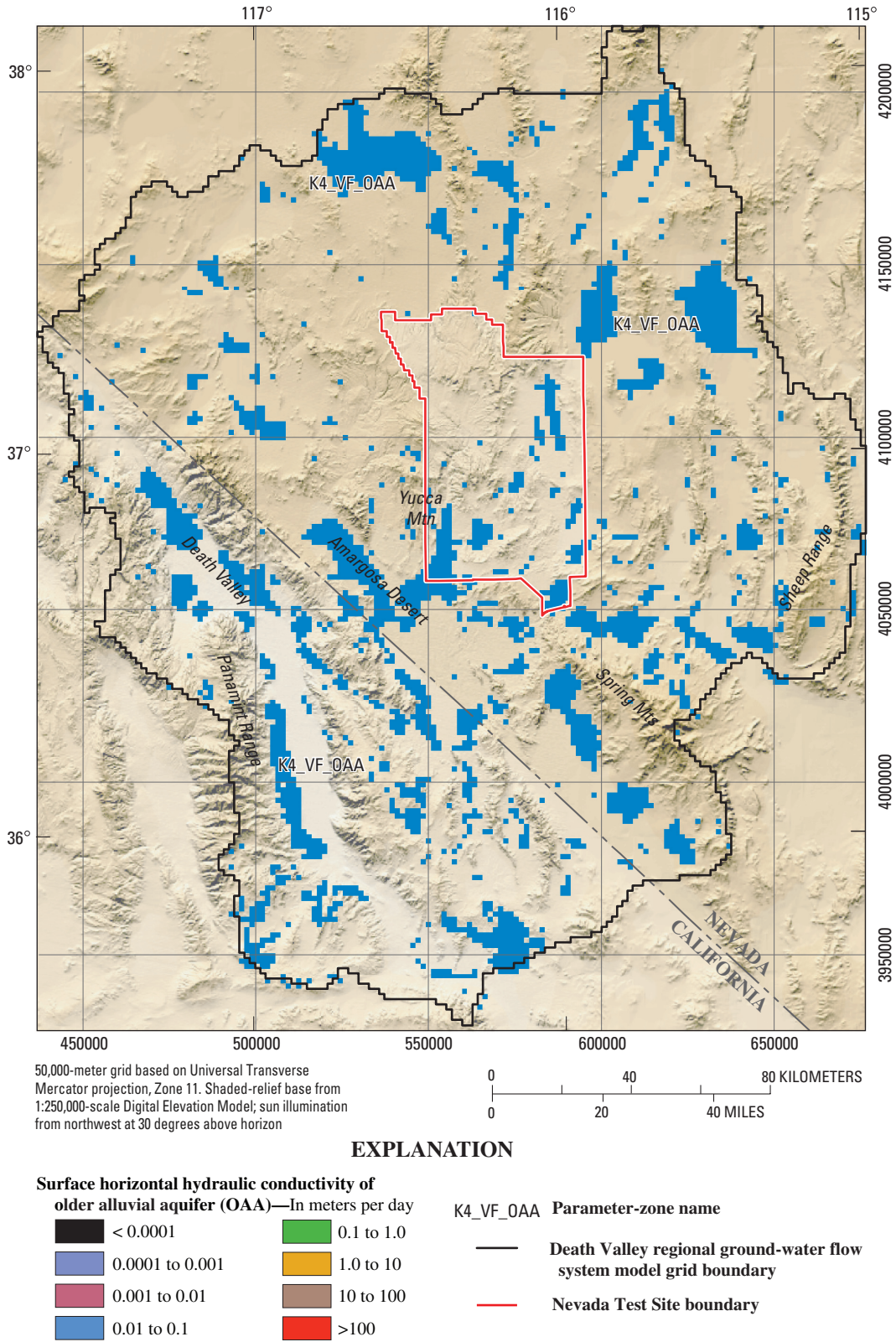
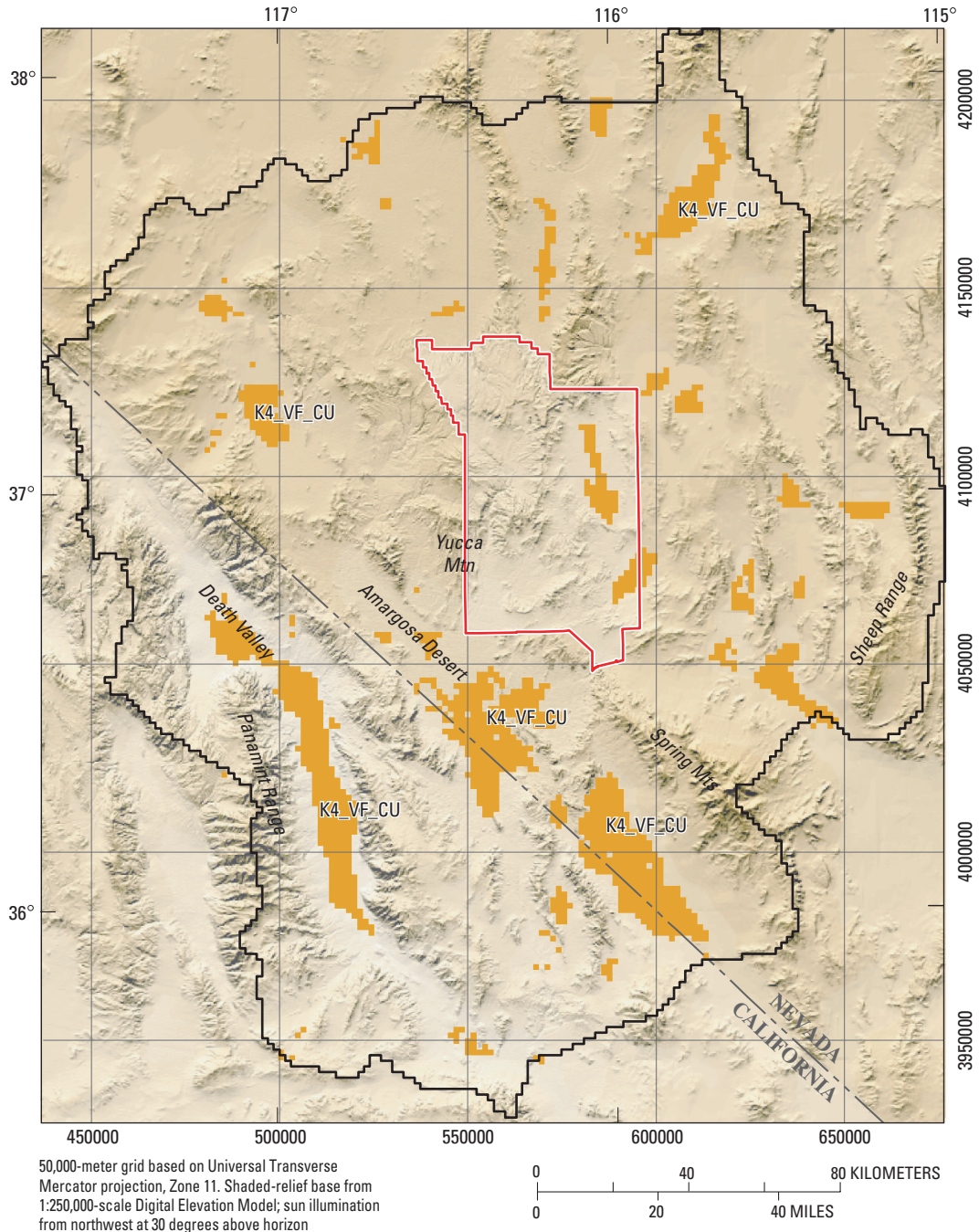










Figure F-32. Hydraulic-conductivity zone parameters, unit thickness, and extent for older alluvial aquifer.



EXPLANATION

Surface horizontal hydraulic conductivity of younger alluvial confining unit (YACU)—
In meters per day

 < 0.0001	 0.1 to 1.0
 0.0001 to 0.001	 1.0 to 10
 0.001 to 0.01	 10 to 100
 0.01 to 0.1	 >100

K4_VF_CU Parameter-zone name



-  Death Valley regional ground-water flow system model grid boundary
-  Nevada Test Site boundary

Figure F-33. Hydraulic-conductivity zone parameters, unit thickness, and extent for younger alluvial confining unit.

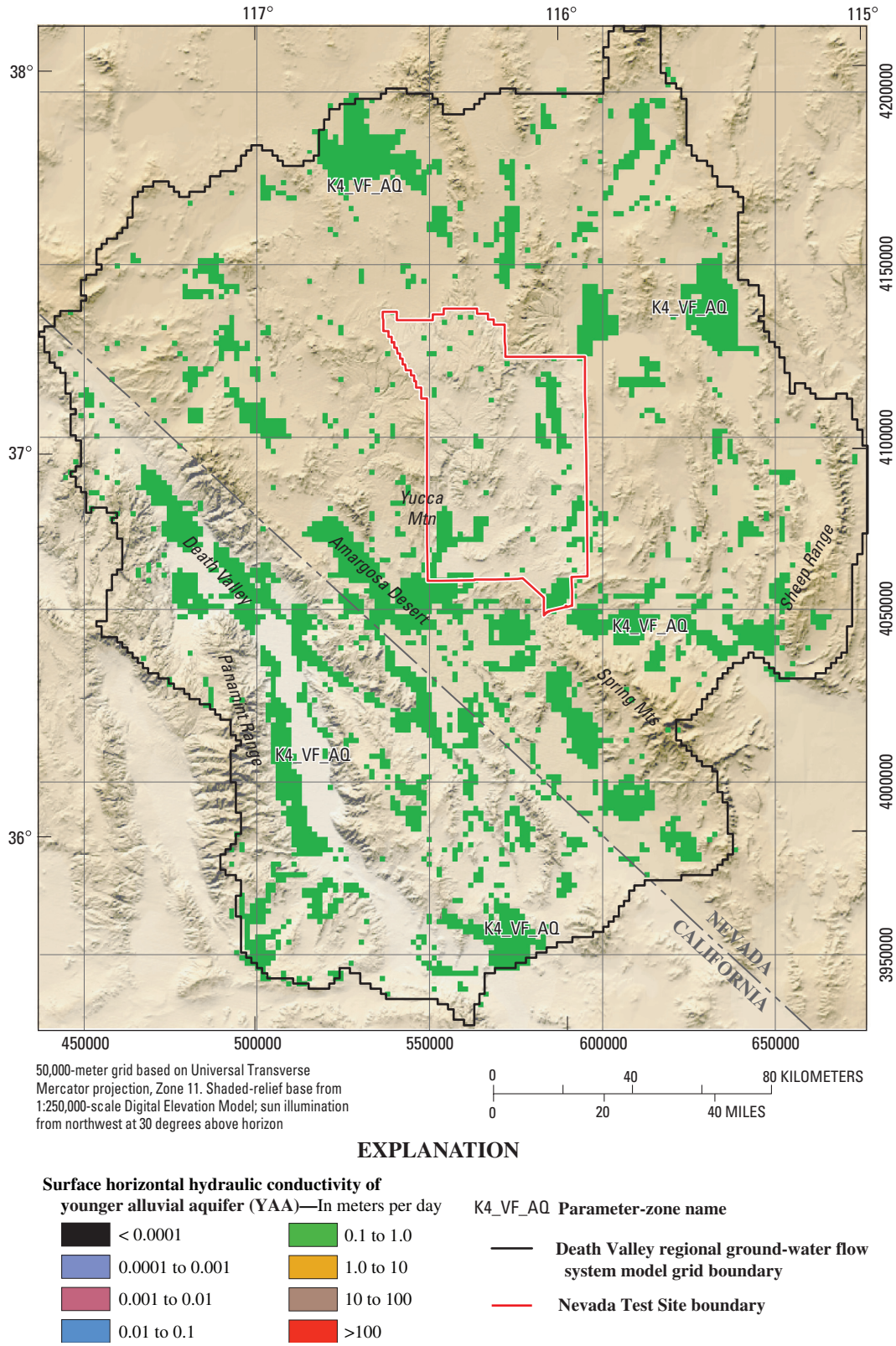


Figure F-34. Hydraulic-conductivity zone parameters, unit thickness, and extent for younger alluvial aquifer unit.

Table F–12. Calibrated depth-decay parameters.

[Abbreviations: LCA, lower carbonate-rock aquifer; LCCU, lower clastic-rock confining unit; NA, not applicable; TSDVS, Tertiary sediments, Death Valley section; UCA, upper carbonate-rock aquifer; UCCU, upper clastic-rock confining unit; VSU, volcanic- and sedimentary-rock unit; YAA, younger alluvial aquifer; YACU, younger alluvial confining unit]

Parameter name	Description	Initial depth-decay parameter value (IT Corp., 1996b)	Depth-decay parameter value (percentage of surface hydraulic conductivity at 1,000 meters)	Composite scaled sensitivity	Coefficient of variation ¹
KDEP_LCA	LCA (except as noted in KDP_LCANO, KDP_LCAT1 and KDEP_NO)	² 0.00102	0.00010 (79.4%)	1.7	NA
KDP_LCANO	LCA (K243GV_LCA, K24ISM_LCA, K243PP_LCA, and K2_DV_LCA)	² 0.00102	0.00002894 (93.6%)	0.4	NA
KDP_LCAT1	(1) LCA_T1 (2) LCA (K2421FLCA)	² 0.00102	0.0015 (3.2%)	3.1	NA
KDP_VOL	Volcanic rocks	³ 0.00256	0.00248 (0.33%)	7.3	NA
KDEP_UCCU	UCCU and UCA	⁴ 0.0015	0.0015 (3.2%)	1.0	NA
KDEP_VFVL	Basin fill (YAA, YACU, OAA, OACU, and LA)	⁵ 0.00563	0.0123 (<0.005%)	0.2	0.5
KDEP_VSUU	Upper VSU	⁶ 0.004	0.0043457 (0.005%)	1.0	0.002
KDEP_VSUL	Lower VSU	⁶ 0.004	0.00012 (75.9%)	0.6	NA
KDEP_NO	(1) LCCU_T1 (2) LCCU (except as noted in KDEP_XL) (3) LCA (K2rr_LCA) (4) LFU (5) SCU (6) XCU (K11CXILCU) (7) ICU	⁷ 0.0012	0.0000001 (99.98%)	7.9×10 ⁻⁴	NA
KDEP_XL	(1) XCU (2) LCCU (K1LCCU_XCU)	⁸ 0.0015	0.00061972 (24%)	1.7	NA

¹Values were not log transformed.

²Mean exponential depth-decay coefficient for carbonate-rock aquifers.

³Mean exponential depth-decay coefficient for volcanic-rock aquifers.

⁴Exponential depth-decay coefficient for the UCCU.

⁵Mean exponential depth-decay coefficient for alluvial (basin-fill) aquifers.

⁶Exponential depth-decay coefficient for TSDVS.

⁷Exponential depth-decay coefficient for LCCU.

⁸Exponential depth-decay coefficient for intrusive rocks.

Vertical Anisotropy

Vertical anisotropy parameters were initially defined for the four major rock types and generally had small CSS values during steady-state simulations (table F–13). Pumping stresses the upper part of the system and tends to force water to flow more vertically than under a natural hydraulic gradient. This resulted in greater sensitivity to vertical anisotropy parameters during transient simulations. The basin-fill units, in which much of the pumpage occurs, were most sensitive (table F–13). These units also are most likely to have stratification that would tend to decrease the vertical conductivity relative to the horizontal (anisotropy ratios greater than 1).

Storage Properties

During calibration, conceptual models simulating the top of the DVRFS model as confined or unconfined model layers were evaluated. Confined conditions were simulated with the capability of the HUF package (Anderman and Hill, 2003). The unconfined simulations were numerically unstable and ultimately were abandoned. For most confined simulations (including the final calibration), the top of the model was defined using simulated hydraulic heads from the previous model run. Because the cones of depression caused by pumpage in this system are fairly modest, simulated results should be very close to results obtained with unconfined simulations.

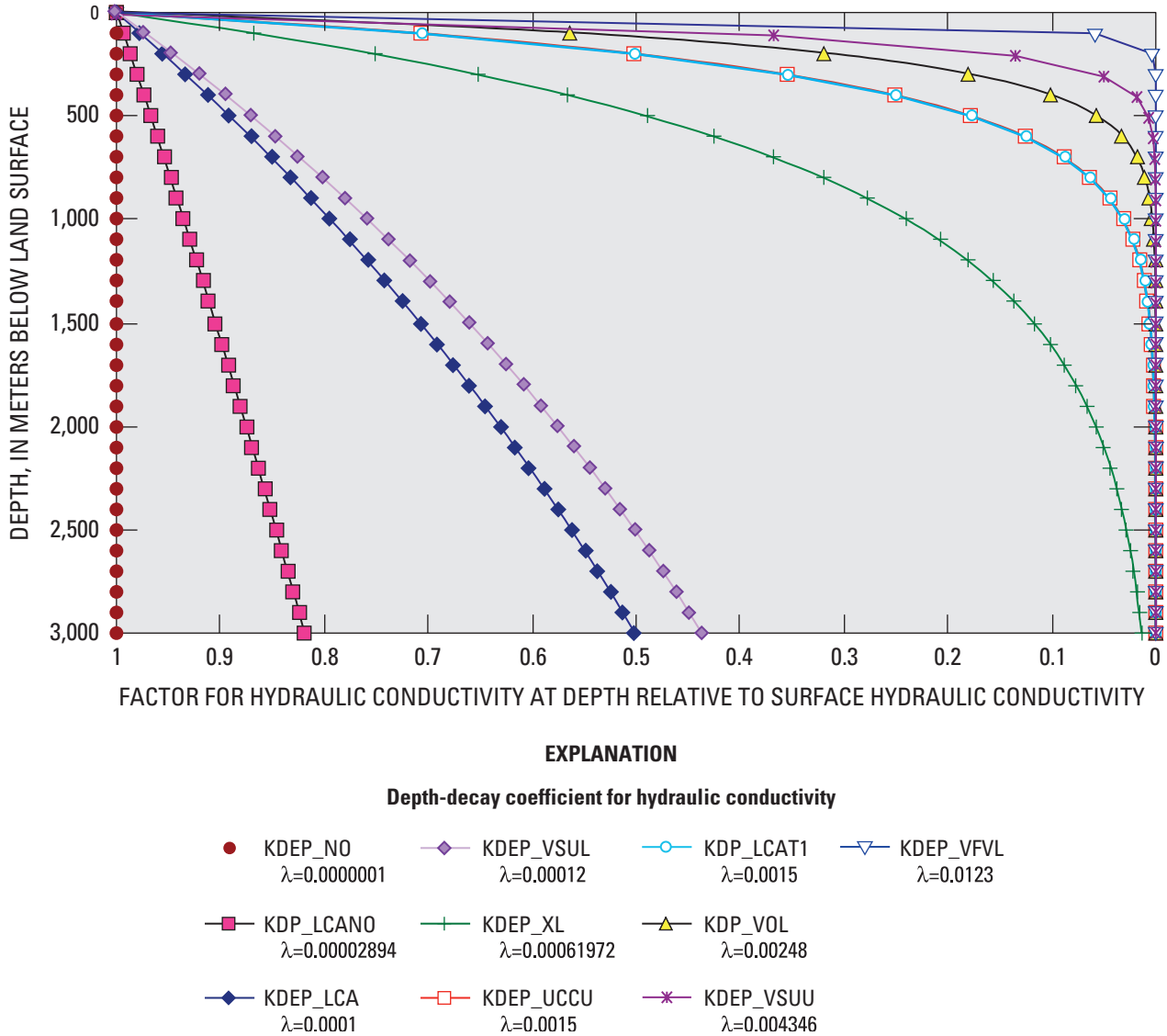


Figure F-35. Hydraulic conductivity values decreasing with depth relative to the surface hydraulic conductivity. The value of each depth-decay parameter is listed for each parameter.

Specific-storage values were determined from literature for the various HGUs in the model domain (table F-14). Specific-storage (S_s) values were used for model layers 2 through 16, and a specific yield (S_y) value was used for layer 1. Storativity values estimated from aquifer tests (Anderson and Woessner, 1992; Belcher and others, 2001) and other modeling studies in the region (Thomas and others, 1996; Schaeffer and Harrill, 1995) are similar to the values used in the DVRFS model (table F-14).

Specifying unique storage property values for each HGU was not necessary. Only those units strongly affected by pumping (predominantly the basin-fill units) were categorized by more than one storage property value. Parameter estimation methods did not provide reasonable storage property values; those values were always unreasonably high. As a result, values of specific storage and specific yield consistent with the

literature (Thomas and others, 1989; Anderson and Woessner, 1992; Schaeffer and Harrill, 1995; Belcher and others, 2001) were specified (set by the user) and the hydraulic conductivities in the basin-fill units, which were most affected by pumping, were re-estimated. Model fit was much better with relatively high values of specific yield. Hence, these values were specified near the upper end of the reasonable range. Errors in simulated heads and discharges associated with errors in storage property values likely are small and were not quantified.

Hydrogeologic Structures

Many of the HFB parameters (fig. F-5) had little effect on the simulation of heads and discharges and were removed as barriers from the flow model. In the final calibration, only nine barriers had a significant effect on heads and discharges

Table F-13. Calibrated vertical anisotropy parameters.

[Abbreviations: ICU, intrusive-rock confining unit; LCA, lower carbonate-rock aquifer; LCA_T1, thrust lower carbonate-rock aquifer; LCCU, lower clastic-rock confining unit; LCCU_T1, thrust lower clastic-rock confining unit; NA, not applicable; OAA, older alluvial aquifer; OACU, older alluvial confining unit; UCCU, upper clastic-rock confining unit; XCU, crystalline-rock confining unit; YAA, younger alluvial aquifer; YACU, younger alluvial confining unit]

Parameter name	Description	Vertical anisotropy value ¹	Composite scaled sensitivity	Coefficient of variation ²
K1_VANI	Confining units (XCU, ICU, UCCU, LCCU, and LCCU_T1)	1.267	0.132	0.5
K2CARBVANI	UCA, LCA, and LCA_T1	1.00	0.125	0.5
K3_VOLVANI	Volcanic-rock units	1.00	0.273	0.47
K4_VFVANIA	Basin-fill aquifers (YAA, OAA, coarser grained parts of upper VSU)	5,000.0	0.119	NA
K4_VFVANIC	Basin-fill confining units (YACU, OACU, finer grained parts of upper VSU)	5,000.0	0.215	NA
K4_VFVANVL	Lower VSU	2.184	0.233	0.5

¹Ratio of horizontal to vertical (values less than 1 indicate higher vertical than horizontal hydraulic conductivity).

²Values were log transformed.

Table F-14. Calibrated storage property values.

[Specific-yield values were used for layer 1, specific-storage values were used for layers 2–16. Values in parentheses for comparison with storage-property values. Abbreviations: ICU, intrusive-rock confining unit; LCCU, lower clastic-rock confining unit; LCCU_T1, thrust lower clastic-rock confining unit; OAA, older alluvial aquifer; OACU, older alluvial confining unit; UCCU, upper clastic-rock confining unit; XCU, crystalline-rock confining unit; YAA, younger alluvial aquifer; YACU, younger alluvial confining unit]

Parameter name	Description	Range of storage properties (specific storage m ⁻¹)	Composite scaled sensitivity	Storage parameter value
STOR_12	Confining units (XCU, ICU, UCCU, LCCU, LCCU_T1); Carbonate-rock aquifers (LCA, LCA_T1, UCA)	¹ 1.5×10 ⁻⁸ – ² 6.3×10 ⁻²	16,127.0	7.0×10 ⁻⁸
STOR_34	Volcanic-rock units; Lower VSU; Basin-fill aquifers (YAA, OAA, LA, upper VSU)	³ 9.7×10 ⁻⁷ – ⁴ 2×10 ⁻²	5,598.5	1.0×10 ⁻⁵
STOR_4VUP	Upper VSU - fine grained, Pahrump Valley	³ 4.7×10 ⁻⁷ – ² 4×10 ⁻²	424.9	7.5×10 ⁻⁵
STOR_4C	Basin-fill confining units (YACU, OACU)	³ 4.7×10 ⁻⁷ – ² 4×10 ⁻²	50.6	5.0×10 ⁻⁵
SY_OTHER	Specific yield for layer 1 in basin-fill units outside the Pahrump Valley (except for upper and lower VSU)	^{1,2,3,4} 0.001 – 0.47	9.5	1.9×10 ⁻¹
SY_PAH	Specific yield for layer 1 in basin-fill units in the Pahrump Valley	^{1,2,3,4} 0.001 – 0.47	13.1	2.0×10 ⁻¹
SY_PUMP	Specific yield for layer 1 in VSU (upper and lower) outside the Pahrump Valley	^{1,2,3,4} 0.001 – 0.47	8.7	1.9×10 ⁻¹

¹Schaeffer and Harrill, 1995.

²Belcher and others, 2001.

³Thomas and others, 1996.

⁴Anderson and Woessner, 1992.

in that they supported the hydraulic gradients (table F-15 and fig. F-5). In particular, the B_LVVSZ_IS parameter (representing part of the LVVSZ) and the B_SOLTARIO parameter (representing the Solitario Canyon fault) have been well documented as to their potential effect on heads in the model domain and had a significant effect on the simulated heads. In most cases, the other potential barriers were found to be unimportant or were adequately represented by the juxtaposition of HGUs in the HFM (Chapter E, this volume).

Recharge

Recharge in the DVRFS model was initially defined using one parameter to vary the net infiltration (Hevesi and others, 2003) throughout the entire model domain by a constant factor (fig. F-6). The CSS value for this parameter during initial model runs was high and generally within the top three most sensitive parameters, indicating that adequate observations existed to describe recharge with additional parameters. Early model runs tended to overestimate net recharge, as was

Table F-15. Calibrated hydraulic characteristic parameters for hydrogeologic structures defined as horizontal-flow barriers.

[Abbreviations: NA, not applicable]

Parameter name	Description	Hydraulic characteristic parameter value (meters per day per meter)	Composite scaled sensitivity	Coefficient of variation ¹
B_HWY95	Highway 95 fault	2.95×10^{-4}	0.046	0.09
B_DVFC_FCR	Death Valley fault zone–Furnace Creek fault zone	1.00×10^{-7}	0.008	0.03
B_LVVSZ_1	Las Vegas Valley shear zone	9.00×10^{-4}	0.005	NA
B_LVVSZ_I2	Las Vegas Valley shear zone	4.19×10^{-8}	0.135	NA
B_PAHRUMP	Pahrump Valley part of Pahrump–Stewart Valley fault zone	5.52×10^{-7}	0.267	0.5
B_LVVSZ_IS	Unnamed splay of the Las Vegas Valley shear zone near Indian Springs	1.1×10^{-8}	0.046	NA
B_DV_N	Northern Death Valley–Furnace Creek fault	2.40×10^{-7}	0.247	NA
B_SOLTARIO	Solitario Canyon fault	4.45×10^{-5}	0.214	NA
B_TC_LINE	Thirsty Canyon lineament	1.00×10^{-7}	0.008	NA

¹Values were log transformed.

evident from comparing the infiltration rates to the ET and spring-flow discharge observations. A recharge zone multiplication array adjusted the net infiltration model (Hevesi and others, 2003) to fit the discharge observations.

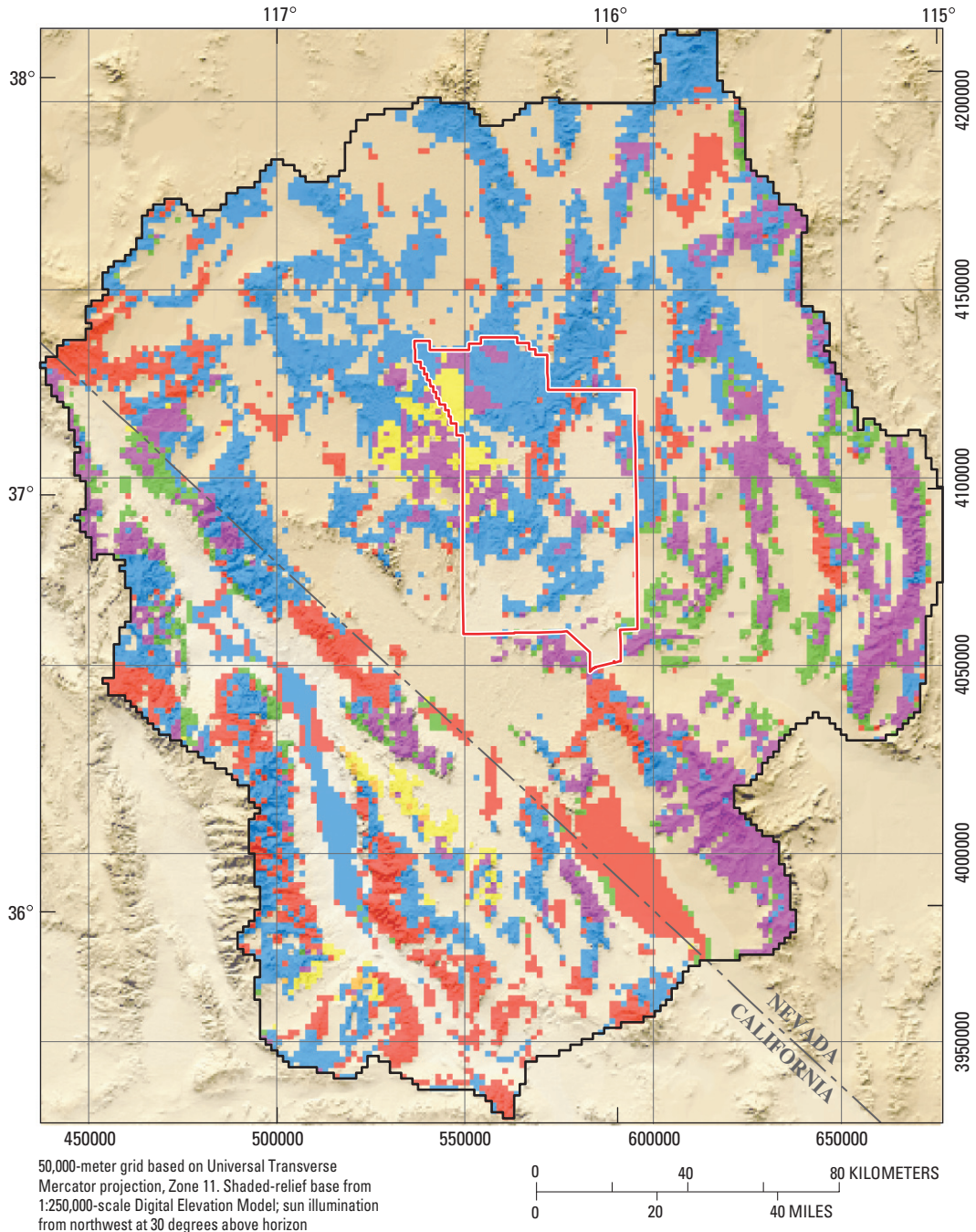
The net-infiltration distribution accounted only for surficial characteristics of the system and not the hydraulic conductivity of the rocks at the water table (Hevesi and others, 2003). Thus, in some areas large recharge rates into rocks with low hydraulic conductivity produced unrealistic simulated hydraulic heads. In reality, the recharge likely was redistributed in the process of percolation. To account for this dynamic, the distribution of recharge was modified by essentially moving high recharge rates from areas where the rocks at the water table were relatively low in permeability to downgradient areas where the rocks at the water table were relatively permeable. This was done by combining net-infiltration rates and the relative permeability of the rocks in the upper five model layers to produce the zones of recharge distribution (fig. F-36). The resulting recharge parameters were multipliers for net infiltration (table F-16).

The parameter zones were created by classifying the top five model layers as either consisting of predominantly (more than 50 percent) relatively higher permeability aquifer material (basin-fill, volcanic-rock, and carbonate-rock aquifers) or relatively lower permeability rocks not identified as aquifers. Cells with aquifer material represent areas where greater permeability would allow rapid infiltration. Because cells with aquifer materials receive most of the infiltration, these cells were further defined by rock type. The logarithm of the infiltration rate was classified into five zones representing areas with no infiltration to those with high infiltration rates. These two classifications (permeability based on rock type and infiltration rates) were combined into the parameters described in table F-16. Some of the parameters were insensitive, so they were combined with parameters having similar recharge multiplier values.

Separate parameters defined for recharge on the high-altitude, carbonate-rock aquifer material contributed the largest volumes of water to the ground-water system (parameters RCH_2 and RCH_8). High recharge rates on the Spring Mountains were necessary to properly simulate discharge in Pahrump Valley, Shoshone and Tecopa basins, Amargosa Desert, and Indian Springs (figs. F-6 and F-36). Parameter RCH_2 was used for recharge on the carbonate-rock aquifer, generally in the Spring Mountains and southern part of the Sheep Range (simulated mean recharge of about 70 millimeters per year [mm/yr]). Parameter RCH_8 was used in the eastern and central western (simulated mean recharge of about 38 mm/yr) part of the model domain. In the final calibration, recharge on the Spring Mountains was 76 percent of the value of net infiltration, whereas recharge on the northeastern and central western parts of the model domain was about 100 percent of the estimate of net infiltration (table F-16). The magnitude of the reduction of net infiltration seems reasonable considering that the composition of the carbonate-rock aquifer material is quite variable between these two areas of the model domain, and the extremely high estimate of net infiltration in the Spring Mountains could not be supported by rocks in the area.

During calibration, a ninth recharge zone was added (RCH_9) where infiltration rates exceeded the hydraulic-conductivity value of the underlying rocks and water ponded more than 20 m above land surface. The recharge rate was assumed to be negligible in these areas, and the recharge parameters (multipliers) in adjacent zones were increased.

In general, the estimated recharge was distributed similarly to the net-infiltration rate of Hevesi and others (2003). For the entire model domain, 92 percent of the net infiltration estimated by Hevesi and others (2003) or 303,415 cubic meters per day was simulated as recharge.



EXPLANATION

Recharge zones and number—

- 2** High infiltration, high permeability
- 3** High to moderate infiltration, low permeability
- 4** Moderate to low infiltration, high permeability
- 5** Low infiltration, low permeability
- 6** Moderate to low infiltration, high permeability with basin fill (and no carbonate or volcanic rocks; none shown)
- 7** Moderate to low infiltration, high permeability with volcanic rocks (and no carbonate rocks)
- 8** Moderate to low infiltration, high permeability with carbonate rocks
- Nevada Test Site boundary**
- Death Valley regional ground-water flow system model grid boundary**

Figure F-36. Recharge zone multiplication array representing infiltration rates and relative permeability in upper five model layers.

Table F-16. Calibrated recharge parameters used as multipliers for infiltration rates defined for the recharge zones.

[NA, not applicable]

Recharge zone number	Relative permeability	Relative infiltration rate	Description	Recharge parameter name	Recharge parameter value ¹	Composite-scaled sensitivity	Coefficient of variation ²
1	NA	None	No infiltration	NA	NA	NA	NA
2	High	High	High infiltration and high permeability (generally carbonate rocks in the Spring Mountains and southern part of the Sheep Range)	RCH_2	0.76	3.22	0.10
3	Low	High to moderate	High to moderate infiltration and low permeability (generally volcanic and(or) clastic rocks)	RCH_35	1.12	3.46	0.13
5	Low	Low	Low infiltration and low permeability (generally volcanic and(or) clastic rocks)	RCH_35	1.12	3.46	0.13
4	High	Moderate to low	Moderate to low infiltration and high permeability on various rock types	RCH_467	1.00	0.115	0.5
6	High	Moderate to low	Moderate to low infiltration and high permeability with basin-fill aquifers present in the upper five layers	RCH_467	1.00	0.115	0.5
7	High	Moderate to low	Moderate to low infiltration and high permeability with volcanic rocks present in the upper five layers	RCH_467	1.00	0.115	0.5
8	High	Moderate to low	Moderate to low infiltration and high permeability with carbonate rocks present in the upper five layers (eastern and central western part of the model domain)	RCH_8	1.00	0.0648	0.5
9	NA	NA	Cells where recharge exceeded hydraulic conductivity	RCH_9	0.000001	0.28×10 ⁻⁸	NA

¹The net-infiltration array values (fig. C-8) are multiplied by this value to calculate the simulated recharge (fig. F-6).

²Values were log transformed.

Ground-Water Discharge

The discharges through ET and spring flow were treated as observations in the flow model, and the conductances of the drain cells were estimated. Initially, the drain cells were divided into five types with the following parameter names (table F-17): (1) DEEP_DRN, warm-water discharge indicates rapid flow from depth and the drain cell is located at the shallowest occurrence of the LCA; (2) UPPER_DRN, flow is through surficial materials that are coarser than playa materials (YAA and OAA); (3) UP_PLY_DRN, flow is through surficial fine-grained playa materials (YACU and OACU); (4) UP_DV_DRN, springs in Death Valley that have substantial salt concentrations; and (5) UP_PAH_DRN, all discharge areas in Pahrump Valley where estimates of discharge over time are available. During calibration, drain conductance parameters were added for the northern part of Death Valley (UP_DVN_DRN) and the Furnace Creek area (FRNCR_DRN).

Hydraulic-Head and Discharge Observations

During calibration, 4,899 observations of hydraulic head and 49 of ground-water discharge and their corresponding weights were evaluated to assess whether the weighting scheme appropriately contributed to model fit. During calibration, weights on five hydraulic-head observations were decreased because of high sensitivity values. Weights on head-change observations in these same locations with particularly large weights also were decreased.

During calibration, the effect of data clustering was examined. The possibility that clustering contributed to the poor fit in areas where observations were limited was tested by grossly increasing the weights on some of the sparsely distributed observations during selected model runs. Because increased weights never significantly improved model fit at these data-sparse locations, calibration difficulties were attributed to some aspect of the model framework or hydrologic conceptualization. The problem then was investigated by examining the hydrologic conceptualization, indicating that

Table F-17. Calibrated drain conductance parameters.

[m/d/m, meter per day per meter; NA, not applicable]

Parameter	Description	Composite scaled sensitivity	Parameter value ¹ (m/d/m)	Coefficient of variation ²
DEEP_DRN	Deep, warm-water springs	1.86	45.6	0.50
UPPER_DRN	Springs in coarse-grained basin-fill deposits	0.70	107.8	0.50
UP_PLY_DRN	Springs in playa deposits	1.78	83.9	0.50
UP_DV_DRN	Death Valley springs with high salt concentrations	0.00855	10,000.0	NA
UP_PAH_DRN	Springs in Pahrump Valley	1.66	195.3	0.50
UP_DVN_DRN	Springs in the northern part of Death Valley	0.145	52.8	0.50
FRNCR_DRN	Spring in the Furnace Creek area	0.00149	10,000.0	NA

¹The parameter value equals the conductance at most cells.²Values were not log transformed.

data clustering is not a significant problem because most of the data clusters are in areas of high hydraulic conductivity, where the sensitivity of hydraulic heads to most parameters is relatively small.

Ground-water discharge observations did not vary throughout the steady-state or transient stress periods, except for Manse and Bennetts Springs in Pahrump Valley. For these springs, one steady-state and two transient discharge observations from 1960 and 1998 were used. All other ground-water discharge observations only appear once in the objective function (eq. 8a). The 49 ground-water discharge observations were combined into 45 discharge observation locations by combining the three observations for Manse and Bennetts Springs into one observation location for each spring.

Modifications also were made to ground-water-discharge observation CVs during the calibration process (but not the observations themselves) because the determination of CVs may not have considered adequately all sources of observation error. Model error, discharge-estimation methods, and magnitude of discharge rate were considered during the calibration process and, where necessary, CVs were modified to reflect (1) the cumulative error, (2) the relative observation importance, and (3) the confidence in the observation.

Final Calibration of Model

As described above, numerous conceptual models were evaluated to test the validity of interpretations of the flow system. For each conceptual model, a new set of parameters was estimated and the resulting simulated hydraulic heads, draw-downs, and ground-water discharges were compared to the observations. Only those conceptual model changes contributing to a significant improvement in model fit were retained. Figures F-37 and F-38 present the estimated parameter values for the final calibration. Figure F-37 shows the values for the hydraulic-conductivity parameters for the confining units, the carbonate-rock units, the volcanic units, and the basin-fill units. Figure F-38 shows the values for the conductances for

the drain parameters, the net-infiltration multiplication factor for the recharge parameters, the values for specific storage and specific yields for the storage property parameters, the values for the vertical anisotropy parameters, and the hydraulic characteristics for the HFB parameters.

Model Evaluation

The calibrated DVRFS model was evaluated to assess the likely accuracy of simulated results. An advantage of using nonlinear regression to calibrate the model is that a substantial methodology exists for model evaluation that facilitates a better understanding of model strengths and weaknesses. A protocol exists to evaluate the likely accuracy of simulated hydraulic heads and ground-water discharges, estimated and specified parameter values and associated sensitivities and confidence intervals, and other measures of parameter and prediction uncertainty. As part of the model evaluation, the regional water budget, the model fit, values of parameter estimates and their associated sensitivities, and boundary flows were evaluated. A qualitative analysis also was performed by comparing the hydrologic conceptual model (Chapter D, this volume) to the overall simulation in several hydrologically significant areas.

Regional Water Budget

The simulated water budgets for the DVRFS for the steady-state prepumping stress period and transient stress period 86 are presented in table F-18 and figure F-39. Stress period 86 (representing year 1997) was used to evaluate the model because there were many observations, and all components except storage were quantified. Many of the observations were quantified with significant accuracy, and some were used as observations in model calibration. The greatest uncertainty is in the representation of recharge.

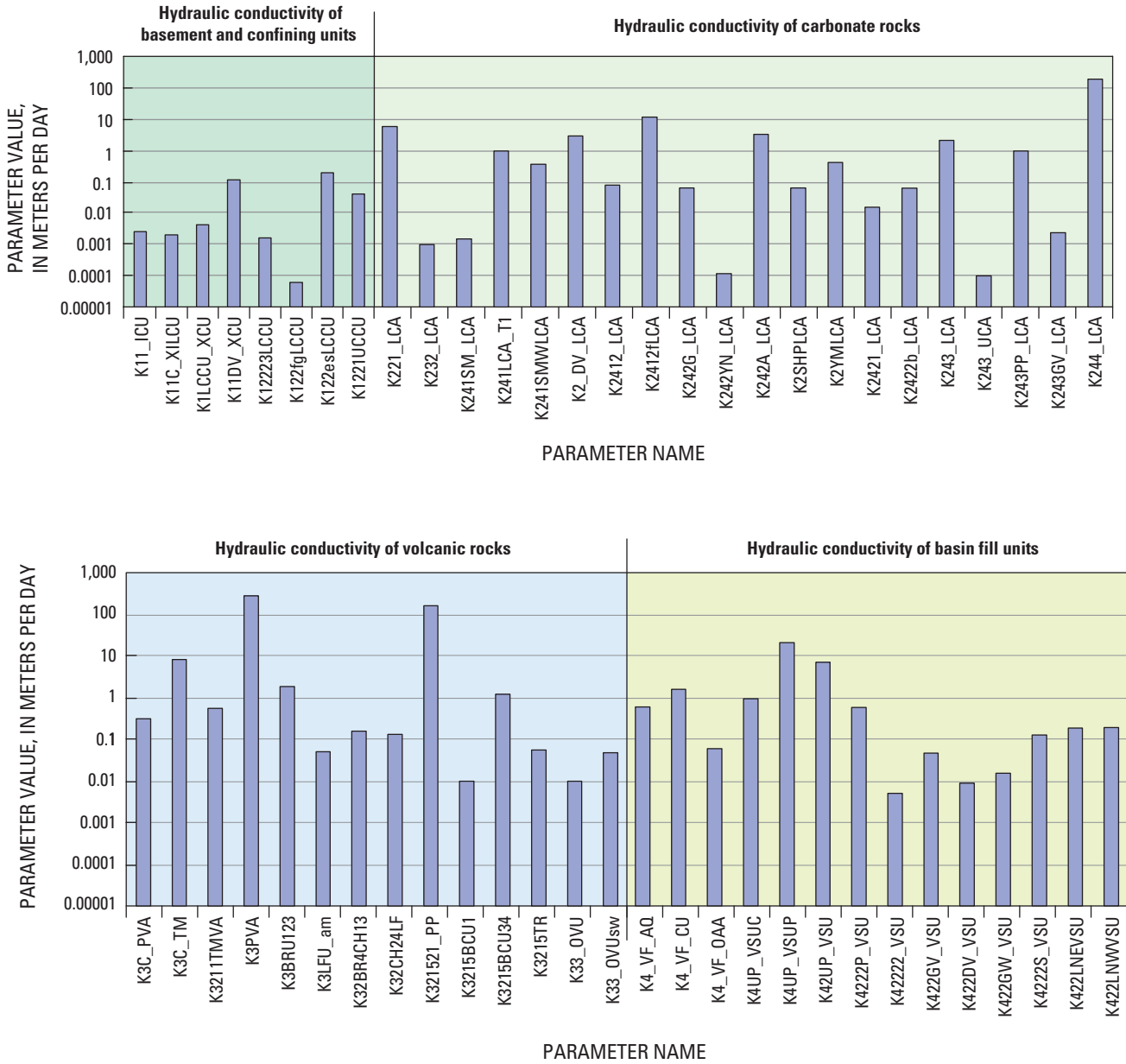


Figure F-37. Parameter values defining hydraulic conductivity for confining units and carbonate rocks, volcanic rocks, and basin-fill units.

Simulated discharges decrease slightly from 361,523 m³/d for the prepumping steady-state stress period to 344,870 m³/d in 1998 (figs. F-39 and F-40). This change can be attributed mostly to pumpage in Pahrump Valley (fig. F-9 and table F-4). In 1997 (transient stress period 86), the sum of observed ground-water discharge is 313,203 m³/d; and the sum of all simulated ground-water discharge is 344,870 m³/d. As of 1998, most of the pumpage came from aquifer storage and is only just beginning to affect the regional discharge from ET and spring flow (fig. F-39).

Flow paths were simulated to evaluate flow directions in the model. For the most part, the model simulates the conceptual model described in Chapter D (this volume). The

major exception was that discharge at the Furnace Creek Wash springs (fig. A-1 in Chapter A, this volume) appears to originate from beneath the north-northwestern part of the Amargosa Desert and areas within the SWNVF rather than from the Spring Mountains through Ash Meadows.

Evaluation of Model Fit to Observations

Model fit is initially evaluated using summary statistics (table F-19) and then through more detailed evaluations, including (1) consideration of results from the prepumping steady-state stress period and the final transient stress period,

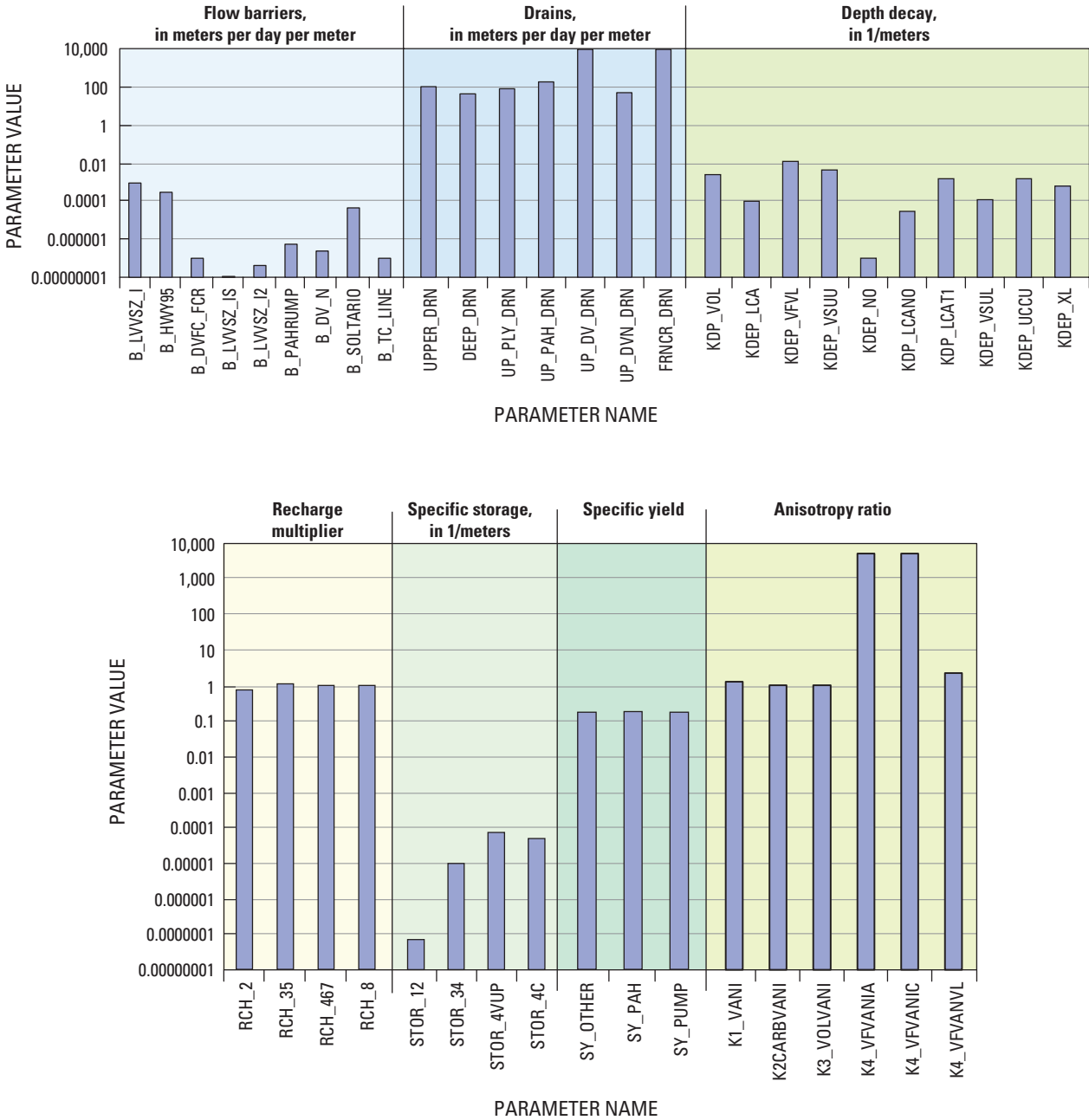


Figure F-38. Parameter values defining flow barriers, drains, and depth decay, recharge, storage, specific yield, and ratio of horizontal to vertical anisotropy.

(2) inspection of hydrographs calculated during transient stress periods, (3) assessment of spatial and temporal distribution of weighted and unweighted residuals, and (4) several graphical analyses. The sum of squared weighted residuals (SOSWR) are shown for completeness but indicate little about model fit. However, the square root of SOSWR divided by the number of observations (Nobs) provides a measure of model fit relative to the weighting that can be compared for different types of observations. A value of 1.0 indicates a match that is, overall, consistent with the observation error evaluation used to determine the weighting. The largest value, 5.4, is for

constant-head boundary flow observations, indicating that the boundary flows are more poorly fit relative to the expected fit than are other types of observations. The second largest value, 3.6, was calculated for discharge observations. The CVs for discharges range from 10 to 71 percent (table F-4). Thus, on average, the difference between observed and simulated discharge can range from 36 to 360 percent of the observed discharge. Although the match to discharges is generally good and considered acceptable (fig. F-41), head-change data fit the observations best, relative to the standard deviations used to weight them.

330 Death Valley Regional Ground-Water Flow System Transient Flow Model
Table F-18. Simulated and observed water budget for the steady-state prepumping stress period and transient stress period 86 (year 1997).

[ET, evapotranspiration; --, not available for combined observations; NA, not applicable]

Water-budget component	Steady-state prepumping stress period				Transient stress period 86, year 1997			
	Observed ¹ (cubic meters per day)	Simulated ¹ (cubic meters per day)	Fractional difference ²	Coefficient of variation	Observed ¹ (cubic meters per day)	Simulated ¹ (cubic meters per day)	Fractional difference ²	Coefficient of variation
Northern Death Valley Subregion								
FLOW IN								
Constant-head segment:								
Clayton	667	7,150	-9.72	0.75	667	7,240	-9.85	0.75
Eureka-Saline	15,100	15,700	-0.04	0.5	15,100	15,906	-0.05	0.5
Stone Cabin-Railroad	12,476	81,500	-5.53	0.96	12,476	85,305	-5.84	0.96
Panamint	15,000	25,400	-0.69	0.5	15,000	25,985	-0.73	0.5
FLOW OUT								
Discharge: ⁶								
Sarcobatus Flat ET	-44,662	-27,458	0.39	--	-44,662	-39,340	0.12	--
Grapevine Canyon Springs	-3,485	-3,245	0.07	--	-3,485	-3,247	0.07	--
Central Death Valley Subregion								
FLOW IN								
Constant-head segment:								
Garden-Coal	⁶ 2,334	12,700	-4.44	0.86	⁶ 2,334	12,678	-4.43	0.86
FLOW OUT								
Constant-head segment:								
Las Vegas	⁶ -3,633	-1,400	0.61	0.96	⁶ -3,633	-1,396	0.62	0.96
Sheep Range	-18,747	-47,390	-1.53	--	-18,747	-47,324	-1.52	--
Pahrangat	⁶ -3,040	-38,210	-11.57	--	⁶ -3,040	-38,548	-11.68	--
Discharge: ⁶								
Penoyer Valley ET	-12,833	-8,040	0.37	0.5	-12,833	-4,890	0.62	0.5
Oasis Valley ET	-20,311	-23,810	-0.17	--	-20,311	-23,630	-0.16	--
Indian Springs area	-2,240	-798	0.64	0.10	-2,240	0	1.00	0.10
Ash Meadows ET	-60,372	-64,106	0.06	--	-60,372	-61,098	-0.01	--
Franklin Well area ET	-1,150	-638	0.45	0.5	-1,150	-520	0.55	0.5
Franklin Lake ET	-3,519	-7,690	-1.19	--	-3,519	-7,240	1.06	--
Death Valley area springs and ET	-128,334	-186,020	-0.45	--	-128,334	-190,690	-0.49	--
Southern Death Valley Subregion								
FLOW IN								
Constant-head segment:								
Silurian	⁶ 500	-1,550	4.10	1.00	⁶ 500	3,710	4.12	1.00
Owlshead	⁶ 1,682	3,670	-1.18	0.89	⁶ 1,680	-1,560	-1.21	0.89
FLOW OUT								
Discharge: ⁶								
Stewart Valley area ET	-3,379	-4,195	-0.24	--	-3,379	-3,842	0.14	--
Pahrump Valley area ET and springs	-32,400	-22,510	0.31	--	-3,378	-9,020	-1.67	--
Tecopa Basin area ET	-21,063	-3,806	0.82	--	-21,063	-3,807	0.82	--
Shoshone Valley area ET	-7,015	-3,620	0.48	--	-7,015	-3,650	0.48	--
Chicago Valley area ET	-1,462	-5,440	-2.72	0.36	-1,462	-5,420	-2.71	0.36

Table F-18. Simulated and observed water budget for the steady-state prepumping stress period and transient stress period 86 (year 1997).—Continued

[ET, evapotranspiration; --, not available for combined observations; NA, not applicable]

Water-budget component	Steady-state prepumping stress period				Transient stress period 86, year 1997			
	Observed ¹ (cubic meters per day)	Simulated ¹ (cubic meters per day)	Fractional difference ²	Coefficient of variation	Observed ¹ (cubic meters per day)	Simulated ¹ (cubic meters per day)	Fractional difference ²	Coefficient of variation
Southern Death Valley Subregion—Continued								
Total IN, constant heads	⁶ 47,759	144,570 (339,601)	--	--	⁶ 47,759	⁷ 149,264 (341,275)	--	--
Pumpage ³	0	0	0	--	--	46,150	--	--
Storage	0	0	0	--	--	221,266	--	--
Recharge	⁴ <342,000	303,415	NA	--	--	303,415	--	--
TOTAL IN:	<397,513	⁷ 447,985 (643,017)	--	--	--	⁷ 723,615 (720,095)	--	--
Total OUT, constant heads	⁶ -25,420	⁷ -87,000 (281,913)	--	--	⁶ -25,420	⁷ -87,000 (-282,306)	--	--
Total, discharge:	-342,225	-361,523	-0.06	--	-313,203	-344,870	-0.07	--
Pumpage	0	0	0	--	NA	-275,978	NA	--
Storage	0	0	0	--	NA	-9,147	NA	--
TOTAL OUT:	--	-448,523 (-342,250)	--	--	NA	-912,301 (-912,302)	NA	--
FLOW IN – FLOW OUT:	--	^{6,7} -538 (-420)	--	--	NA	^{5,7} -192,206 (-194)	--	--

¹Negative values indicate flow out of the model domain.

²Calculated as (observed–simulated)/observed.

³Simulated inflows are mostly from irrigation return flows and injection. A minor part of this is from well-bore inflow between pumping nodes connecting model layers in the Multi-Node Well package (Halford and Hanson, 2002).

⁴Total net infiltration from Hevesi and others (2003). Not used as an observation.

⁵The global budget error from the model in parenthesis. Steady-state is -0.07 percent, transient is -0.02 percent.

⁶Observed constant-head flow is less than that reported in table D-4 (this volume) because of no-flow boundaries applied in the model to subsegments where flow is less than 1,000 cubic meters per day.

⁷Value in parenthesis is cumulative numbers and takes into account flow in and out of given constant head segments. Individual constant head fluxes are composite numbers.

⁸Portions of Death Valley discharge are in northern and southern Death Valley subregion.

The standard error of regression (eq. 9) provides an overall measure of model fit. For the steady-state and transient simulations the standard error of the regression equals 2.7 (table F-19), which indicates that overall model fit is 2.7 times worse than would be consistent with the observation error statistics used to determine observation weights.

Ground-Water Discharge and Boundary Flow

Matching natural ground-water discharge from ET and springs was generally more difficult than matching hydraulic heads and hydraulic-head changes (table F-4) but provided important information for calibration. The overall fit of simulated ground-water discharge and boundary flow to observations is unbiased; simulated values plotted against

observations are randomly scattered about the 1 to 1 line (fig. F-42A). Flow associated with the Stone Cabin–Railroad boundary segment (fig. A2-3 in Appendix 2, this volume) is an outlier where simulated flow into the model is higher than the observed flow. Most water entering the model along this northern boundary segment discharges at Sarcobatus Flat, where simulated discharge rates are less than the observed value. Fractional differences show how close the match was; the CV reflects expected observation error. If the model fits the observations in a manner that on average is as expected, the fractional differences would, on average, be similar to the CVs (table F-4). For the constant-head boundary flows, one weighted residual is greater than, and one weighted residual is less than, three times the standard error. Eighty-seven percent of the constant head boundary flows are within three times the standard error of regression.

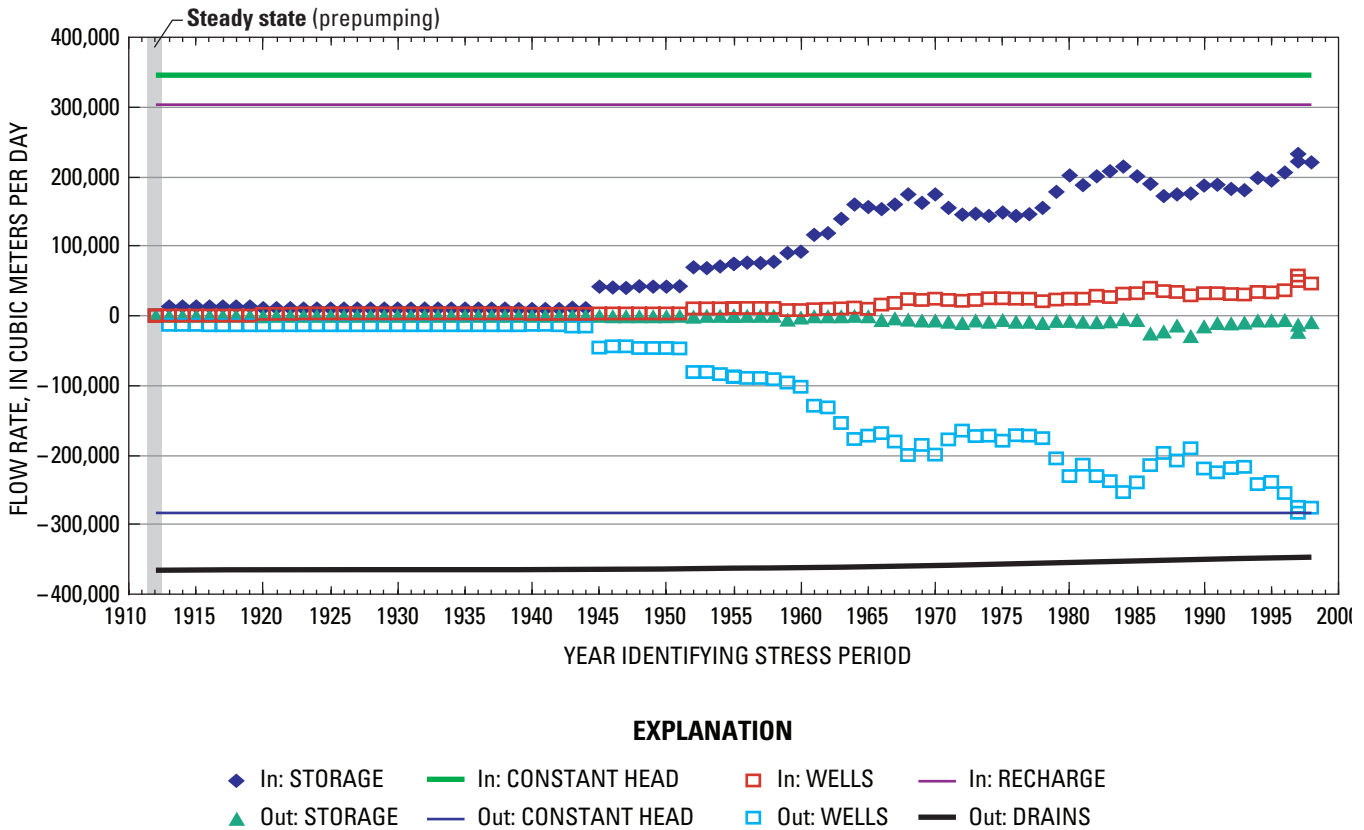


Figure F-39. Total simulated and observed ground-water discharge from evapotranspiration and spring flow for steady state and transient stress periods of the transient model.

Noting that ground-water discharges have been assigned a negative sign indicating flow out of the model, the weighted residuals for ground-water discharges appear to vary randomly about a value of zero with a slight overall bias toward being positive, indicating that simulated discharges in these areas are greater than observed discharges (fig. F-43). The greatest positive unweighted ground-water discharge residuals (simulated greater than observed) by volume (absolute value greater than 10,000 cubic meters/day) are at Death Valley (Cottonball Basin, middle, and Mesquite Flat) (OBS-DV-COTTN, OBS-DV-MIDDL, and OBS-DV-MESQU). The greatest negative unweighted ground-water discharge residuals (simulated less than observed) are at Sarcobatus-northeastern (OBS-SARCO-NE), early observations at Manse Spring in Pahump (OBS-PAH-MANS) and upper Tecopa Valley (OBS-TC-TECOP). The two major discharge areas that contribute the largest error to the model are Death Valley and the Shoshone/Tecopa area. Two of the weighted residuals for ground-water discharges are greater than 8.2 and one is less than -8.2, indicating that 94 percent of the flow-weighted residuals are within three times the standard error of the regression. For the constant-head boundary flows, one weighted residual is greater than, and one weighted residual is less than three times the standard error. Eighty-seven percent of the constant head boundary flows are within three times the regression standard error.

The graph of weighted residuals for ground-water discharge (fig. F-43) indicates how well the model reproduces the observed discharges. An absolute value of 1.0 or less indicates that the residual was less than the standard deviation of the observation error. Weighted residuals that exceed 3.0 are considered to be large. For 35 of the 49 discharge observations, simulated ground-water discharge values are less than three times the standard error (fig. F-44). Simulated discharge from the regional ground-water discharge areas is shown in figure F-45. For these major discharge areas, simulated discharges are within one standard deviation, except at the Shoshone/Tecopa area and Death Valley.

Hydraulic Heads

Comparison of prepumping, steady-state simulated hydraulic heads (figs. F-46 and F-47) with the potentiometric surface of D’Agnese and others (1998) and the potentiometric surface of Appendix 1 (this volume) indicates that the DVRFS model results adequately depict major features of the hydraulic-head distribution. Local mounds of perched water (D’Agnese and others, 1998) are not represented in this simulation. In general, areas of nearly flat and steep hydraulic gradients are appropriately located and important hydraulic gradients are represented:

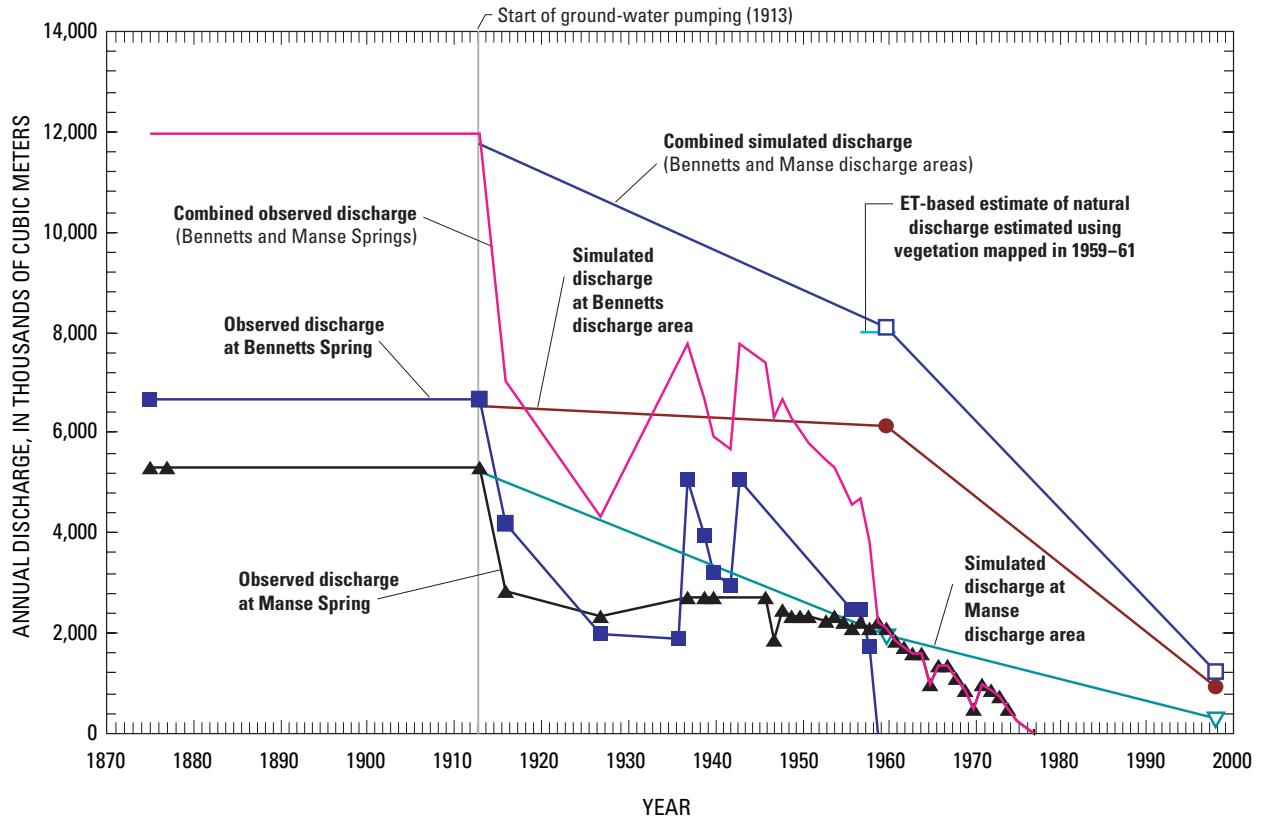


Figure F-40. Simulated and observed annual discharge from regional springs in Pahrump Valley.

Table F-19. Summary statistics for measure of model fit.

[SOSWR, sum of squared weighted residuals; Nobs, number of observations]

Type of observation	Number of observations	Average positive weighted residual	Average negative weighted residual	SOSWR	[SOSWR/Nobs] ^{1/2}
Hydraulic head	2,227	2.1	-1.8	22,702	3.2
Hydraulic-head changes—transient ¹	2,672	1.6	-1.4	13,361	2.2
Discharge	49	2.9	-2.3	637	3.6
Constant-head boundary flow	15	3.7	-3.3	438	5.4
Total	4,963	1.8	-1.6	37,146	2.7
Other statistics					
Number of defined parameters	100				
Number of estimated parameters	Variable				
Standard error of the regression	2.7				

¹Steady-state head observations are included with transient head observations if they are (1) classified as steady-state conditions and (2) located where there were no head observations during the initial steady-state stress period.

- (1) The potentiometric-surface trough on Pahute Mesa, although subdued in the simulation, is represented;
- (2) The generally west-to-east hydraulic gradient in the volcanic rocks at Yucca Mountain is simulated;
- (3) The upward vertical hydraulic gradients from the carbonate-rock aquifer at Yucca Mountain are represented in the simulation (pl. 2, hydrograph [HG] 26); and
- (4) The downward vertical hydraulic gradients in recharge areas of the Spring Mountains (pl. 2) and parts of Pahute Mesa (pl. 2, HG 18, 20, and 28) and upward vertical hydraulic gradients in discharge areas in Pahrump Valley (pl. 2, HGs 11, 12, and 14) and Ash Meadows (pl. 2, HG 1) are represented.

Simulated values plotted against observations generally fall on the 1 to 1 line, indicating a good model fit (fig. F-42B). The fit of simulated to observed hydraulic heads is generally

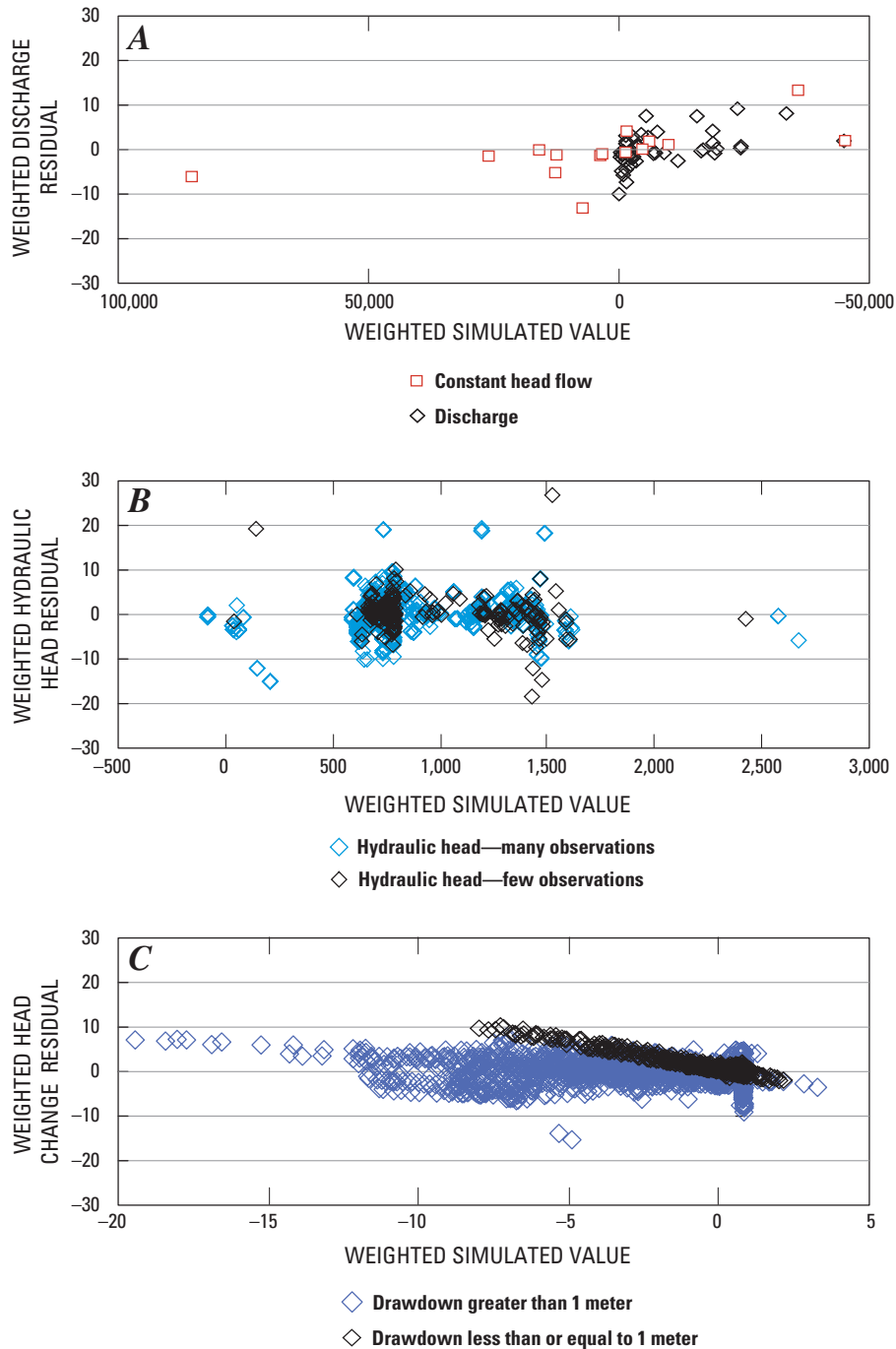


Figure F-41. Weighted residuals and simulated equivalent for (A) hydraulic head, (B) head change, and (C) constant-head flow and discharge.

good (unweighted residuals with absolute values less than 10 m) in most areas of nearly flat hydraulic gradients and moderate (residuals with absolute values of 10 to 20 m) in the remainder of the nearly flat hydraulic gradient areas (primarily in Pahrump Valley) (fig. F-46). The fit of simulated to observed heads is poorer (residuals with absolute values of greater than 20 m) in areas of steep hydraulic gradient. Poorest fit to observed hydraulic heads is in the vicinity of the

steep hydraulic gradient along the Eleana Range and western part of Yucca Flat, and in the southern part of the Owlshead Mountains (fig. F-46). The fits also are poor in the southern part of the Bullfrog Hills and the north-northwestern part of the model domain. Most of these larger residuals can be attributed to (1) insufficient representation of the hydrogeology in the HFM, (2) misinterpretation of water levels, (3) model error associated with grid cell size, or (4) a combination of the first three factors.

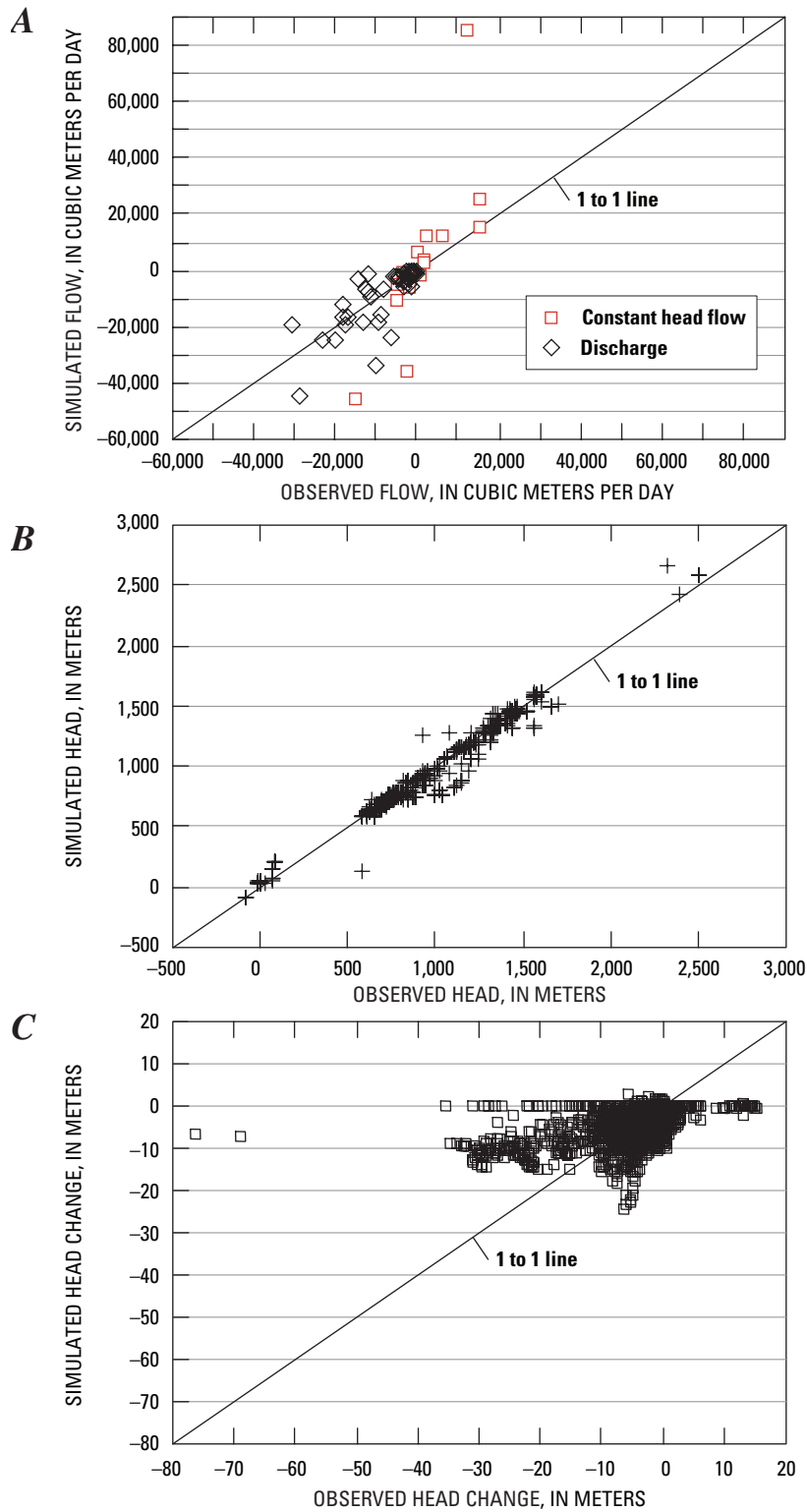


Figure F-42. Weighted observed value compared to weighted simulated values for (A) hydraulic head, (B) head change, and (C) constant-head flow and discharge.

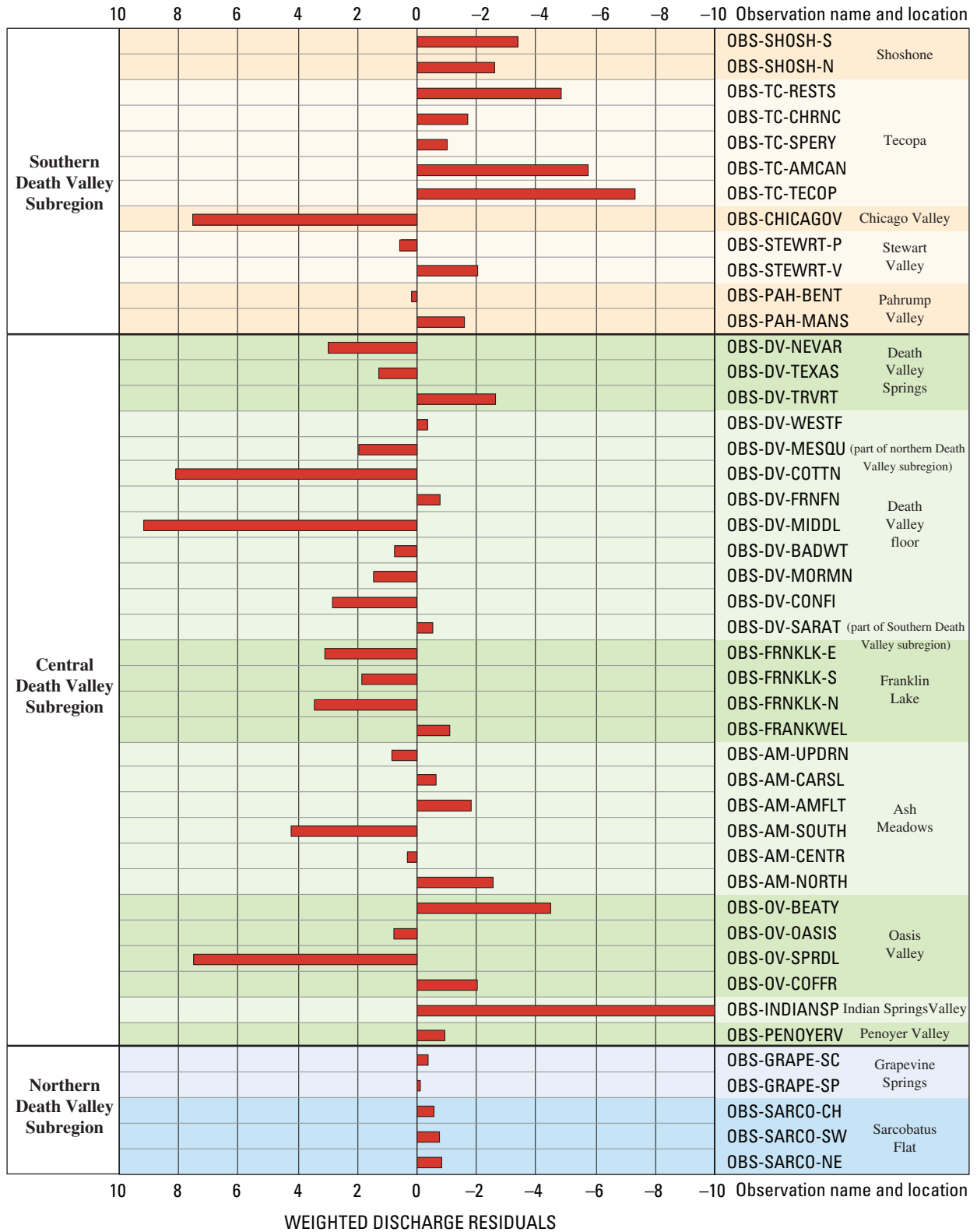


Figure F-43. Ground-water discharge weighted residuals (observed minus simulated).

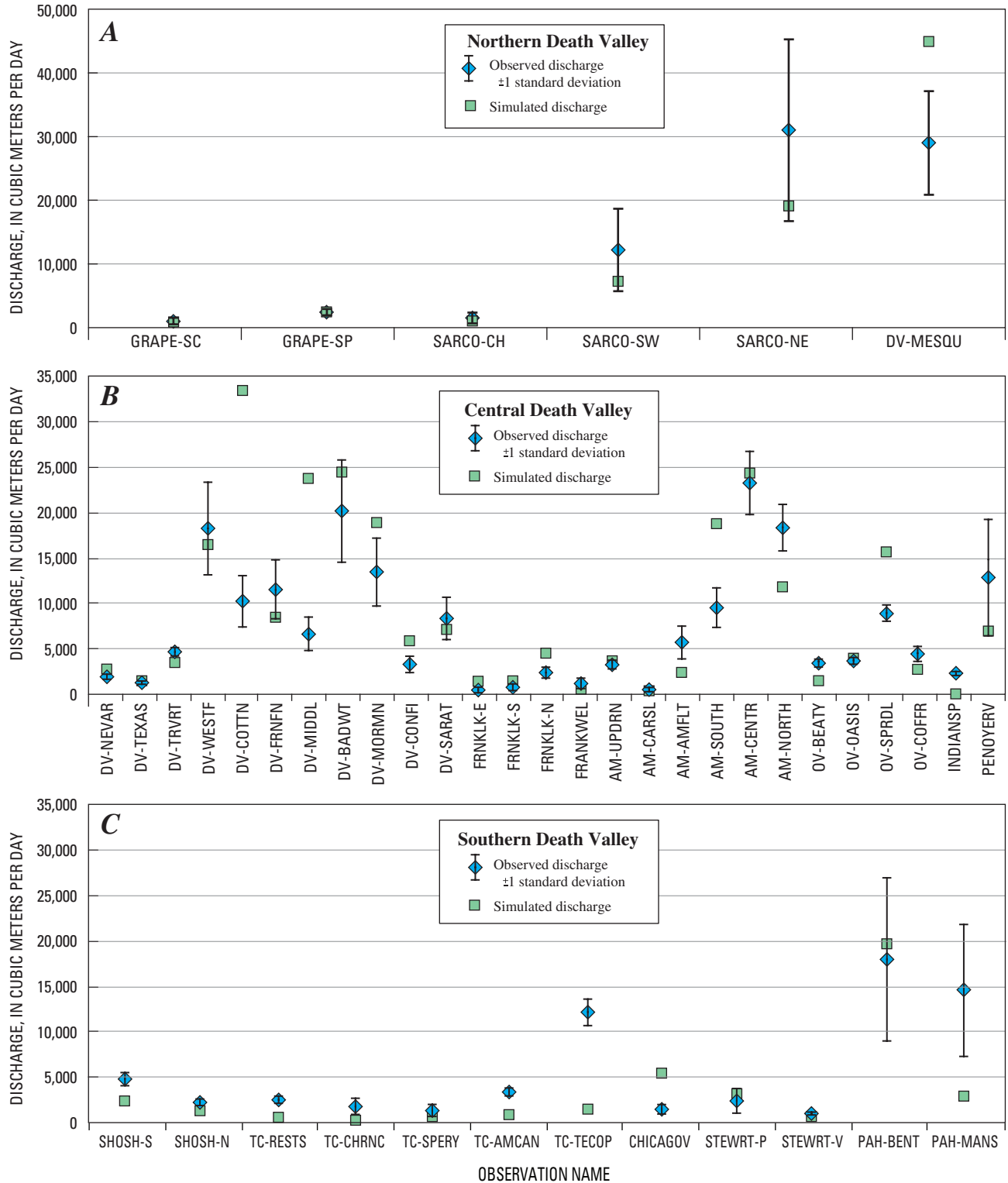


Figure F-44. Observed and simulated ground-water discharge by subregion: (A) Northern Death Valley, (B) Central Death Valley, and (C) Southern Death Valley with expected observed discharge variation.

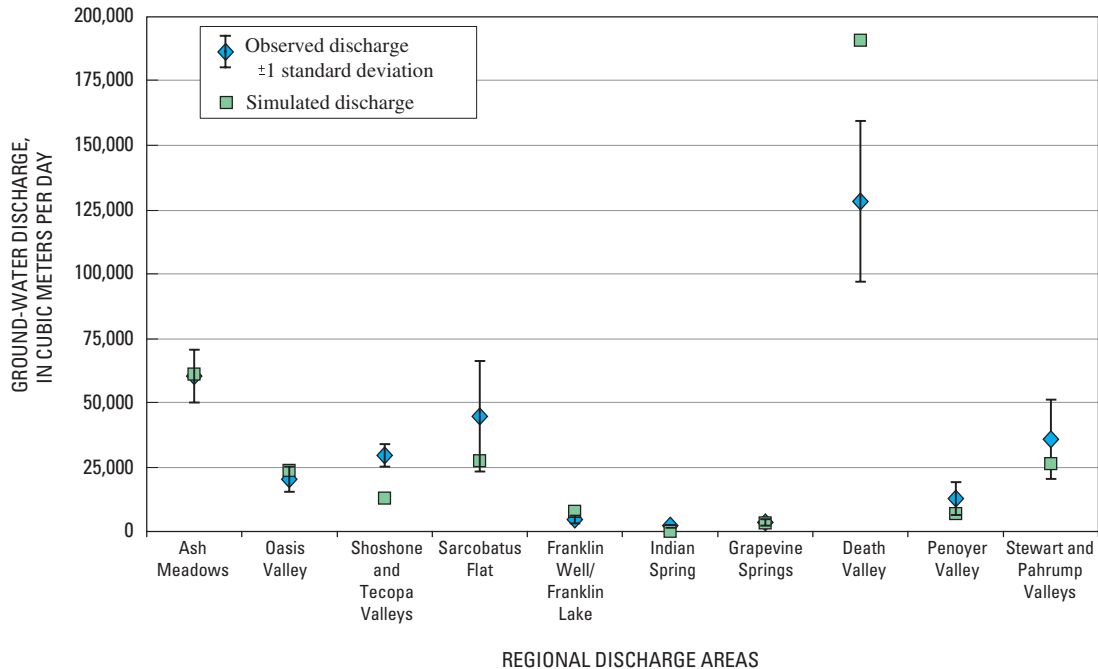


Figure F-45. Observed and simulated ground-water discharge observations by major discharge area with expected observation discharge variation.

Patterns in the spatial distribution of weighted residuals indicate a nonrandom distribution, indicating some model error (fig. F-47). In the northwestern part of the Amargosa Desert, weighted residuals are of moderate magnitude, but heads are consistently simulated lower than observations near the Bullfrog Hills and the slopes of the Funeral Mountains. Heads also are consistently simulated higher than in the northeastern arm of the Amargosa Desert and along the slopes of the southern part of the Funeral Mountains. Although a number of well-matched observations exist, weighted residuals also indicate that heads are simulated higher than observations at the northern part of Pahute Mesa and lower than observations on the southeastern part of Pahute Mesa (fig. F-47). There are four simulated head values of 2,500 m near the peak of the Spring Mountains; these simulated values are greater than observations, possibly indicating model bias. Where concentrated hydraulic-head observations are available for the remainder of the model domain, the distribution of the weighted residuals is random (fig. F-41B).

When plotted against simulated values, most of the weighted residuals for hydraulic heads vary randomly about a value of zero (fig. F-41B). However, 13 head-change weighted-residual values are greater than +8.2, which is three times the regression standard error of 2.7; 3 values are less than -8.2. Thirty-one hydraulic-head weighted-residual values are greater than 8.2; 26 values are less than -8.2. For normally distributed values, only 3 in 1,000 on average would be so different from the expected value. Here, out of about 4,900 observations, 57 are greater in absolute value than three times the standard error of the regression, with most of those being

positive. Although this distribution is slightly biased, it is still largely random. Many of the head observations with large negative weighted residuals can be attributed to steep hydraulic gradients or potentially perched water levels (D'Agnese and others, 1997; D'Agnese and others, 2002). Many of the large positive weighted residuals are along the northern and southern parts of the model boundary, where considerable uncertainty exists in the hydrogeology.

Changes in Hydraulic Heads for the Transient Stress Periods

Changes in hydraulic heads for the transient stress periods were evaluated by assessing head residuals and by examining hydrographs. Weighted values of head change do not fall along a 1 to 1 line, indicating bias (fig. F-42C). Overall, the simulated head change is less than the observed head change, and not enough drawdown was simulated. Additionally, two outliers are located south of Beatty, Nev., where model-predicted drawdown is about 7 m, but 70 m or more of drawdown was observed. The clustering of head changes about the simulated model value of 0 is a result of generally underpredicting drawdown; many simulated head-change values are within about 5 m of observed head changes.

The simulated heads were compared with observed heads by using hydrographs from 869 of the wells in the model domain. Representative hydrographs (pl. 2) are, for the most part, grouped by wells from different pumping areas. In general, the simulated head changes match the observed head changes. Discrepancies between the simulated heads

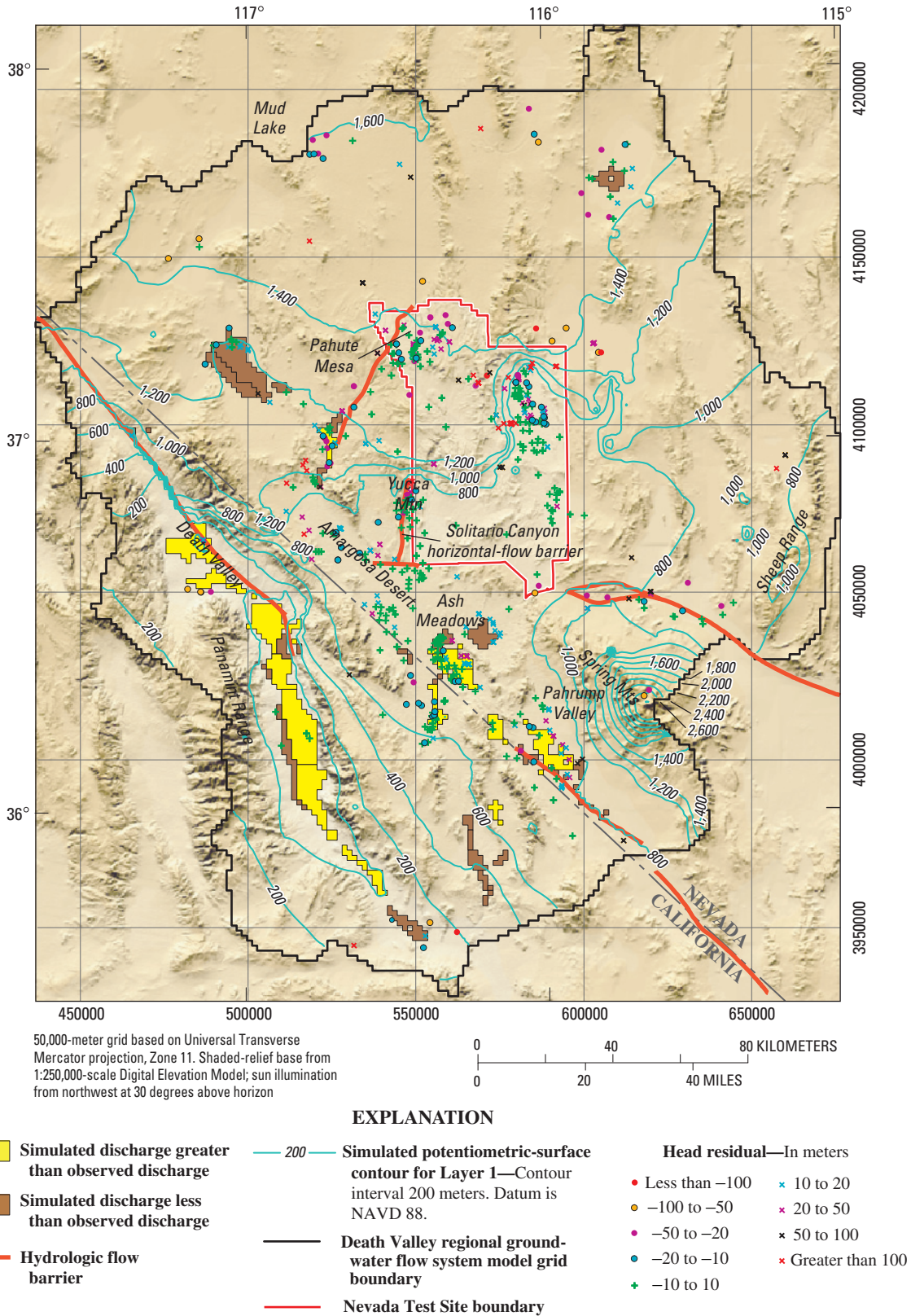


Figure F-46. Steady-state stress period hydraulic-head residuals (observed minus simulated) and simulated potentiometric surface for uppermost active model layer.

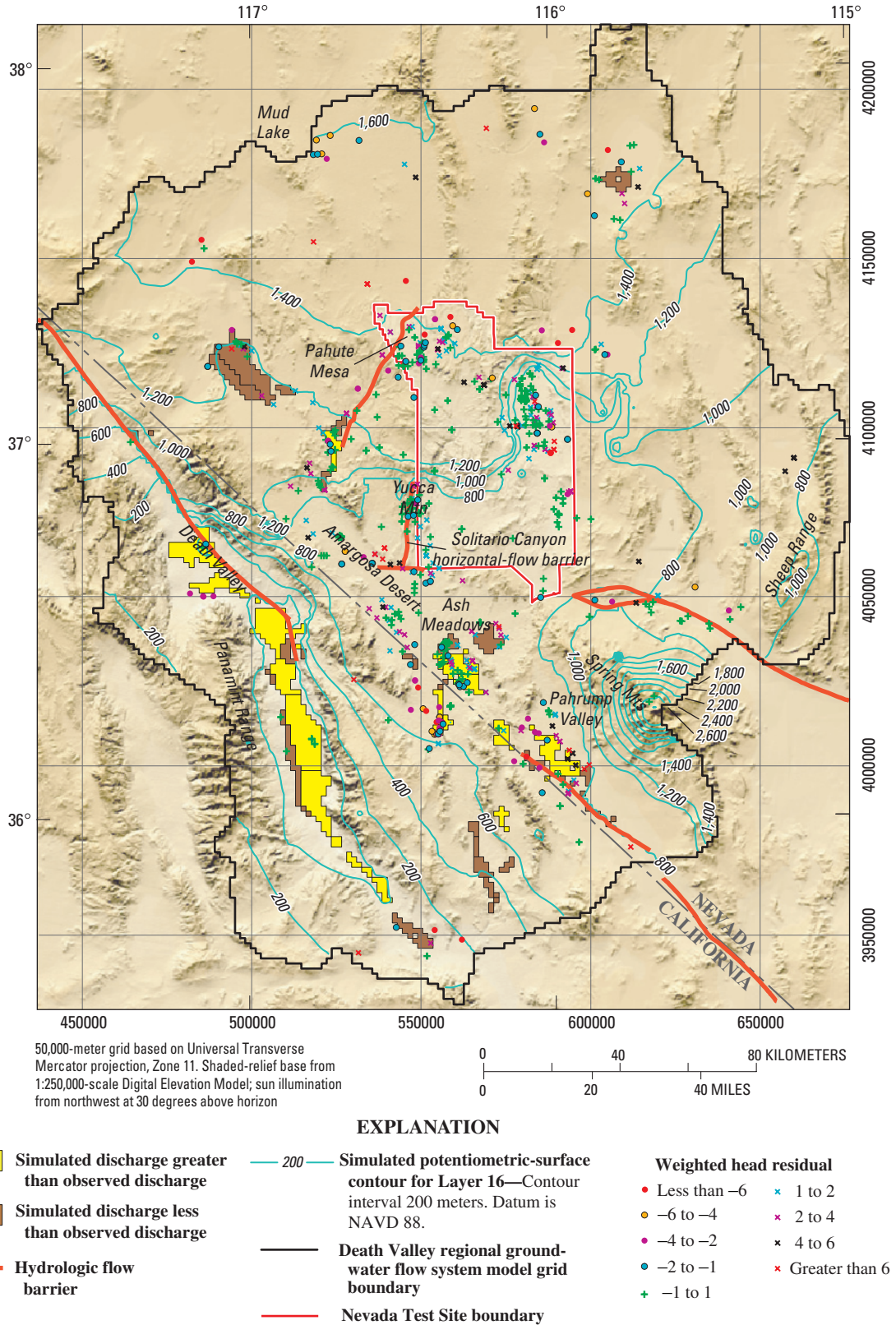


Figure F-47. Steady-state stress period hydraulic-head weighted residuals (observed minus simulated) and simulated potentiometric surface for uppermost active model layer 16.

and the observed heads may be caused, in part, by assuming that pumping is constant during each calendar year. For some areas, the match between simulated and observed values likely could be improved with better estimates of the quantity and temporal distribution of pumping.

For wells in the Amargosa Desert and Penoyer Valley, the observed heads began declining in the 1960's and 1970's, respectively (pl. 2), and these declines were generally matched by simulated heads. The hydrogeologic system at Pahrump Valley appears to be complicated as a result of large amount of pumpage over various time periods from various basin-fill units. Observed heads began to decline significantly in the 1960's and the declines continued, for most locations in Pahrump Valley, until the late 1980's. In some areas, heads are still declining, but in other areas, heads began to recover in the 1990's. Examination of the simulated hydrographs (pl. 2) shows that in some areas in Pahrump Valley these features are matched and in other areas they are not. Because of the complex hydrogeologic system in Pahrump Valley, a more detailed model would be needed to simulate head changes more accurately. The transient simulation is discussed in more detail in the "Evaluation of Hydrologically Significant Areas" section.

Normality of Weighted Residuals and Model Linearity

Linear confidence intervals on estimated parameters are valid only if the model correctly represents the system; that is, weighted residuals are normally distributed and the model is effectively linear. However, normal probability plots for the weighted residuals (not presented here) were not linear. The R^2_N statistic (Hill, 1998, p. 23) equaled 0.871, indicating that the normal probability plot is significantly nonlinear. Correlations among weighted residuals caused by the fitting of the simulated values to the observations could cause the deviation from a straight line. Model linearity was statistically tested using the modified Beale's measure (Cooley and Naff, 1990). The modified Beale's measure calculated for the transient simulation equals 212. This value indicates that the model is highly nonlinear (modified Beale's measure greater than 0.66). This lack of normality of the weighted residuals and the degree of nonlinearity of the model indicate that linear confidence intervals for parameter values may not be valid.

Evaluation of Estimated Parameter Values and Sensitivities

Most of the parameters estimated during model calibration were related to hydraulic conductivity (horizontal hydraulic conductivity, horizontal-flow barriers, drain conductances, vertical anisotropy, and depth decay). Of the 100 defined parameters, 23 were estimated in the steady-state simulation, and 32 were estimated in the transient simulation (fig. F-48 and tables F-8—F-11). The other defined parameters were not estimated because *CSS* and/or *PCC* values indicate that

there is inadequate information to estimate them. Compared to field-measured hydraulic-conductivity estimates (Belcher and others, 2001), estimated parameter values appeared realistic (figs. F-37 and F-38, tables F-8—F-11), revealing very little indication of model error.

Evaluation of Boundary Flows

Although simulated values of flow for each boundary segment (or subsegment) differ somewhat from those reported by Harrill and Bedinger (Appendix 2, this volume), except for the Silurian segment, the direction of flow is simulated accurately and the flows are generally matched well within their estimated error. For the Silurian segment, simulated flow is about 1,500 m³/d out of the model domain, rather than an inflow of 500 m³/d. Despite the generally low-permeability rocks along most of the western boundary, estimates indicate a potential for flow into the model domain across the Clayton, Eureka, Saline, Panamint, and, to a lesser degree, the Owlshead boundary segments (Appendix 2, this volume). The model simulates net flow greater than 1,000 m³/d into the model domain at these segments. Net flow out of the model domain with a net flow greater than 1,000 m³/d across the Las Vegas, Sheep Range, Pahrnatag, and the Silurian boundary segments is simulated. The simulated flow out of the system at parts of the Pahrnatag and Sheep Range boundary segments and the inflow across the Stone Cabin–Railroad boundary segment are much greater than estimated. These differences may result from inaccuracies in the HFM or in the boundary-flow estimates.

Evaluation of Hydrologically Significant Areas

The simulation of the conceptual hydrologic model presented in Chapter D (this volume) was evaluated in several hydrologically significant areas. These areas are: (1) the Sheep Range; (2) the Pahrnatag Range; (3) northern Death Valley and Sarcobatus Flat; (4) the pumping centers of Pahrump Valley, Penoyer Valley, and the Amargosa Desert; and (5) the NTS area (including Yucca Mountain). Hydrochemical, isotopic, and thermal data (see Chapter D, this volume) were used, where possible, to help delineate the flow system and assess whether simulated flow paths were reasonable. These hydrochemical characteristics are used as qualitative information to help in the calibration of the flow model and to indicate where flow directions and magnitudes are reasonable.

Sheep Range

In the original conceptual model of the flow system, the boundary of the model was placed at the flow system boundary in the vicinity of the Sheep Range, which was assumed to coincide with the approximate trace of the Gass Peak thrust fault (fig. F-49 and Chapter D, this volume). On the basis of examination of the limited regional-potential data

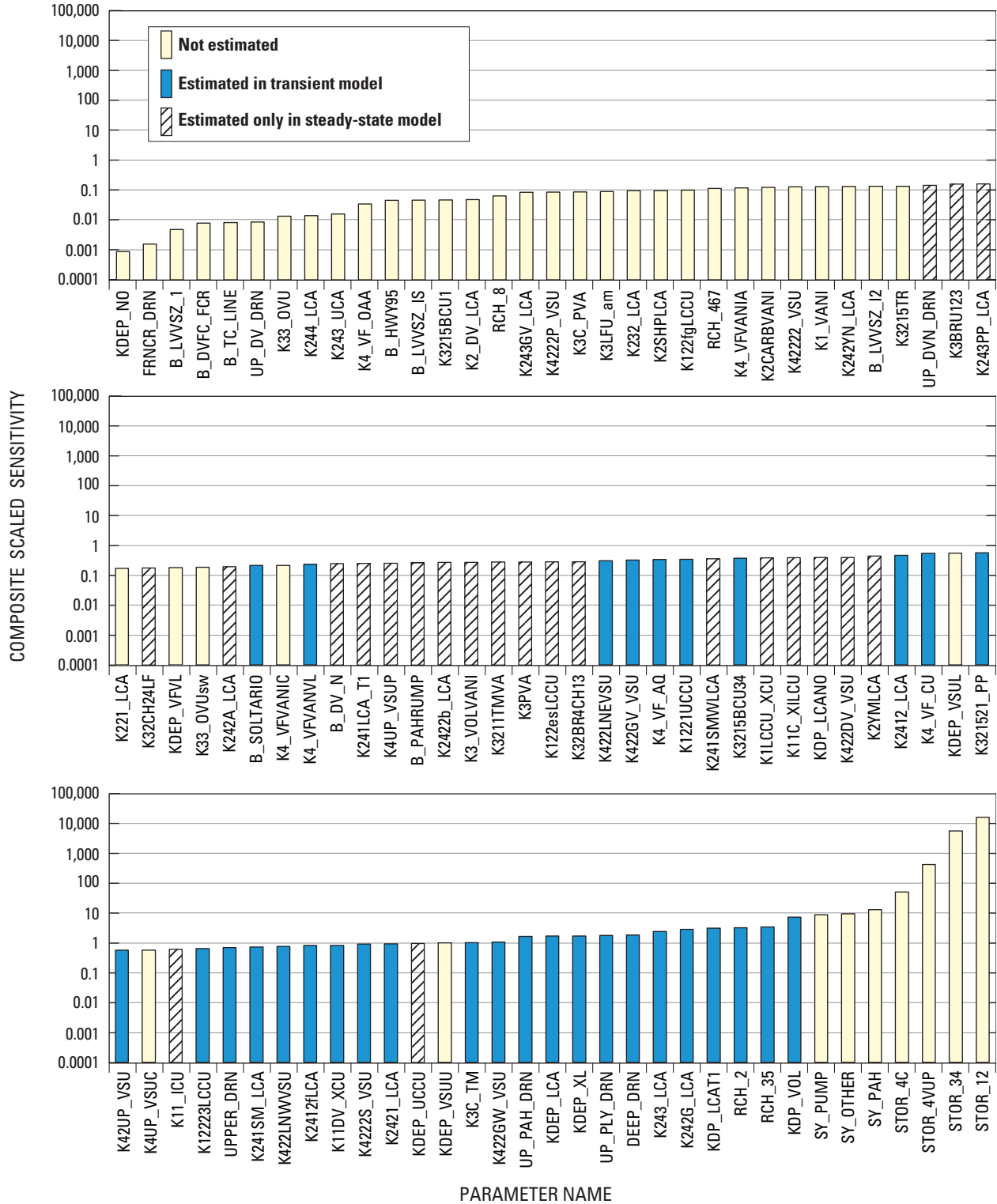


Figure F-48. Composite scaled sensitivities for all parameters. Parameter RCH_9 had a composite-sealed sensitivity of virtually zero and is not included in the figure.

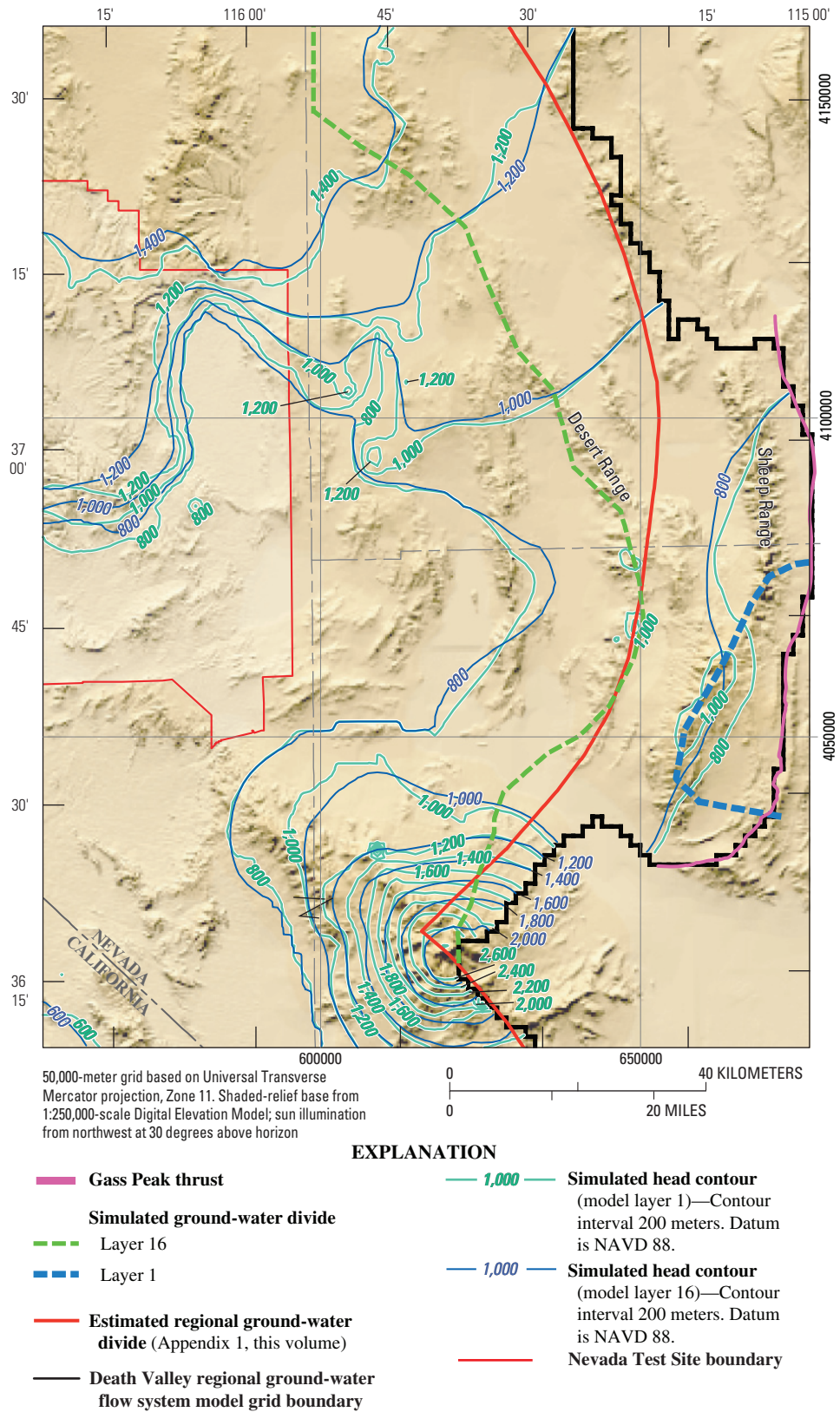


Figure F-49. Model boundary and ground-water divide near Sheep Range with simulated potentiometric surface from model layers 1 and 16.

(Appendix 1, this volume), the flow system boundary actually may be west of the model boundary in the approximate location of the Desert Range (fig. F-49 and pl. 1), and flow east of this ground-water divide would be to the Colorado River ground-water flow system. In the upper layers of the model (layer 1, for example), the location of this ground-water divide is controlled primarily by topography and the presence of recharge areas (fig. F-49). Simulated recharge on the southern Sheep Range exits the model domain to the east.

The simulated ground-water divide is not a vertical plane, and in the deeper parts of the model, the position of the divide is controlled by geology and regional hydraulic gradients. The LCCU in the upper plate of the Gass Peak thrust is modeled in the HFM (Chapter E, this volume) thinner than previous geologic interpretations (Chapter B, this volume), indicating a less effective barrier to ground-water flow. Simulated head for the lower model layers representative of the deep regional system (layer 16, for example), indicates a ground-water divide in the general area of the regional ground-water divide estimated from regional potentiometric data (fig. F-49, pl. 1, and Appendix 1). Differences in the simulated ground-water divide with depth are owing to the scarcity of head data and the relatively large simulated vertical hydraulic conductivity in this area.

Pahranagat Range

Early studies describe the Ash Meadows ground-water basin as potentially receiving ground-water flow from the Pahranagat Range (fig. A-1, and Chapter D, this volume). On the basis of more recent studies (Chapter D, this volume), little to no flow is simulated from the Pahranagat Range to Ash Meadows. An overall net outflow is simulated along the Pahranagat boundary segment. Water enters the system along the Garden-Coal boundary segment and exits along the northern part of the Pahranagat boundary segment. Flow also is simulated entering the model domain across the Pahranagat boundary segment and exiting through the Sheep Range boundary segment.

Northern Part of Death Valley and Sarcobatus Flat

Although the observed heads and spring flow and flow across the Eureka Saline boundary segment appear to be adequately simulated, discharge from drains representing ET is simulated much higher than observed (figs. F-46 and F-47). The steep hydraulic gradient required to simulate discharge to Grapevine Springs and reasonable ET rates in northern Death Valley was maintained by specifying an HFB along the northern Death Valley fault zone. Although geologically reasonable, the extremely low permeability barrier required to produce the observed discharge from Grapevine Springs resulted in simulated heads that are above land surface on the floor of

Death Valley and upgradient from this fault zone. Given the current HFM (Chapter E, this volume), this feature is required to simulate discharge at Grapevine Springs.

This HFB, however, could not simulate the observed discharge at Sarcobatus Flat, even with local recharge. Inflow along the northern model boundary (Stone Cabin–Railroad and Clayton boundary segments) in excess of that estimated (Appendix 2, this volume) was required to simulate heads and observed discharge at Sarcobatus Flat. The excess inflow, the configuration of the HFM, and the constant heads specified along the Stone Cabin–Railroad boundary segment resulted in heads being simulated above land surface at Mud Lake (fig. F-46 and F-47). The simulated discharge at Sarcobatus Flat was less than observed (figs. F-44–F-47).

Pahrump Valley

Although the general trends, heads, and drawdowns are approximated on a regional scale, the DVRFS model appears to lack sufficient detail to accurately simulate ground-water flow in the complex basin-fill system of Pahrump Valley (fig. A-1 in Chapter A, this volume). Heads respond differently to pumping over short distances, so that the heads are accurately simulated in some areas of Pahrump Valley but not in others (pl. 2).

Examination of selected hydrographs for Pahrump Valley (pl. 2, HG 11–17) shows the variable heads and drawdown. In general, trends are simulated; however, spikes are not. The pumping induces hydraulic gradients that increase and decrease with changes in pumping over the simulation period (pl. 2, HG 11, 12, and 14). Pumping in this area appears to decrease from the 1950's on, while pumping in other areas, often in shallower wells, increases (pl. 2, HG 11–14). Plate 2 (HG 11, 13, and 16) shows that the simulated trends are matched fairly well and most of the effects in this area are in layers 1 and 2 (pl. 2, HG 11); however, the simulated trends are subdued (HG 12). A prominent feature of HG 12 is that head observations with the highest weights are matched well, and head observations with lower weights are matched less well, indicating that the lower weights may be contributing to the subdued nature of the hydrograph. In the northern part of Pahrump Valley, wells in model layer 1 are much less affected by pumping than wells in the deeper model layers, with maximum drawdown occurring in the 1990's. Because pumping occurs mostly in the eastern and central parts of the valley, there has been little effect from pumping in the western part of the valley (pl. 2, HG 15). The effect of some of the more recent, larger pumping rates in the eastern part of the valley can be seen on the map of head change (pl. 2) and on HG 13 (pl. 2). A small amount of drawdown in the southeastern part of Pahrump Valley is indicated by a long-term water-level record (pl. 2, HG 17). The simulated heads in this area are less than observed but replicate the small drawdown over time.

In order to simulate the change in natural discharge due to pumping in the Pahrump Valley (including both ET and spring flow), three values of discharge were estimated

from various data for Bennetts and Manse Springs areas (Chapter C, this volume). The discharge observations represent that the springs went dry prior to the end of the simulation period, although ET continued (fig. F-40). Simulated discharge and discharge observations are matched relatively well from 1959 to 1961; however, discharge prior to and after this period is not simulated as accurately. Although a general trend of decreasing simulated discharge with time is evident (fig. F-40), the decrease is not at the same rate as observed. Early-time discharge observations are simulated lower than expected, and late-time observations are simulated higher than expected.

Penoyer Valley

Little is known about the hydrogeology of Penoyer Valley (fig. A-1 in Chapter A, this volume). Given that many of the drains simulating ET in the valley are dry, and the discharge rate is greatly underestimated, the drain altitudes may be simulated higher than is reasonable or the hydrogeologic conditions may not be represented correctly. Most of the wells in the Penoyer Valley are shallow and some areas are affected by drawdown. Head observations (figs. F-46 and F-47) and hydrographs (pl. 2, HG 21-23) show that heads and general trends of head change are matched where pumping does and does not occur. In most areas, heads are matched within 10 m, while in isolated areas, the unweighted head residuals reach 20 m (fig. F-46 and pl. 2). As in other areas, abrupt changes in heads shown in the hydrographs are not simulated. Although this area is adjacent to the model boundary, flow across these boundary segments does not appear to be affected by the pumping. The proximity of the constant-head boundary may also be influencing the high head residuals in this area. To match these head observations, unrealistically low hydraulic conductivity values and high specific storage values were required.

Amargosa Desert

The Amargosa Desert has two main centers of pumping, Ash Meadows and Amargosa Farms. At Ash Meadows, heads generally are matched well in the shallow model layers (layers 1-3) and generally show a small upward hydraulic gradient (pl. 2, HG 1-3 and fig. F-46). In the deeper model layers (fig. F-47), such as those representing the carbonate-rock aquifer at Devils Hole (pl. 2, HG 27), heads are not matched as well and show a small downward hydraulic gradient. Despite the poor fit of simulated and observed head at Devils Hole (pl. 2, HG 27), a small amount of drawdown can be seen in the 1970's and some recovery in late 1970's to early 1980's, simulating the hydraulic connection between the basin-fill units, where pumping is occurring, and the LCA.

Except for a few wells, very little drawdown is seen in the hydrographs (pl. 2). Because of the numerous wells in the area (fig. F-9), most completed without casing, and the simulation

of the hydraulic connection between layers with the MNW package, heads appear to begin to increase in model layer 1 in the 1980's (pl. 2, HG 1). Because of the lack of information required to define the effects of the well-bore inflow, the simulation of flow from higher heads in deeper parts of the system through inactive well bores into lower heads in shallower parts of the system may be incorrect. Drawdown from pumping in nearby wells is superimposed on this increase.

In the Amargosa Farms area, there generally is a good match of simulated to observed heads (<10-m residuals, fig. F-46; pl. 1, HG 4-9), though the match is poor for some wells (pl. 2, HG 10). On the adjacent alluvial fans sloping up to the Funeral Mountains, simulated heads are somewhat lower than observations. Heads are also less well matched in the northwest arm of the Amargosa Desert (fig. F-46, pl. 2, HG 10). Pumping rates in this northwestern area are lower than in other areas in the Amargosa Desert, resulting in less drawdown with strong upward hydraulic gradients. In most areas, the trend of head changes resulting from changes in pumping is matched reasonably well in the model (pl. 2, HG 4-10). Spikes generally are not matched well (pl. 1, HG 8), but some small head changes (pl. 2, HG 5) appear to be local effects and are matched well.

Nevada Test Site and Yucca Mountain

At the NTS, recharge and discharge areas are represented by downward and upward hydraulic gradients in a number of the deeper wells (pl. 2, HG 18-20 and 28). Some heads are simulated higher than observed values, and others are simulated lower than observed values (fig. F-46; pl. 2, HG 18-20). There has been minimal pumping at the NTS, and, as a result, little drawdown is observed in simulated hydrographs (pl. 2, HG 18-20). Fenelon (2000) describes NTS wells in which pumping effects were evident, as is shown in HGs 18 and 28 (pl. 2). More than 10 m of drawdown is measured and simulated in some wells (pl. 2, HG 28).

At Yucca Mountain, simulated hydraulic gradients are generally upward from the carbonate-rock aquifer into the volcanic rocks (pl. 2, HG 26). The potentiometric surface at and to the east of Yucca Mountain is generally flat and the simulated heads are mostly within 10 m of the observations (fig. F-46; pl. 2, HG 25 and 26). The steep hydraulic gradient at the northern end of Yucca Mountain may be caused by perched water levels (Luckey and others, 1996). Because of this possibility, head observations in wells associated with this steep hydraulic gradient were given lower weights. Because of these lower weights and the inability of the model to simulate such a steep hydraulic gradient at a regional scale, a steep hydraulic gradient is simulated, but not as steep as observed. Heads are lower than observations to the north and higher than observations to the south (fig. F-46). A moderate hydraulic gradient on the western side of Yucca Mountain, likely associated with the Solitario Canyon fault (fig. F-46), was simulated by an HFB at the location of the fault. Although some pumping has

occurred periodically for water supply and tests associated with the hydrogeologic characterization of Yucca Mountain, little drawdown is observed at a regional scale.

Model Evaluation Summary

The evaluation of the DVRFS transient model described on the preceding pages indicates that the model simulates observed values reasonably well. The three-dimensional aspects of the flow system are simulated with downward hydraulic gradients in recharge areas and upward hydraulic gradients in discharge areas. Most wells are in discharge areas and as a result, observations and hydrographs are biased to show upward hydraulic gradients.

Pumping from both shallow and deeper layers of the model is imposed early in the transient simulation. Simulation of increased pumping, mostly from the shallow layers for stress periods corresponding to the 1950's and 1980's, resulted in local drawdown cones and reversals of hydraulic gradients. Since 1998, most of the pumpage has come from ground-water storage in the system. A small amount of flow comes from a decrease in discharge at ET areas and springs (mostly in Pahrump Valley). The model underestimates this decrease in natural discharge in Pahrump Valley.

Generally, the simulated boundary flows matched the estimated boundary flows well within their estimated error. Changes in flow across the model boundary segments are negligible, indicating that the effects of pumping have not reached the model boundary.

Evaluation of model fit on the basis of weighted residuals of heads and discharges reveals one or more types of model error: (1) large positive weighted residuals for some head observations in steep hydraulic-gradient areas indicate that simulated heads in these areas are significantly lower than the observations, (2) large negative weighted residuals for ground-water discharge rates in Death Valley indicate that the simulated discharge rate is greater than the observations, (3) large positive weighted residuals for ground-water discharge rates at Sarcobatus Flat indicate that the simulated discharge is smaller than the observations, and (4) positive weighted residuals for ground-water discharge rates in Pahrump Valley in the transient simulations indicate that the simulated discharge rates are greater than the observations.

Model Improvements

The transient model is based on up-to-date geologic and hydrogeologic framework models of the regional flow system. The models represent an intensive integration and synthesis of the available hydrogeologic data and interpretations for the DVRFS.

Data and Data Analysis

The DVRFS ground-water flow model described in this report reflects the current representation of hydrogeologic and hydrologic data for the region. This current understanding affects nearly every aspect of the flow system and improves the constraints on the conceptual and numerical flow models. Improvements in data and data analysis include:

- More detailed description and delineation of the basin-fill units over the entire DVRFS model domain, particularly in the Amargosa Desert,
- Increased understanding of the volcanic-rock stratigraphy at the NTS and Yucca Mountain based on recent drilling,
- Evaluation of recharge using surface-process modeling,
- More accurate and comprehensive measurement of natural ground-water discharge (ET and spring flow),
- More complete compilation and analysis of hydraulic-head and pumpage data, especially in areas not included in previous models, and
- Evaluation of boundary inflows and outflows, resulting in a more realistic depiction of the flow system than in previous conceptual models.

Model Construction and Calibration

In addition to advances in data collection, compilation, and analysis, the ways in which these data were applied in the modeling process also represent significant advances in simulating hydrogeologic systems. For example:

- The DVRFS model simulates transient, long-term regional-scale changes in hydraulic heads and discharges that result from pumpage.
- Using the HUF package allowed the HGU's to be defined independently of model layers, linking the HFM and the flow models more directly. This linkage facilitated testing many different conceptual models.

Model Limitations

All models are based on a limited amount of data and thus are necessarily simplifications of actual systems. Model limitations are a consequence of uncertainty in three basic aspects of the model, including inadequacies or inaccuracies in (1) observations used in the model, (2) representation of geologic complexity in the HFM, and (3) representation of the ground-water flow system in the flow model. It is important to understand how these characteristics limit the use of the model.

Observation Limitations

Observations of hydraulic-head and ground-water discharge, and estimates of boundary flows, constrain model calibration through parameter estimation. Uncertainty in these observations introduces uncertainty in the results of flow-model simulations. Although head and discharge observations were thoroughly analyzed prior to and throughout calibration, there was uncertainty regarding (1) the quality of the observation data, (2) appropriateness of the hydrogeologic interpretation, and (3) the representation of observations in the flow model.

Quality of Observations

The clustering of head observations limits the flow model because it results in the overemphasis of many observations in isolated areas, thus biasing those parts of the model. Outside the Yucca Mountain, NTS, Amargosa Desert, and Pahrump Valley areas, water-level data are sparse, both spatially and temporally. A method of better distributing weights for these situations would reduce model uncertainty.

Some hydraulic-head observations used in the steady-state calibration likely are affected by pumping. Many observations in agricultural areas represent measurements made in pumping wells. Because many of the wells in the Amargosa Desert and Pahrump Valley were drilled at the start of, or after, ground-water development, it is difficult to assess which of these observations best represents prepumping conditions.

The errors in estimates of the model boundary flow also affect the accuracy of the model. Any unknown, and thus unsimulated, flow diminishes model accuracy, and improving the boundary-flow estimates can reduce model uncertainty.

Interpretation of the Observations

It is difficult to assess whether certain head observations represent the regional saturated-zone or local perched-water conditions. Areas of steep hydraulic gradient, which are important features in the regional ground-water flow system, also may be an artifact of perched water levels. The uncertainty used to weight head observations in recharge areas commonly was increased because large head residuals indicated the possibility of perched water. Decreasing the number of observations, or reducing observation weights, increased model uncertainty. Further evaluation of potentially perched water levels in these areas may help to reduce model uncertainty.

Most discharge observations were computed on the basis of vegetated areas, and it is assumed that these areas are similar to their size prior to ground-water development. In some areas, such as Pahrump Valley, this assumption may not be entirely valid because local pumping already had lowered water levels and decreased the size of the discharge areas. The uncertainty in the discharge observations increases uncertainty in the flow model.

Representation of Observations

Because of the small distance affected and comparably large grid-cell size, simulating drawdowns near wells with small pumpage rates (less than 700 m³/d) was difficult because the cones of depression are small relative to the size of the model grid. This limitation may be resolved by creating a higher resolution model, lowering the weights on the observations, or by removing these head-change observations from the model.

The altitude assigned to drains affected the ability of the model to simulate ground-water conditions accurately. The altitude of drains used to simulate discharge through ET and spring flow likely approximates the extinction depth for all discharge areas, particularly in areas with highly variable root depth of plants and discontinuous areas of capillary fringe. Penoyer Valley is an example of a discharge area that may have a zone of fairly extensive capillary effects contributing to ET. The observed heads are lower than the drain altitudes, and the Penoyer Valley drain, or any drain with similar relative heads, will not discharge if the heads are simulated accurately.

Incised drainages and other focused discharge areas are difficult to simulate accurately at a grid resolution of 1,500 m because in many cases, the hydraulic conductivity of the HGUs at the land surface controls the simulated discharge. In situations where this methodology does not control flow, a consistent method for assigning drain conductance needs to be used.

Hydrogeologic Framework Limitations

The accuracy of the ground-water flow model depends on the accuracy of the hydrogeologic conceptual model. Limitations exist in the ground-water flow model because of the difficulties inherent in the interpretation and representation of the complex geometry and spatial variability of hydrogeologic materials and structures in both the HFM and the flow model.

Complex Geometry

Geometric complexity of hydrogeologic materials and structures is apparent throughout the model domain. One notable example is the Las Vegas Valley Shear Zone (LVVSZ). Simulation of heads in this area is limited by the current understanding of fault-system geometry and the accuracy and resolution of its representation in the HFM and in the ground-water flow model.

Similarly, the steep hydraulic gradient that extends from the Groom Range through the Belted and Eleana Ranges to Yucca Mountain and the Bullfrog Hills is inadequately simulated because of an incomplete understanding of the complex geometries in this area. However, the steep hydraulic gradient also is simulated inadequately because of simplifications inherent in the HFM and ground-water flow model construction and discretization.

Complex Spatial Variability

The spatial variability of material properties of the HGUs and structures is represented to some degree in the model (Chapter B, this volume). Incorporating these features in the flow model substantially improved the simulation; however, the model remains a significantly simplified version of reality, resulting in imperfect matching of hydraulic gradients and heads affected by detailed stratigraphy not represented in the HFM. In the ground-water flow model, the assumption of homogeneity within a given HGU or hydraulic-conductivity zone removes the potential effects of smaller scale variability. A particularly noteworthy area where poor model fit exists is in the vicinity of Oasis Valley and the Bullfrog Hills. In this area, the observed effects of hydrothermal alteration are characterized incompletely by data and inadequately represented in the HFM and the ground-water flow model. Many of the inadequacies in the simulation of heads within the SWNVF are caused in part by the underrepresentation of local-scale hydrogeologic complexities in the HFM and the ground-water flow model.

Flow Model Limitations

Three basic limitations of the flow model are inherent in its construction. These inaccuracies are in (1) representation of the physical framework, (2) representation of the hydrologic conditions, and (3) representation of time.

Representation of Physical Framework

While the 1,500-m resolution of the flow model grid is appropriate to represent regional-scale conditions, higher resolution would improve simulation accuracy, particularly in areas of geologic complexity. The large grid cells tend to generalize important local-scale complexities that affect regional hydrologic conditions. To represent more local dynamics, smaller grid cells throughout the model (or local refinement around selected features or in critical areas in the model domain) would be required.

Representation of Hydrologic Conditions

The hydrologic conditions represented by the model are expressed as boundary conditions and include recharge, lateral boundary flows, discharge from ET and springs, and pumpage. Of these boundary conditions, the most significant is recharge. The main limitation in the representation of recharge is the inaccurate estimation of net infiltration that likely is owing in large part to the assumption that net infiltration results in regional recharge. The net-infiltration model likely overestimates recharge in many parts of the model domain because it is assumed that all infiltrating water that passes the root zone ultimately reaches the water table. This assumption ignores the possibility that infiltrating water could be intercepted and

either diverted or perched by a lower permeability layer in the unsaturated zone, or the possibility of deep evaporation from the unsaturated zone. This limitation may be resolved by including in the flow model a means to account for deep, unsaturated zone processes that may act to reduce or redistribute infiltrating water.

Limitations in the definition of lateral boundary flow are the result of incomplete understanding of natural conditions. Because very little data exist in the areas defined as lateral flow-system boundary segments, all aspects of the assigned boundary conditions are poorly known. Despite these uncertainties, the data used to characterize these boundary flows have been thoroughly analyzed for this model. The model does not simulate the complex process of ET but accounts for the ground-water discharge attributed to ET through use of the Drain package for MODFLOW-2000. ET by native vegetation was studied extensively. Future revisions of the DVRFS model might be improved by using a more complex ET package instead of the Drain package. This package could incorporate spatially varying parameters to simulate direct recharge, soil moisture, and vegetative growth.

Representation of Time

The year-long stress periods simulated in the model limit its temporal applicability to dynamics that change over at least several years. Simulation of seasonal dynamics using shorter stress periods could be advantageous to account for the seasonal nature of irrigation pumpage. Such a simulation would require seasonal definition of hydrologic conditions.

Appropriate Uses of the Model

Because the DVRFS model was constructed to simulate regional-scale ground-water flow, it can be used to answer questions regarding ground-water flow issues at that scale. For example, interactions can be considered between hydraulic heads, discharge, pumping, and flow direction and magnitude on a regional scale.

The model can provide boundary conditions for the development of local-scale models, such as those being developed by the Department of Energy for both the NNSA/NSO and ORD programs. Consistency between regional and local models must be ensured. Advances in linking regional- and local-scale models may allow for simultaneous calibration and uncertainty analysis. Although regional scale by design, the DVRFS model includes many local-scale features and site-specific data. Local features include facies changes and pumpage from one or a few wells. In some circumstances the model could be used to evaluate the regional consequences of such local features. Yet, some regional consequences and all local consequences would be evaluated most effectively using local-scale models in combination with simulations from the regional model.

The model can be used to evaluate alternative conceptualizations of the hydrogeology that are likely to have a regional effect. These might include the effects of increased recharge caused by climate change, different interpretations of the extent or offset of faults, or other conceptual models of depositional environments that would affect the spatial variation of hydraulic properties.

The model also can be used to provide insight about contaminant transport. Flow direction and magnitude are appropriately represented using particle tracking methods as long as the particle paths are interpreted to represent regional, not local, conditions. The model may be a useful tool for evaluating advective-transport flow paths that are at least several times longer than the length of a 1,500-m model cell (Hill and others 2001; Tiedeman and others, 2003).

Increased urbanization in southern Nevada necessitates the development of ground-water resources. The model can be used for examining the effects of continued or increased pumpage on the regional ground-water flow system to effectively manage ground-water resources within conflicting land-use management policies.

Summary

The Death Valley regional ground-water flow system was simulated by a three-dimensional (3D) model that incorporates a nonlinear least-squares regression technique to estimate aquifer parameters. The model was constructed with MODFLOW-2000, a version of the U.S. Geological Survey 3D, finite-difference, modular ground-water flow model in which nonlinear regression may be used to estimate model parameters that result in the best fit to measured heads and discharges.

The model consists of 16 layers, on a finite-difference grid of 194 rows and 160 columns, and uniform, square model cells with a dimension of 1,500 meters (m) on each side. Model layers are simulated under confined flow conditions, so that the top of each layer and its thickness are defined. Although the top of the actual flow system is unconfined, the model accounts for the position of the simulated potentiometric surface in the top model layer to account for the thickness of the top layer and approximate unconfined flow conditions. Prepumping conditions were used as the initial conditions for the transient-state calibration of the model. Transmissivity is temporally constant and is spatially defined by hydrogeologic units (HGUs) and zones within some of these units. Storage properties were constant in time.

The model design was based on a 3D hydrogeologic framework model (HFM) that defines the physical geometry and composition of the surface and subsurface materials of 27 HGUs through which ground water flows. The HFM defines the geometry of the HGUs in the model domain (the area inside the model boundary).

Several conceptual models were evaluated during calibration to test the validity of various interpretations about the flow system. The evaluation focused on testing alternative hypotheses concerning (1) the location and type of flow system boundaries, (2) the definition of recharge areas, and (3) variations in interpretation of the hydrogeologic framework. For each conceptual model, a new set of parameters was estimated, and the resulting simulated hydraulic heads, drawdowns, ground-water discharges, and boundary flows were compared to observed values. Only those conceptual model changes contributing to a significant improvement in model fit were retained in the final calibrated model.

Ground-water flow into the model is from the simulation of infiltration of direct precipitation (recharge) and, to a lesser extent, from the simulation inflow across the model boundary. The distribution of simulated recharge varies spatially but is held at a constant rate for the entire simulation period. Ground-water flow out of the model primarily is through simulated ET, spring flow and pumping, and, to a lesser extent, by outflow across the model boundary. Observations of the combined discharge by ET and spring flow and estimated boundary flows were used to calibrate the model.

Boundary flows into and out of the model domain were simulated using head-dependent boundaries that were assigned the regional potentiometric surface altitude. Because previous models of the system generally used no-flow boundaries, the representation of inflow and outflow across the model boundary from adjacent systems are significantly different. In particular, ground-water flow from the north is simulated to sustain heads in the northern parts of the Nevada Test Site and, in particular, discharge around Sarcobatus Flat.

The final calibration was evaluated to assess the accuracy of simulated results by comparing measured and expected values with simulated values. The fit of simulated heads to observed hydraulic heads is generally good (residuals with absolute values less than 10 m) in most areas of nearly flat hydraulic gradients, and moderate (residuals with absolute values of 10 to 20 m) in the remainder of the areas of nearly flat hydraulic gradients. The poorest fit of simulated heads to observed hydraulic heads (residuals with absolute values greater than 20 m) is in steep hydraulic-gradient areas in the vicinity of Indian Springs, western Yucca Flat, and the southern Bullfrog Hills. Most of these inaccuracies can be attributed to (1) insufficient representation of the hydrogeology in the HFM, (2) misinterpretation of water levels, and (3) model error associated with grid cell size.

Ground-water discharge residuals are fairly random, with as many areas in which simulated discharges are less than observed discharges as areas in which simulated discharges are greater than observed. The largest unweighted ground-water discharge residuals are in Death Valley and Sarcobatus Flat (northeastern area). The two major discharge areas that contribute the largest volumetric error to the model are the Shoshone/Tecopa area and Death Valley. Positive

weighted residuals were computed in transient simulations of the Pahrump Valley that may indicate a poor definition of hydraulic properties and(or) discharge estimates, especially near Bennetts Spring.

Parameter values estimated by the regression analyses were reasonable—that is, within the range of expected values. As with any model, uncertainties and errors remain, but this model is considered an improvement on previous representations of the flow system.

The model is appropriate for evaluation of regional-scale processes. These include the assessment of boundary conditions of local-scale models, the evaluation of alternative conceptual models, the approximation of aspects of regional-scale advective transport of contaminants, and the analysis of the consequences of changed system stresses, such as those that would be imposed on the system by increasing pumpage.

Inherent limitations result from uncertainty in three basic aspects of the model: inadequacies or inaccuracies in observations used in the model, in the representation of geologic complexity in the HFM, and representation of the ground-water flow system in the flow model. It is important to understand how these characteristics limit the use of the model. These basic aspects of the model are represented at a regional scale, and the use of the model to address regional-scale issues or questions is the most appropriate use of the model.

References Cited

- Anderman, E.R., and Hill, M.C., 2000, MODFLOW-2000, The U.S. Geological Survey modular ground-water flow model—Documentation of the hydrogeologic-unit flow (HUF) package: U.S. Geological Survey Open-File Report 00–342, 89 p.
- Anderman, E.R., and Hill, M.C., 2003, MODFLOW-2000, The U.S. Geological Survey modular ground-water flow model—Three additions to the hydrogeologic-unit flow (HUF) package—Alternative storage for the uppermost active cells (STYP parameter type), flows in hydrogeologic units, and the hydraulic conductivity depth-dependence (KDEP) capability: U.S. Geological Survey Open-File Report 03–347, 36 p. Accessed April 14, 2004, at <http://water.usgs.gov/nrp/gwsoftware/modflow2000/modflow2000.html>
- Anderman, E.R., Hill, M.C., and Poeter, E.P., 1996, Two-dimensional advective transport in ground-water flow parameter estimation: *Ground Water*, v. 34, no. 6, p. 1001–1009.
- Anderson, M.P., and Woessner, W.W., 1992, Applied ground-water modeling—Simulation of flow and advective transport: San Diego, Calif., Academic Press, Inc., 381 p.
- Bard, Jonathon, 1974, Nonlinear parameter estimation: New York, Academic Elsevier, 476 p.
- Bedinger, M.S., Langer, W.H., and Reed, J.E., 1989, Ground-water hydrology, in Bedinger, M.S., Sargent, K.A., and Langer, W.H., eds., Studies of geology and hydrology in the Basin and Range Province, southwestern United States, for isolation of high-level radioactive waste—Characterization of the Death Valley region, Nevada and California: U.S. Geological Survey Professional Paper 1370–F, p. 28–35.
- Belcher, W.R., Elliott, P.E., and Geldon, A.L., 2001, Hydraulic-property estimates for use with a transient ground-water flow model for the Death Valley regional ground-water flow system, Nevada and California: U.S. Geological Survey Water-Resources Investigations Report 01–4210, 28 p., accessed on September 1, 2004 at <http://water.usgs.gov/pubs/wri/wri014210/>
- Cooley, R.L., and Naff, R.L., 1990, Regression modeling of ground-water flow: U.S. Geological Survey Techniques of Water-Resources Investigations, book 3, chap. B4, 232 p.
- D’Agnese, F.A., Faunt, C.C., Turner, A.K., and Hill, M.C., 1997, Hydrogeologic evaluation and numerical simulation of the Death Valley regional ground-water flow system, Nevada and California: U.S. Geological Survey Water-Resources Investigations Report 96–4300, 124 p.
- D’Agnese, F.A., Faunt, C.C., and Turner, A.K., 1998, An estimated potentiometric surface of the Death Valley region, Nevada and California, using geographic information systems and automated techniques: U.S. Geological Survey Water-Resources Investigations Report 97–4052, 15 p., 1 plate.
- D’Agnese, F.A., O’Brien, G.M., Faunt, C.C., Belcher, W.R., and San Juan, Carma, 2002, A three-dimensional numerical model of prepumping conditions in the Death Valley regional ground-water flow system, Nevada and California: U.S. Geological Survey Water-Resources Investigations Report 02–4102, 114 p.
- DeMeo, G.A., Lacznik, R.J., Boyd, R.A., Smith, J.L., and Nylund, W.E., 2003, Estimated ground-water discharge by evapotranspiration from Death Valley, California, 1997–2001: U.S. Geological Survey Water-Resources Investigations Report 03–4254, 27 p.
- Fenelon, J.M., 2000, Quality assurance and analysis of water levels in wells on Pahute Mesa and vicinity, Nevada Test Site, Nye County, Nevada: U.S. Geological Survey Water-Resources Investigations Report 00–4014, 68 p.
- Grasso, D.N., 1996, Hydrology of modern and late Holocene lakes, Death Valley, California: U.S. Geological Survey Water-Resources Investigations Report 95–4237, 53 p.

- Halford, K.J., and Hanson, R.T., 2002, User guide for the drawdown-limited, multi-node well (MNW) package for the U.S. Geological Survey's modular three-dimensional finite-difference ground-water flow model, versions MODFLOW-96 and MODFLOW-2000: U.S. Geological Survey Open-File Report 02-293, 33 p.
- Harbaugh, J.W., Banta, E.R., Hill, M.C., and McDonald, M.G., 2000, MODFLOW-2000, The U.S. Geological Survey's modular ground-water flow model—User guide to modularization concepts and the ground-water flow process: U.S. Geological Survey Open-File Report 00-92, 121 p.
- Hevesi, J.A., Flint, A.L., and Flint, L.E., 2003, Simulation of net infiltration and potential recharge using a distributed parameter watershed model of the Death Valley region, Nevada and California: U.S. Geological Survey Water-Resources Investigations Report 03-4090, 91 p.
- Hill, M.C., 1998, Methods and guidelines for effective model calibration: U.S. Geological Survey Water-Resources Investigations Report 98-4005, 90 p.
- Hill, M.C., Banta, E.R., Harbaugh, A.W., and Anderman, E.R., 2000, MODFLOW-2000, The U.S. Geological Survey's modular ground-water flow model—User guide to the observation, sensitivity, and parameter-estimation procedures and three post-processing programs: U.S. Geological Survey Open-File Report 00-184, 209 p., accessed September 1, 2004, at <http://water.usgs.gov/nrp/gwsoftware/modflow2000/modflow2000.html>
- Hill, M.C., Cooley, R.L., and Pollock, D.W., 1998, A controlled experiment in ground-water flow model calibration: *Ground Water*, v. 36, no. 3, p. 520-535.
- Hill, M.C., Ely, M.D., Tiedeman, C.R., O'Brien, G.M., D'Agnesse, F.A., and Faunt, C.C., 2001, Preliminary evaluation of the importance of existing hydraulic-head observation locations to advective-transport predictions, Death Valley regional flow system, California and Nevada: U.S. Geological Survey Water-Resources Investigations Report 00-4282, 82 p., accessed September 1, 2004, at <http://water.usgs.gov/pubs/wri/wri004282/>
- Hill, M.C., and Tiedeman, C.R., 2003, Weighting observations in the context of calibrating ground-water models, in Kovar, Karel, and Zbynek, Hrkal, eds., Calibration and reliability in groundwater modeling, a few steps closer to reality: International Association Hydrological Sciences Publication 277, p. 196-203.
- Hsieh, P.A., and Freckleton, J.R., 1993, Documentation of a computer program to simulate horizontal-flow barriers using the U.S. Geological Survey modular three-dimensional finite difference ground-water flow model: U.S. Geological Survey Open-File Report 92-477, 32 p.
- IT Corporation, 1996, Underground Test Area subproject, Phase I data analysis task, volume IV, Hydrologic parameter data documentation package: Report ITLV/10972-181 prepared for the U.S. Department of Energy, 8 volumes, various pagination.
- Laczniak, R.J., Smith, J.L., Elliott, P.E., DeMeo, G.A., Chatigny, M.A., and Roemer, G.J., 2001, Ground-water discharge determined from estimates of evapotranspiration, Death Valley regional flow system, Nevada and California: U.S. Geological Survey Water-Resources Investigations Report 01-4195, 51 p.
- Luckey, R.R., Tucci, Patrick, Faunt, C.C., Ervin, E.M., Steinkampf, W.C., D'Agnesse, F.A., and Patterson, G.L., 1996, Status of understanding of the saturated-zone ground-water flow system at Yucca Mountain, Nevada as of 1995: U.S. Geological Survey Water-Resources Investigations Report 96-4077, 71 p.
- Miller, G.A., 1977, Appraisal of the water resources of Death Valley, California-Nevada: U.S. Geological Survey Open-File Report 77-728, 68 p.
- Moreo, M.T., Halford, K.J., La Camera, R.J., and Laczniak, R.J., 2003, Estimated ground-water withdrawals from the Death Valley regional flow system, 1913-1998, Nevada and California: U.S. Geological Survey Water-Resources Investigations Report 03-4245, 28 p.
- Poeter, E.P. and Hill, M.C., 1997, Inverse modeling, a necessary next step in ground-water modeling: *Ground Water*, v. 35, no. 2, p. 250-260.
- Potter, C.J., Sweetkind, D.S., Dickerson, R.P., Kilgore, M.L., 2002, Hydrostructural maps of the Death Valley regional flow system, Nevada and California: U.S. Geological Survey Miscellaneous Field Studies MF-2372, 2 sheets, 1:250,000 scale, 14 pages of explanatory text.
- Prudic, D.E., Harrill, J.R., and Burbey, T.J., 1995, Conceptual evaluation of regional ground-water flow in the carbonate-rock province of the Great Basin, Nevada, Utah, and adjacent States: U.S. Geological Survey Professional Paper 1409-D, 102 p.
- Rantz, S.E. (compiler), 1982, Measurement and computation of stream flow: U.S. Geological Survey Water-Supply Paper 2175, v. 1, p. 181-183.
- Reiner, S.R., Laczniak, R.J., DeMeo, G.A., Smith, J.L., Elliott, P.E., Nylund, W.E., and Fridrich, C.J., 2002, Ground-water discharge determined from measurements of evapotranspiration, other available hydrologic components, and shallow water-level changes, Oasis Valley, Nye County, Nevada: U.S. Geological Survey Water-Resources Investigations Report 01-4239, 65 p.

- Schaefer, D.H., and Harrill, J.R., 1995, Simulated effects of proposed ground-water pumping in 17 basins of east-central and southern Nevada: U.S. Geological Survey Water-Resources Investigations Report 95-4173, 71 p.
- Sweetkind, D.S., and White, D.K., 2001, Facies analysis of Late Proterozoic through Lower Cambrian clastic rocks of the Death Valley regional ground-water system and surrounding areas, Nevada and California: U.S. Geological Survey Open-File Report 01-351, 13 p.
- Thomas, J.M., Carlton, S.M., and Hines, L.B., 1989, Ground-water flow and simulated response to selected developmental alternatives in Smith Creek Valley, a hydrologically closed basin in Lander County, Nevada: U.S. Geological Survey Professional Paper 1409-E, 57 p.
- Tiedeman, C.R., Hill, M.C., D'Agnesse, F.A., and Faunt, C.C., 2003, Methods for using ground-water model predictions to guide hydrogeologic data collection with application to the Death Valley regional groundwater flow system: *Water Resources Research*, v. 39, no. 1, p. 5-1 to 5-17.
- Van Denburgh, A.S., and Rush, F.E., 1974, Water-resources appraisal of Railroad and Penoyer Valleys, east-central Nevada: Nevada Department of Conservation and Natural Resources Ground-Water Resources—Reconnaissance Series Report 60, 61 p.
- Waddell, R.K., 1982, Two-dimensional, steady-state model of ground-water flow, Nevada Test site and vicinity, Nevada-California: U.S. Geological Survey Water-Resources Investigations Report 84-4267, 72 p.